GOX 2023 Program Key

AC Advanced Characterization Techniques
BG Bulk Growth
DI Dielectric Interfaces
EG Epitaxial Growth
EP Electronic and Photonic Devices, Circuits and Applications
ET Electronic Transport and Breakdown Phenomena
HM Heterogeneous Material Integration
KEY Keynote Address
MD Material and Device Processing and Fabrication Techniques
TM Theory, Modeling and Simulation

Key to Session/Paper Numbers

Sessions sponsored by multiple topics are labeled with all acronyms (e.g. **AC+ET+HM**), then a dash followed by the first two characters of the day of the week: **Mo**nday, **Tu**esday, **We**dnesday, then a single letter for **M**orning, **A**fternoon, **P**oster, and finally a number indicating the starting time slot for the paper.
Example: EG+BG-TuA-3 (Bulk/Epitaxy Session, Tuesday Afternoon, 2:15 pm).

GOX 2023 Program Overview

Room /Time	Bansal Atrium	Davis Hall 101
MoM		**KEY-MoM: Keynote Address I** **AC+TM-MoM: Characterization/Modeling I** **EG-MoM: Bulk/Epitaxial I**
MoA		**EP+HM+MD-MoA: Processes/Devices I** **AC+DI+HM+TM-MoA: Characterization/Modeling II**
MoP	**Poster Sessions**	
TuM		**KEY-TuM: Keynote Address II** **TM-TuM: Characterization/Modeling III** **AC+MD-TuM: Characterization/Modeling IV**
TuA		**EG+BG-TuA: Bulk/Epitaxy II** **MD+AC+EP-TuA: Process/Devices II**
TuP	**Poster Sessions**	
WeM		**KEY-WeM: Keynote Address III** **EG+BG+MD-WeM: Epitaxial III** **EP+ET+MD-WeM: Process/Devices III**

Monday Morning, August 14, 2023

Room Davis Hall 101

Keynote Address
Session KEY-MoM
Keynote Address I
Moderators:
Michael Scarpulla, University of Utah,
Uttam Singisetti, University of Buffalo, SUNY

8:30am	**Welcome and Opening Remarks**
8:45am	**INVITED: KEY-MoM-2** Gallium Oxide as a Material for Power Device Applications, ***Akito Kuramata,*** Novel Crystal Technology, Inc., Japan
9:00am	

Advanced Characterization Techniques
Session AC+TM-MoM
Characterization/Modeling I
Moderators:
Michael Scarpulla, University of Utah,
Uttam Singisetti, University of Buffalo, SUNY

9:15am	**AC+TM-MoM-4** Electric Field Induced Defect Redistribution at Ni-Ga_2O_3 Interfaces, ***Daram Ramdin****, H. Huang, S. Dhara, S. Rajan, J. Hwang, L. Brillson,* The Ohio State University
9:30am	**AC+TM-MoM-5** Charge State Transition Levels of Ni in β-Ga_2O_3 Crystals from Experiment and Theory: Eminently Suitable Candidate for Compensation, ***Palvan Seyidov****,* Leibniz-Institut für Kristallzüchtung, Germany*; J. Basile Varley,* Lawrence Livermore National Laboratory*; Z. Galazka, T. Chou, A. Popp, K. Irmscher, A. Fiedler,* Leibniz-Institut für Kristallzüchtung, Germany
9:45am	**AC+TM-MoM-6** Comparative Study of Temperature-Dependent Bandgap Transitions in Ga_2O_3 Polymorphs, ***Benjamin M. Janzen****, N. Hajizadeh, M. Meißner, M. Marggraf, C. Hartung,* Technical University of Berlin, Germany*; Z. Galazka,* Leibniz-Institut für Kristallzüchtung, Berlin, Germany*; P. Mazzolini, A. Sacchi, R. Fornari,* Department of Mathematical, Physical and Computer Sciences, University of Parma, Italy*; C. Petersen, H. von Wenckstern, M. Grundmann,* Universität Leipzig, Felix-Bloch-Institut für Festkörperphysik, Germany*; E. Kluth, M. Feneberg, R. Goldhahn,* Otto-von-Guericke-University Magdeburg, Germany*; T. Oshima,* Department of Electrical and Electronic Engineering, Saga University, Japan*; T. Kato, H. Nishinaka,* Faculty of Electrical Engineering and Electronics, Kyoto Institute of Technology, Japan*; J. Varley,* Lawrence Livermore National Laboratory*; M. Wagner,* Paul-Drude-Institut für Festkörperelektronik, Germany
10:00am	**AC+TM-MoM-7** Strain and Composition Dependencies in $(Al_xGa_{1-x})_2O_3$ Alloys, ***Rafal Korlacki****, J. Knudtson, M. Stokey, M. Hilfiker,* University of Nebraska-Lincoln*; V. Darakchieva,* Lund University, Sweden*; M. Schubert,* University of Nebraska-Lincoln
10:15am	**AC+TM-MoM-8** 10 kV Ga_2O_3 Schottky Rectifier Operational at 200 ℃, ***Yuan Qin****, M. Xiao, M. Potter, Y. Ma,* Center of Power Electronics Systems, Virginia Polytechnic Institute and State University*; J. Spencer,* Naval Research Laboratory*; Z. Du,* Ming Hsieh Department of Electrical Engineering, University of Southern California*; A. Jacobs,* Naval Research Laboratory*; K. Sasaki,* Novel Crystal Technology Inc., Japan*; H. Wang,* Ming Hsieh Department of Electrical Engineering, University of Southern California*; M. Tadjer,* Naval Research Laboratory*; Y. Zhang,* Center of Power Electronics Systems, Virginia Polytechnic Institute and State University
10:30am	**BREAK**

Epitaxial Growth
Session EG-MoM
Bulk/Epitaxial I
Moderator:
Hongping Zhao, Ohio State University

10:45am	**INVITED: EG-MoM-10** Advances in the MOCVD Growth of β-Ga_2O_3 and Related Heterostructures, ***Andrei Osinsky****,* Agnitron Technonolgy, Inc.*; F. Alema,* Agnitron Technology, Inc.
11:00am	
11:15am	**EG-MoM-12** MOVPE of (100) β-Ga2O3 for Vertical Power Devices - Challenges to Epitaxial Growth Process, ***Andreas Popp****, T. Chou, S. Bin Anooz, R. Grüneberg, V. Thuy, J. Rehm, A. Akhtar, Z. Galazka, P. Seyidov, K. Irmscher,* LEIBNIZ-INSTITUT FÜR KRISTALLZÜCHTUNG im Forschungsverbund Berlin e.V, Germany*; M. Albrecht,* LEIBNIZ-INSTITUT FÜR KRISTALLZÜCHTUNG im Forschungsverbund Berlin e., Germany*; A. Fiedler,* LEIBNIZ-INSTITUT FÜR KRISTALLZÜCHTUNG im Forschungsverbund Berlin e.V, Germany
11:30am	**EG-MoM-13** MOCVD Epitaxy of (010) β-Ga_2O_3 with Fast Growth Rate and the Role of Carbon in Charge Compensation, ***Lingyu Meng****, A. Bhuiyan, D. Yu, H. Zhao,* The Ohio State University
11:45am	**EG-MoM-14** Controllable Deep Acceptor Doping in MOCVD β-Ga_2O_3 to Compensate Parasitic Interface Charges, ***Fikadu Alema****,* Agnitron Technology*; T. Itoh,* Materials Department, University of California, Santa Barbara*; W. Brand, A. Osinsky,* Agnitron Technology*; J. Speck,* Materials Department, University of California, Santa Barbara
12:00pm	**EG-MoM-15** Si Accumulation on Ga_2O_3 Surfaces, ***Jon McCandless****, C. Gorsak, V. Protasenko, D. Schlom, M. Thompson, H. Xing, H. Nair, D. Jena,* Cornell University

	Room Davis Hall 101	
1:45pm	**INVITED: EP+HM+MD-MoA-1** Gallium Oxide – Heterogenous Integration with Diamond for Advanced Device Structures*, H. Kim, A. Bhat, A. Nandi, V. Charan, I. Sanyal, A. Mishra, Z. Abdallah, M. Smith, J. Pomeroy, D. Cherns, **Martin Kuball**,* University of Bristol, UK	**Electronic and Photonic Devices, Circuits and Applications** **Session EP+HM+MD-MoA** **Processes/Devices I** **Moderator:** **Yuhao Zhang**, Virginia Tech
2:00pm		
2:15pm	**EP+HM+MD-MoA-3** Highly Scaled β-Ga2O3 MOSFET with 5.4 MV/cm Average Breakdown Field and Near 50 GHz fMAX*, **Chinmoy Nath Saha**, A. vaidya,* SUNY at Buffalo*; A. Bhuiyan, L. Meng,* Ohio State University*; S. Sharma,* SUNY at Buffalo*; H. Zhao,* Ohio State University*; U. Singisetti,* SUNY at Buffalo	
2:30pm	**EP+HM+MD-MoA-4** Demonstration of a β-Ga_2O_3 Lateral Diode Full-Wave Rectifier Monolithic Integrated Circuit*, **Jeremiah Williams**, J. Piel, A. Islam, N. Hendricks, D. Dryden, N. Moser,* Air Force Research Laboratory, Sensors Directorate*; W. Wang,* Wright State University*; K. Liddy, M. Ngo,* Air Force Research Laboratory, Sensors Directorate*; N. Sepelak,* KBR Inc.*; A. Green,* Air Force Research Laboratory, Sensors Directorate	
2:45pm	**EP+HM+MD-MoA-5** Improved Breakdown Strength of Lateral β-Ga_2O_3 MOSFETs Using Aerosol-Spray-Printed hBN-BCB Composite Encapsulation*, **Daniel Dryden**,* Air Force Research Laboratory, Sensors Directorate*; L. Davidson,* KBR, Inc.*; K. Liddy, J. Williams, T. Pandhi, A. Islam, N. Hendricks, J. Piel,* Air Force Research Laboratory, Sensors Directorate*; N. Sepelak,* KBR, Inc.*; D. Walker, Jr., K. Leedy,* Air Force Research Laboratory, Sensors Directorate*; T. Asel, S. Mou,* Air Force Research Laboratory, Materials and Manufacturing Directorate, USA*; F. Ouchen,* KBR, Inc.*; E. Heckman, A. Green,* Air Force Research Laboratory, Sensors Directorate	
3:00pm	**EP+HM+MD-MoA-6** Wafer-Scale β-Ga_2O_3 Field Effect Transistors with MOCVD-Grown Channel Layers*, **Carl Peterson**,* University of California Santa Barbara*; F. Alema,* Agnitron Technology Incorporated*; Z. Ling, A. Bhattacharyya,* University of California Santa Barbara*; S. Roy,* University of California at Santa Barbara*; A. Osinsky,* Agnitron Technology Incorporated*; S. Krishnamoorthy,* University of California Santa Barbara	
3:15pm	**EP+HM+MD-MoA-7** Modelling of Impedance Dispersion in Lateral β-Ga-$_2O_3$ MOSFETs Due to Parallel Conductive Si-Accumulation Layer*, **Zequan Chen**, A. Mishra, A. Bhat, M. Smith, M. Uren,* University of Bristol, UK*; S. Kumar, M. Higashiwaki,* National Institute of Information and Communications Technology, Japan*; M. Kuball,* University of Bristol, UK	
3:30pm	**BREAK**	
3:45pm	**INVITED: AC+DI+HM+TM-MoA-9** The Physics of Low Symmetry Semiconductors: Gallium Oxide for the Future of Green Energy as Example*, **Mathias Schubert**, R. Korlacki, M. Stokey, M. Hilfiker,* University of Nebraska-Lincoln, USA*; S. Knight,* Linkoping University, Sweden*; S. Richter,* Lund University, Sweden*; A. Ruder,* University of Nebraska-Lincoln, USA*; A. Papamichael, V. Stanishev,* Linkoping University, Sweden*; J. Speck,* University of California Santa Barbara*; V. Darakchieva,* Lund University, Sweden	**Advanced Characterization Techniques** **Session AC+DI+HM+TM-MoA** **Characterization/Modeling II** **Moderator:** **Mike Thompson**, Cornell University
4:00pm		
4:15pm	**AC+DI+HM+TM-MoA-11** Investigation of Split Vacancy and Interstitial Defects and Ionic Diffusion Mechanisms in β-Ga_2O_3: A Direct Approach via Master Diffusion Equations*, **Channyung Lee**, E. Ertekin,* University of Illinois Urbana-Champaign	
4:30pm	**AC+DI+HM+TM-MoA-12** Hybrid Metal/low-k/$BaTiO_3$/β-Ga_2O_3 Metal-Insulator-Semiconductor Junctions Enable Electric Field of 6.8 MV/cm*, **Ashok Dheenan**, S. Dhara,* Ohio State University*; A. Islam, A. Green,* Air Force Research Laboratory*; S. Rajan,* Ohio State University	
4:45pm	**AC+DI+HM+TM-MoA-13** Towards Controlled Transfer of (001) β-Ga_2O_3 to (0001) 4H-SiC Substrates*, **Michael Liao**,* National Research Council Postdoctoral Fellow at the U.S. Naval Research Laboratory*; K. Huynh,* University of California Los Angeles*; J. Lundh,* National Research Council Postdoctoral Fellow at the U.S. Naval Research Laboratory*; M. Tadjer, K. Hobart,* U.S. Naval Research Laboratory*; M. Goorsky,* University of California Los Angeles	

Advanced Characterization Techniques
Room Bansal Atrium - Session AC-MoP
Advanced Characterization Techniques Poster Session I
5:15 – 7:15 pm

AC-MoP-1 Photoluminescence Mapping of Gallium Oxide, ***Matthew McCluskey***, Washington State University

AC-MoP-2 Linearly Polarized UV, Blue, and IR Photoluminescence from β-Ga_2O_3, *J. Cooke, M. Lou,* ***Mike Scarpulla***, University of Utah; *A. Bhattacharyya,* University of California, Santa Barbara; *X. Cheng, Y. Wang,* University of Utah; *S. Krishnamoorthy,* University of California, Santa Barbara; *B. Sensale-Rodriguez,* University of Utah

AC-MoP-3 Non-Uniformity and Hysteresis of Capacitance-Voltage Doping Profiling in Β-Ga_2O_3, ***Jian Li***, *A. Charnas, B. Noesges, A. Neal, T. Asel, Y. Kim, S. Mou,* Air Force Research Laboratory, Materials and Manufacturing Directorate, USA

AC-MoP-4 Scanning Transmission Electron Microscopy (S/TEM) Investigation of γ-Ga_2O_3 Defective Layers In Aluminum and Scandium Alloyed β-Ga_2O_3, ***Andrew Balog***, The Pennsylvania State University; *A. Chmielewski,* CEMES-CNRS, France; *R. Lavelle, L. Miao,* The Pennsylvania State University; *J. Jesenovec, B. Dutton,* Washington State University; *C. Lee, E. Ertekin,* University of Illinois at Urbana Champaign; *J. McCloy,* Washington State University; *N. Alem,* The Pennsylvania State University

Bulk Growth
Room Bansal Atrium - Session BG-MoP
Bulk Growth Poster Session I
5:15 – 7:15 pm

BG-MoP-1 MOCVD Development for Growth of Ga_2O_3 Over Large Areas, ***Muhammad Ali Johar***, *A. Feldman, G. Provost, K. Vasudevan,* Structured Materials Industries, Inc; *L. Lyle,* Pennsylvania State University; *L. Porter,* Carnegie Mellon University, USA; *A. Popp,* Leibniz-Institut für Kristallzüchtung (IKZ); *G. Tompa,* Structured Materials Industries, Inc

BG-MoP-2 Quality Improvement of Sn-doped β-Ga_2O_3 Single Crystal by Optimizing Temperature Gradient Control in Growth Zone, ***Su-Min Choi***, *H. Jang, S. Seo, M. Chae, M. Park, Y. Jang,* Department of Advanced Materials Engineering, Dong-Eui University, Republic of Korea; *Y. Moon, Y. Sung, J. Kang,* AXEL, Republic of Korea; *Y. Shin, S. Bae,* Korea Institute of Ceramic Engineering and Technology, Republic of Korea; *W. Lee,* Department of Advanced Materials Engineering, Dong-Eui University, Republic of Korea

BG-MoP-4 Various Crystal Planes and their Characteristics obtained from β-Ga_2O_3 Single Crystal Blocks Grown by the Multi-slit Structure of the EFG Method, *Y. MOON,* AXEL, Republic of Korea; ***HUIYEON JANG***, Dongeui University, Republic of Korea; *Y. SUNG,* AXEL, Republic of Korea; *S. CHOI, M. CHAE, S. SEO, M. PARK, Y. JANG, W. LEE,* Dongeui University, Republic of Korea; *Y. SHIN, S. BAE,* Korea Institute of Ceramic Engineering and Technology, Republic of Korea; *T. LEE, H. KIM,* Korea Institute of Industrial Technology, Republic of Korea; *J. KANG,* AXEL, Republic of Korea

BG-MoP-5 Investigation of Defects in(100) and (001) β-Ga_2O_3Single Crystal GrownbyEFG Method, *M. Choi,* Korea Institute of Ceramic Engineering and Technology/Pusan National University, Republic of Korea; ***Yun-Ji Shin***, Korea Institute of Ceramic Engineering and Technology, Republic of Korea; *W. Jeong, T. Gu, A. Shin, S. Cho,* Korea Institute of Ceramic Engineering and Technology/Pusan National University, Republic of Korea; *Y. Moon, J. Kang,* AXEL, Republic of Korea; *W. Lee,* Dong-Eui University, Republic of Korea; *S. Jeong,* Korea Institute of Ceramic Engineering and Technology, Republic of Korea; *S. Harada,* Nagoya University, Japan; *K. Ishiji,* Kyushu Synchrotron Light Research Center, Japan; *H. Lee,* Pusan National University, Republic of Korea; *S. Bae,* Korea Institute of Ceramic Engineering and Technology, Réunion

Dielectric Interfaces
Room Bansal Atrium - Session DI-MoP
Dielectric Interfaces Poster Session I
5:15 – 7:15 pm

DI-MoP-1 Dielectric Lifetime Enhancement of in-situ MOCVD Al_2O_3 on β-Ga_2O_3 Using Temperature Modulated Deposition, ***Saurav Roy***, *A. Bhattacharyya, C. Peterson, S. Krishnamoorthy,* University of California Santa Barbara

Electronic and Photonic Devices, Circuits and Applications
Room Bansal Atrium - Session EP-MoP
Electronic and Photonic Devices, Circuits and Applications Poster Session I
5:15 – 7:15 pm

EP-MoP-2 Anisotropy Nature of NiO_x/β-Ga_2O_3*p-n* Heterojunctions on (-201), (001), and (010) β-Ga_2O_3 Substrates, ***Dinusha Herath Mudiyanselage***, *D. Wang, H. Fu,* Arizona State University

EP-MoP-3 Ultrathin Films of Amorphous Gallium Oxide for Ultra-Fast Solar-Blind Photodetectors, ***Damanpreet Kaur***, *M. Kumar,* Indian Institute of Technology Ropar, India

Epitaxial Growth
Room Bansal Atrium - Session EG-MoP
Epitaxial Growth Poster Session I
5:15 – 7:15 pm

EG-MoP-1 A Study of the Critical Thickness for Phase Transition of α-Gallium Oxide Grown on Sapphire Substrates by MOCVD, ***Cheng-Han Lee***, *C. Gorsak, H. Nair,* Department of Materials Science and Engineering, Cornell University

EG-MoP-2 Epitaxial Growth of β-Ga_2O_3 Films on Mgo Substrate via Mist Chemical Vapor Deposition Method, ***Takumi Ikenoue***, Kyoto University, Cronell University, Japan; *Y. Cho, V. Protasenko, C. Savant, B. Cromer,* Cornell University; *M. Miyake, T. Hirato,* Kyoto University, Japan; *M. Thompson, D. Jena, H. Xing,* Cornell University

EG-MoP-3 Fluid Analysis of MIST-CVD Chamber for Uniformity Improvement in Gallium Oxide Epitaxial Growth, ***Jungyeop Hong***, *Y. Jung, D. Chun, J. Park, N. Joo, T. Kim,* Hyundai Motor Company, Republic of Korea

EG-MoP-6 The Effect of Excess Ga on Electron Transport in *β*-Ga_2O_3 Grown via Plasma Assisted Molecular Beam Epitaxy, ***Thaddeus Asel***, *B. Noesges, Y. Kim, A. Neal, S. Mou,* Air Force Research Laboratory, Materials and Manufacturing Directorate, USA

EG-MoP-7 Low-Pressure Chemical Vapor Deposition of Ultrawide Bandgap $LiGa_5O_8$ Thin Films, ***Kaitian Zhang***, *L. Meng, H. Huang,* The Ohio State University; *J. Sarker,* University of Buffalo, SUNY; *A. Bhuiyan,* The Ohio State University; *B. Mazumder,* University of Buffalo, SUNY; *J. Hwang, H. Zhao,* The Ohio State University

EG-MoP-8 Controlling Si Dopant Profiles in n-type *β*-Gallium Oxide, ***Brenton Noesges***, *Y. Kim, A. Neal, S. Mou, T. Asel,* Air Force Research Laboratory, Materials and Manufacturing Directorate, USA

EG-MoP-9 Silicon-doped *β*-Ga2O3 Films Grown at 1 µm/h by Suboxide Molecular-Beam Epitaxy, ***Kathy Azizie***, *F. Hensling, C. Gorsak,* Cornell University; *Y. Kim,* Air Force Research Laboratory; *N. Pieczulewski,* Cornell University; *D. Dryden,* Air Force Research Laboratory; *M. Senevirathna, S. Coye,* Clark Atlanta University; *S. Shang,* Penn State University; *J. Steele, P. Vogt, N. Parker, Y. Birkhölzer, J. McCandless, D. Jena, H. Xing,* Cornell University; *Z. Liu,* Penn State University; *M. Williams,* Clark Atlanta University; *A. Green,* Air Force Research Laboratory; *D. Schlom,* Cornell University

EG-MoP-10 Epitaxial Growth of Metastable Ga_2O_3 Polymorphs Using MOCVD and HVPE, ***Jingyu Tang***, *M. Moneck, M. Weiler, K. Jiang, R. Davis, L. Porter,* Carnegie Mellon University

EG-MoP-11 Pulsed Laser Deposition of α-Ga_2O_3 on M-Plane Al_2O_3: Growth Regime, Growth Process and Structural Properties, ***Clemens Petersen***, University Leipzig, Felix Bloch Institute for Solid State Physics, Semiconductor Physics Group, Leipzig, Germany; *S. Vogt, H. von Wenckstern, M. Grundmann,* University Leipzig, Felix Bloch Institute for Solid State Physics, Semiconductor Physics Group, Germany

EG-MoP-4 High-Quality Power Device Grade β-Ga_2O_3 on 4H-SiC via Metal Organic Chemical Vapor Deposition, *I. Sanyal, A. Nandi,* ***Martin Kuball***, University of Bristol, UK

Heterogeneous Material Integration
Room Bansal Atrium - Session HM-MoP
Heterogeneous Material Integration Poster Session I
5:15 – 7:15 pm

HM-MoP-1 Characterization of Sputtered P-Type Nickel Oxide for Ga_2O_3 Devices, ***Joseph Spencer***, Naval Research Laboratory; *Y. Ma, B. Wang, M. Xiao,* Virginia Tech; *A. Jacobs, J. Hajzus,* Naval Research Laboratory; *A. Mock,* Weber State University; *T. Anderson, K. Hobart,* Naval Research Laboratory; *Y. Zhang,* Virginia Tech; *M. Tadjer,* Naval Research Laboratory

Material and Device Processing and Fabrication Techniques
Room Bansal Atrium - Session MD-MoP
Material and Device Processing and Fabrication Techniques Poster Session I
5:15 – 7:15 pm

MD-MoP-2 Characteristics of n-ITO/Ti/Au Multilayer for Ohmic Contact on β-Ga_2O_3 Epitaxial Layer, ***Yusup Jung***, *H. Kim, S. Kim,* Powercubesemi Inc., Republic of Korea; *Y. Jung, D. Chun,* Hyundai Motor Company, Republic of Korea; *T. Kang, S. Kyoung,* Powercubesemi Inc., Republic of Korea

MD-MoP-3 β-Ga_2O_3 Schottky and Heterojunction Diodes Operating at Temperatures Up to 600°C, ***Kingsley Egbo***, *S. Schaefer, W. Callahan, B. Tellekamp, A. Zakutayev,* National Renewable Energy Laboratory

MD-MoP-4 Structural Properties of Ga_2O_3 Surfaces Treated by Nitrogen Radical Irradiation, ***Kura Nakaoka***, *S. Taniguchi, T. Kitada, M. Higashiwaki,* Department of Physics and Electronics, Osaka Metropolitan University, Japan

MD-MoP-6 Process Optimization of Sputtered High-K (Sr,Ba,Ca)Tio_3 for Ga_2O_{-3} Dielectric Layers, ***Bennett Cromer***, *C. Gorsak, W. Zhao, L. Li, H. Nair, J. Hwang, B. Van Dover, D. Jena, G. Xing,* Cornell University

MD-MoP-7 Electrical Characteristics of MOCVD Grown β-Ga_2O_3 Schottky Diodes on (010) β-Ga_2O_3 Substrates, ***Sudipto Saha***, University at Buffalo-SUNY; *L. Meng, D. Yu, A. Bhuiyan,* Ohio State University; *H. Zhao,* ohio State University; *U. Singisetti,* University at Buffalo-SUNY

	Room Davis Hall 101	
8:30am	**KEY-TuM-1** Welcome and Opening Remarks	**Keynote Address** **Session KEY-TuM** **Keynote Address II** **Moderators:** **Uttam Singisetti**, University of Buffalo, SUNY, **Joel Varley**, Lawrence Livermore National Laboratory
8:45am	**INVITED: KEY-TuM-2** Bulk Single Crystals and Physical Properties of β-$(Al_xGa_{1-x})_2O_3$ Grown by the Czochralski Method, ***Zbigniew Galazka***, LEIBNIZ-INSTITUT FÜR KRISTALLZÜCHTUNG, Germany	
9:00am		
9:15am	**INVITED: TM-TuM-4** Electron–Phonon Effects and Temperature-Dependence of the Electronic Structure of Monoclinic *β*-Ga_2O_3 from First Principles, ***Elif Ertekin**, C. Lee,* University of Illinois at Urbana-Champaign, USA; *M. Scarpulla, N. Rock, A. Islam,* University of Utah	**Theory, Modeling and Simulation** **Session TM-TuM** **Characterization/Modeling III** **Moderators:** **Uttam Singisetti**, University of Buffalo, SUNY, **Joel Varley**, Lawrence Livermore National Laboratory
9:30am		
9:45am	**TM-TuM-6** Ab-Initio Calculation of Low Field Electron Transport in Disordered Bulk β-$(Al_xGa_{1-x})_2O_3$ Semiconductor Alloy, ***Ankit Sharma**, U. Singisetti,* University at Buffalo-SUNY	
10:00am	**TM-TuM-7** Quantitative Modelling of Defect Concentrations in β-Ga_2O_3 for Equilibrium, Full Quenching, and Generalized Quenching Scenarios, ***Khandakar Aaditta Arnab**, I. Maxfield,* University of Utah; *C. Lee, E. Ertekin,* University of Illinois at Urbana Champaign; *J. Varley,* Lawrence Livermore National Laboratory; *Y. Frodason,* University of Oslo, Norway; *M. Scarpulla,* University of Utah	
10:15am	**TM-TuM-8** Exploring Gallium Oxide (β-Ga_2O_3) Drift Layer Design: Theoretical Analysis and Trade-offs, ***Sundar Isukapati**, S. DeBoer, S. Jang,* SUNY Polytechnic Institute, Albany; *Y. Jung,* Hyundai Motor Company, Republic of Korea; *W. Sung,* SUNY Polytechnic Institute, Albany	
10:30am	**BREAK**	
10:45am	**INVITED: AC+MD-TuM-10** Defects in Ga_2O_3: An Ultra-high Resolution Electron Microscopy Study, ***Nasim Alem**,* The Pennsylvania State University; *A. Chmielewski,* CEMES-CNRS, France	**Advanced Characterization Techniques** **Session AC+MD-TuM** **Characterization/Modeling IV** **Moderator:** **Baishakhi Mazumder**, University of Buffalo, SUNY
11:00am		
11:15am	**AC+MD-TuM-12** Sub-oxide Ga to Enhance Growth Rate of β-Ga_2O_3 by Plasma-assisted Molecular Beam Epitaxy, ***Zhuoqun Wen**, K. Khan, E. Ahmadi,* University of Michigan, Ann Arbor	
11:30am	**AC+MD-TuM-13** Microscopic-Scale Defect Analysis on Ga_2O_3 through Microscopy, *M. Kim,* NIST-Gaithersburg, Republic of Korea; *A. Winchester, O. Maimon,* NIST-Gaithersburg; *S. Koo,* KwangWoon University, Korea; *Q. Li,* George Mason University; ***Sujitra Pookpanratana**,* NIST-Gaithersburg	
11:45am	**AC+MD-TuM-14** Characterization and Processing Improvements for Fabricating and Polishing β-Ga2O3 Substrates, ***Robert Lavelle**, D. Snyder, W. Everson, D. Erdely, L. Lyle, N. Alem, A. Balog,* Penn State University; *N. Mahadik, M. Liao,* Naval Research Laboratory	
12:00pm		

	Room Davis Hall 101	
1:45pm	**INVITED: EG+BG-TuA-1** Suitable Orientation for Homoepitaxial Growth of Gallium Oxide, ***Kohei Sasaki**, A. Kuramata,* Novel Crystal Technology, Inc., Japan	**Epitaxial Growth** **Session EG+BG-TuA** **Bulk/Epitaxy II** **Moderator:** **Sriram Krishnamoorthy**, University of California Santa Barbara
2:00pm		
2:15pm	**EG+BG-TuA-3** Pushing the Al composition limit up to 99% in MOCVD β-$(Al_xGa_{1-x})_2O_3$ films using TMGa as Ga precursor, ***A F M Anhar Uddin Bhuiyan**, L. Meng, H. Huang, J. Hwang, H. Zhao,* The Ohio State University	
2:30pm	**EG+BG-TuA-4** Fast Growth and Characterization of Undoped β-Ga_2O_3 on 2-Inch Substrates Using a Horizontal Hot-Wall MOVPE System, ***Kazutada Ikenaga**,* Tokyo University of Agriculture and Technology / TAIYO NIPPON SANSO CORPORATION, Japan*; J. Yoshinaga, P. Guanxi,* TAIYO NIPPON SANSO CORPORATION, Japan*; H. Tozato, T. Okuyama, K. Goto, Y. Kumagai,* Tokyo University of Agriculture and Technology, Japan	
2:45pm	**INVITED: EG+BG-TuA-5** MBE Growth and Properties of Ultra-wide Bandgap Oxide Layers Spanning 5.0 - 9.0 eV Energy Gaps, ***Debdeep Jena**,* Cornell University	
3:00pm		
3:15pm	**EG+BG-TuA-7** Structural Defect Formation and Propagation in Fe-doped Czochralski-grown b-Ga_2O_3 Boules, ***Luke Lyle**,* Pennsylvania State University - Applied Research Lab*; R. Lavelle,* Penn State University - Applied Research Lab*; D. Erdely,* Pennsylvania State University - Applied Research Lab*; W. Everson,* Penn State University - Applied Research Lab*; A. Balog, N. Alem,* Pennsylvania State University*; D. Snyder,* Pennsylvania State University - Applied Research Lab	
3:30pm	**BREAK**	
3:45pm	**MD+AC+EP-TuA-9** Large Area Trench β-Ga_2O_3 Schottky Barrier Diode with Extreme-K Dielectric Resurf, ***Saurav Roy**, A. Bhattacharyya,* University of California Santa Barbara*; J. Cooke,* University of Utah*; C. Peterson,* University of California Santa Barbara*; B. Rodriguez,* University of Utah*; S. Krishnamoorthy,* University of California Santa Barbara	**Material and Device Processing and Fabrication Techniques** **Session MD+AC+EP-TuA** **Process/Devices II** **Moderator:** **Yuhao Zhang**, Virginia Tech
4:00pm	**MD+AC+EP-TuA-10** Fabrication and Characteristics of Ga_2O_3 MOSFET using p-NiO for Normally-off Operation, ***Daehwan Chun**, Y. Jung, J. Park, J. Hong, N. Joo, T. Kim,* Hyundai Motor Company, Republic of Korea	
4:15pm	**MD+AC+EP-TuA-11** On the Mg-Diffused Current Blocking Layer for Ga_2O_3 Vertical Diffused Barrier Field-Effect-Transistor (VDBFET), ***Ke Zeng**, Z. Bian, S. Chowdhury,* Stanford University	
4:30pm	**MD+AC+EP-TuA-12** Electrical Properties of p-NiO/β-Ga_2O_3 Vertical PN Heterojunction Diode for Power Device Applications, ***Youngkyun Jung**, D. Chun,* Hyundai Motor Company, Republic of Korea	
4:45pm	**MD+AC+EP-TuA-13** Effects of Oxygen Reactive Ion Etching and Nitrogen Radical Irradiation on Electrical Properties of Ga_2O_3 Schottky Barrier Diodes, ***Shota Sato**, K. Eguchi,* Department of Physics and Electronics, Osaka Metropolitan University, Japan*; Z. Wang,* National Institute of Information and Communications Technology, Japan*; T. Kitada, M. Higashiwaki,* Department of Physics and Electronics, Osaka Metropolitan University, Japan	

Advanced Characterization Techniques
Room Bansal Atrium - Session AC-TuP
Advanced Characterization Techniques Poster Session II
5:15 – 7:15 pm

AC-TuP-1 Photoluminescence Spectroscopy of Cr^{3+} in β-Ga_2O_3 and $(Al_{0.1}Ga_{0.9})_2O_3$, ***Cassandra Remple***, Materials Science & Engineering Program, Washington State University; *L. Barmore,* Dept. of Physics and Astronomy, Washington State University; *J. Jesenovec, J. McCloy,* Institute of Materials Research, Materials Science & Engineering Program, Washington State University; *M. McCluskey,* Dept. of Physics and Astronomy, Washington State University

AC-TuP-2 Determining the Effects of Traps on the Effective Mobility of β-Ga_2O_3 MOSFETs using the Split C-V Method in Dark and Illumination Conditions and Pulsed I-V, ***Ory Maimon***, George Mason University; *N. Moser,* Air Force Research Lab; *D. Chamria,* Colgate University; *K. Liddy, A. Green, K. Chabak,* Air Force Research Lab; *S. Pookpanratana, P. Shrestha,* National Institute of Standards and Technology (NIST); *Q. Li,* George Mason University

AC-TuP-3 Advanced Characterization Methods for Scale-up and Improvement of β-Ga2O3 Substrates, ***Robert Lavelle***, *D. Snyder, W. Everson, D. Erdely, L. Lyle, A. Balog, N. Alem,* Penn State University

AC-TuP-4 Vacancies in Electron Irradiated β-Ga_2O_3 Probed with Positrons, ***Marc Weber***, *C. Halverson,* Washington State University; *B. Dutton, C. Remple,* Washington State University, United States Minor Outlying Islands (the); *M. McCluskey,* Washington State University, US, United States Minor Outlying Islands (the); *M. Scarpulla,* University of Utah; *J. McCloy,* Washington State University, United States Minor Outlying Islands (the)

AC-TuP-5 Artificial Intelligence Assisted Vacancy Detection via 3D Microscopy in Doped and Undoped Ga_2O_3, ***Prachi Garg***, *J. Sarker,* Department of Materials Design and Innovation, University at Buffalo; *A. Uddin Bhuiyan, L. Meng,* Department of Electrical and Computer Engineering, The Ohio State University; *H. Zhao,* Department of Electrical and Computer Engineering & Department of Materials Science and Engineering, The Ohio State University; *K. Reyes, B. Mazumder,* Department of Materials Design and Innovation, University at Buffalo

AC-TuP-6 Silicon Ion Implantation in β-Ga_2O_3: Effect of Temperature on Atomic Damage and Recovery, ***Naomi Pieczulewski***, *K. Gann,* Cornell University; *T. Asel, B. Noesges,* Air Force Research Laboratory; *K. Heinselman,* National Renewable Energy Laboratory; *M. Thompson, D. Muller,* Cornell University

AC-TuP-8 Kinetics of Compensation in Sn-doped Ga_2O_3 During O_2 Annealing Revealed by FTIR and Modelling, *J. High, H. Yang, N. Rock,* ***Mike Scarpulla***, University of Utah

AC-TuP-9 Cation Vacancy and Dopant Diffusion in β-Ga2O3, ***Nathan David Rock***, *A. Levin,* University of Utah; *A. Bhattacharyya,* University of California Santa Barbara; *H. Yang, B. Eisner,* University of Utah; *S. Krishnamoorthy,* University of California Santa Barbara; *M. Scarpulla,* University of Utah

Bulk Growth
Room Bansal Atrium - Session BG-TuP
Bulk Growth Poster Session II
5:15 – 7:15 pm

BG-TuP-5 β-Ga_2O_3 Single Crystal Growth by EFG Method using Die with Multi-Slit Structure, ***Yeon-Geun Seong***, *Y. Moon,* Axel, Republic of Korea; *H. Jang, S. Choi, C. Min-Ji, S. Seo, M. Park, Y. Jang, W. Lee,* Dongeui University, Republic of Korea; *J. Kang,* Axel, Republic of Korea

Electronic and Photonic Devices, Circuits and Applications
Room Bansal Atrium - Session EP-TuP
Electronic and Photonic Devices, Circuits and Applications Poster Session II
5:15 – 7:15 pm

EP-TuP-6 Investigating the Properties of β-Ga_2O_3 Schottky Diodes on MOCVD-Grown (001) Drift Layer, ***Prakash P. Sundaram***, University of Minnesota, USA; *F. Alema, A. Osinsky,* Agnitron Technology; *S. Koester,* University of Minnesota, USA

EP-TuP-8 Operation of β-Ga2O3 Field-effect Transistors at 650 °C, ***James Spencer Lundh***, *H. Masten,* National Research Council Postdoctoral Fellow residing at US Naval Research Laboratory (DC); *F. Alema, A. Osinsky,* Agnitron Technology, Inc.; *A. Jacobs, K. Hobart, T. Anderson, M. Tadjer,* US Naval Research Laboratory

Heterogeneous Material Integration
Room Bansal Atrium - Session HM-TuP
Heterogeneous Material Integration Poster Session II
5:15 – 7:15 pm

HM-TuP-1 Bond-and-Thin Process for Making Heterogeneous Substrate with a Thin Ga_2O_3 Layer om Polycrystalline SiC Substrate, ***Alex Usenko***, *A. Caruso,* University of Missouri-Kansas City; *S. Bellinger,* Semiconductor Power Technologies

HM-TuP-3 Design of 10 kV P-Diamond/I-Ga_2O_3/N-Ga_2O_3 Power PN Diodes, ***Hunter Ellis***, *K. Fu,* Department of Electrical and Computer Engineering, University of Utah

HM-TuP-5 Heterogeneous Material Integration, ***Yash Mirchandani***, Syrnatec

HM-TuP-6 Si/Ga_2O_3 and GaAsP/Ga_2O_3 P-N Diodes via Semiconductor Grafting, *J. Zhou, D. Kim, H. Jang, Q. Lin,* ***Jiarui Gong***, University of Wisconsin - Madison; *F. Alema, A. Osinsky,* Agnitron Technology Inc.; *K. Chabak, G. Jessen,* Air Force Research Laboratory; *S. Pasayat,* University of Wisconsin - Madison; *C. Cheung, V. Gambin,* Northrop Grumann; *C. Gupta, Z. Ma,* University of Wisconsin - Madison

Material and Device Processing and Fabrication Techniques
Room Bansal Atrium - Session MD-TuP
Material and Device Processing and Fabrication Techniques Poster Session II
5:15 – 7:15 pm

MD-TuP-1 Growth of Room Temperature Polycrystalline β-Gallium Oxide Thin Film, ***Damanpreet Kaur***, *M. Kumar,* Indian Institute of Technology Ropar, India

MD-TuP-2 Performance and Traps of Ga_2O_3 Schottky Barrier Diodes with Mesa Structure, ***Min-Yeong Kim***, NIST-Gaithersburg, Republic of Korea; *O. Maimon,* NIST-Gaithersburg; *N. Hendricks, N. Moser,* Air Force Research Laboratory, USA; *S. Pookpanratana,* NIST-Gaithersburg; *S. Koo,* KwangWoon University, Korea; *Q. Li,* George Mason University

MD-TuP-4 Evolution of Lattice Distortions Throughout Various Stages of (010) β-Ga_2O_3 Substrate Preparation, ***Michael Liao***, National Research Council Postdoctoral at the U.S. Naval Research Laboratory; *N. Mahadik,* Naval Research Laboratory; *R. Lavelle, D. Snyder, W. Everson, D. Erdely, L. Lyle, N. Alem, A. Balog,* Penn State University; *T. Anderson,* Naval Research Laboratory

MD-TuP-5 Investigation of In-Plane Anisotropy of In-situ Ga etching on (010) β-Ga_2O_3, ***Abishek Katta***, Arizona State University; *F. Alema, W. Brand, A. Osinsky,* Agnitron Technologies; *N. Kalarickal,* School of Electrical, Computer and Energy Engineering, Arizona State University

MD-TuP-6 Understanding Ohmic Contacts to N+ Doped (010) β-Ga_2O_3 by Both In-Situ MOCVD Doping and Silicon Ion Implantation, ***Kathleen Smith***, *K. Gann, C. Gorsak, N. Pieczulewski, H. Nair, M. Thompson, D. Jena, H. Xing,* Cornell University

MD-TuP-7 Heteroepitaxial Growth of $ZnGa_2O_4$ by Post-Deposition Annealing of ZnO on Ga_2O_3 Substrate, ***Stefan Kosanovic***, *K. Sun,* University of Michigan, Ann Arbor; *U. Mishra,* University of California Santa Barbara; *E. Ahmadi,* University of Michigan, Ann Arbor

MD-TuP-8 Revitalizing Fractured β-Ga_2O_3 Nanomembranes: Nanogap Recovery for Enhanced Charge Transport Performance, *M. Hasan, J. Lai,* ***Jung-Hun Seo***, University at Buffalo

MD-TuP-9 Impact of Magnetron Sputtered Ultra-Thin Layer of Fe-Doped β-Ga_2O_3 on Gallium Oxide Schottky Contacts, ***Adetayo Adedeji***, Elizabeth City State University; *J. Merrett,* Air Force Research Laboratory, Aerospace Systems Directorate; *J. Lawson, C. Ebbing,* University of Dayton Research Institute

MD-TuP-10 An Investigation of (001) β-Ga_2O_3 Etching via Heated H_3PO_4, ***Steve Rebollo***, *T. Itoh, S. Krishnamoorthy, J. Speck,* University of California, Santa Barbara

MD-TuP-11 An Organic, Direct Bonded Copper, Multi-Layered, Ultra-Low Inductance Package for High-Power UWBG MOSFETs, *J. Major, J. Calder, S. Zhao,* ***Faisal Khan***, National Renewable Energy Laboratory

Theory, Modeling and Simulation
Room Bansal Atrium - Session TM-TuP
Theory, Modeling and Simulation Poster Session
5:15 – 7:15 pm

TM-TuP-1 Investigation of Oxygen Interstitial Diffusion Pathways in β-Ga2O3, ***Grace McKnight***, *C. Lee, E. Ertekin,* University of Illinois at Urbana-Champaign

TM-TuP-2 Optoelectronic Properties of $(In,Ga)_2O_3$ using First Principles Calculations*, E. Welch,* Prairie View A&M University*; P. Borges,* Federal University of Vicosa - Rio Paranaiba, Brazil*; **Luisa Scolfaro**, M. Talukder, R. Droopad,* Texas State University

TM-TuP-3 Modeling of β-$(Al_xGa_{1-x})_2O_3/Ga_2O_3$ High Electron Mobility Transistor (HEMT) and Current Aperture Vertical Electron Transistor (CAVET)*, **Dawei Wang**, D. Herath Mudiyanselage, H. Fu,* Arizona State University

TM-TuP-4 Electronic Band Structure and Excitons in $LiGaO_2$ and $LiGa_5O_8$*, N. Dadkhah,* Case Western Reserve University*; K. Dabsamut,* Kasetsart University, Thailand*; **Walter R. L. Lambrecht**,* Case Western Reserve University

TM-TuP-5 Two–Dimensional Analytical Modeling of the Surface Potential of a Double–Gate Vertical Fin–Shaped Ga_2O_3 Power Transistor*, **Twisha Titirsha**, M. Hossain, M. Shuvo, Q. Huang, J. Gahl, S. Islam,* University of Missouri, Columbia

	Room Davis Hall 101	
8:30am	**KEY-WeM-1** Welcome and Opening Remarks	**Keynote Address** **Session KEY-WeM** **Keynote Address III** **Moderators:** **Hari Nair**, Cornell University, **Uttam Singisetti**, University of Buffalo, SUNY
8:45am	**INVITED: KEY-WeM-2** Gallium Oxide Microelectronics for Department of Air Force Applications, ***Kelson Chabak***, Air Force Research Laboratory	
9:00am		
9:15am	**EG+BG+MD-WeM-4** Growth of α-$(Al_xGa_{1-x})_2O_3$ by Suboxide Molecular-Beam Epitaxy, ***Jacob Steele***, *K. Azizie, N. Pieczulewski, J. McCandless, D. Muller, H. Xing, D. Jena,* Cornell University*; T. Onuma,* Kogakuin University, Japan*; D. Schlom,* Cornell University (USA) and Leibniz-Institut für Kristallzüchtung (Germany)	**Epitaxial Growth** **Session EG+BG+MD-WeM** **Epitaxial III** **Moderators:** **Hari Nair**, Cornell University, **Uttam Singisetti**, University of Buffalo, SUNY
9:30am	**EG+BG+MD-WeM-5** Structural, Electrical, and Thermal Characterization of CIS-MOCVD β-Ga_2O_3 Epitaxial Buffer Layers, ***Hannah Masten***, Naval Research Laboratory*; G. Alvarez,* Cornell University*; C. Halverson,* Washington State University*; M. Liao, J. Lundh,* Naval Research Laboratory*; F. Alema, A. Osinsky,* Agnitron Technology*; A. Jacobs,* Naval Research Laboratory*; M. Weber,* Washington State University*; Z. Tian,* Cornell University*; K. Hobart, M. Tadjer,* Naval Research Laboratory	
9:45am	**EG+BG+MD-WeM-6** Electrical and Optical Properties of Melt-Grown Mn Doped β-Ga_2O_3 , ***Benjamin Dutton***, *C. Remple, J. Jesenovec,* Washington State University*; J. Varley, L. Voss,* Lawrence Livermore National Laboratory*; M. McCluskey, J. McCloy,* Washington State University	
10:00am	**EG+BG+MD-WeM-7** Mg and Zn Counter doping of Homoepitaxial β-Ga_2O_3 Grown by Molecular Beam Epitaxy, ***Stephen Schaefer***, *K. Egbo, S. Harvey, A. Zakutayev, B. Tellekamp,* National Renewable Energy Laboratory	
10:15am	**EG+BG+MD-WeM-8** Optimizing Si Implantation and Annealing in β-Ga_2O_3, ***Katie Gann***, *N. Pieczulewski,* Cornell University*; T. Asel,* Air Force Research Laboratory*; C. Gorsak,* Cornell University*; K. Heinselman,* national renewable Energy Laboratory*; K. Smith, J. McCandless,* Cornell University*; B. Noesges,* Air Force Research Lab*; G. Xing, D. Jena, H. Nair, D. Muller, M. Thompson,* Cornell University	
10:30am	**BREAK**	
10:45am	**INVITED: EP+ET+MD-WeM-10** Recent Progress of Ga_2O_3 Power Technology: Large-Area Devices, Packaging, and Applications, ***Yuhao Zhang***, Virginia Tech	**Electronic and Photonic Devices, Circuits and Applications** **Session EP+ET+MD-WeM** **Process/Devices III** **Moderator:** **Marko Tadjer**, Naval Research Laboratory
11:00am		
11:15am	**EP+ET+MD-WeM-12** Forward and Reverse Current Transport of (001) β-Ga_2O_3 Schottky Barrier Diodes and TiO_2/β-Ga_2O_3 Heterojunction Diodes with Various Schottky Metals, ***Nolan Hendricks***, AFRL, UCSB*; E. Farzana,* UCSB*; A. Islam, D. Dryden, J. Williams,* Air Force Research Lab*; J. Speck,* UCSB*; A. Green,* Air Force Research Lab	
11:30am	**EP+ET+MD-WeM-13** Vertical β-Ga_2O_3 Diodes with PtO_x/Interlayer Pt Schottky Contact and High Permittivity Dielectric Field Plate for Low Loss and High Breakdown Voltage, ***Esmat Farzana***, *S. Roy, S. Krishnamoorthy, J. Speck,* University of California Santa Barbara	
11:45am	**EP+ET+MD-WeM-14** Ni/TiO_2/β-Ga_2O_3 Heterojunction Diodes with NiO Guard Ring Simultaneously Increasing Breakdown Voltage and Reducing Turn-on Voltage, *J. Williams, N. Hendricks,* Air Force Research Lab*;* ***Weisong Wang***, Wright State University*; A. Adams,* Apex Micro Devices*; J. Piel, D. Dryden, K. Liddy,* Air Force Research Lab*; N. Sepelak,* KBR Inc.*; B. Morell,* Cornell University*; A. Miesle,* University of Dayton*; A. Islam, A. Green,* Air Force Research Lab	
12:00pm	**EP+ET+MD-WeM-15** Fabrication of Self Aligned β-Ga_2O_3 Junction Barrier Schottky Diodes with NiO Field Termination, ***Joseph Spencer***, Naval Research Laboratory*; B. Wang, M. Xiao,* Virginia Tech*; A. Jacobs, T. Anderson, K. Hobart,* Naval Research Laboratory*; Y. Zhang,* Virginia Tech*; M. Tadjer,* Naval Research Laboratory	
12:15pm	**EP+ET+MD-WeM-16** Ni/$BaTiO_3$/β-Ga2O3 Solar-Blind UV Photodetectors with Deep Etch Edge Termination, ***Nathan Wriedt***, *S. Rajan,* Ohio State University	
12:30pm	**Best Paper Awards, e-Surveys, and Closing Remarks**	

Author Index

Bold page numbers indicate presenter

— X —

— Y —

— Z —

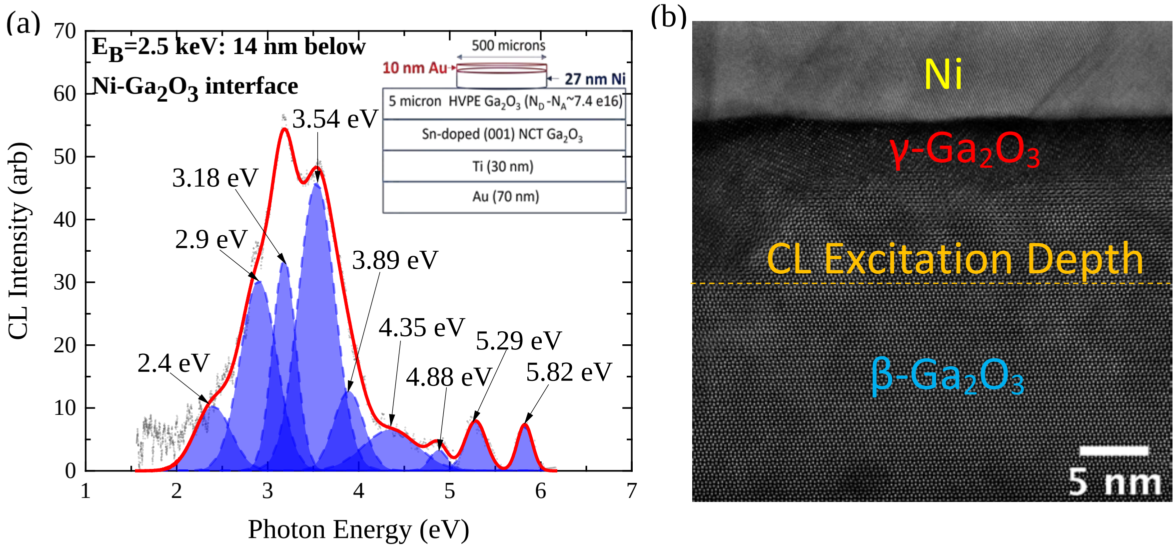

Figure 1: Characterization of near Ni-Ga_2O_3 interfacial region using (a) CLS & (b) STEM. CLS reveals pronounced above bandgap emissions that correlate with a defective γ phase region observed in STEM.

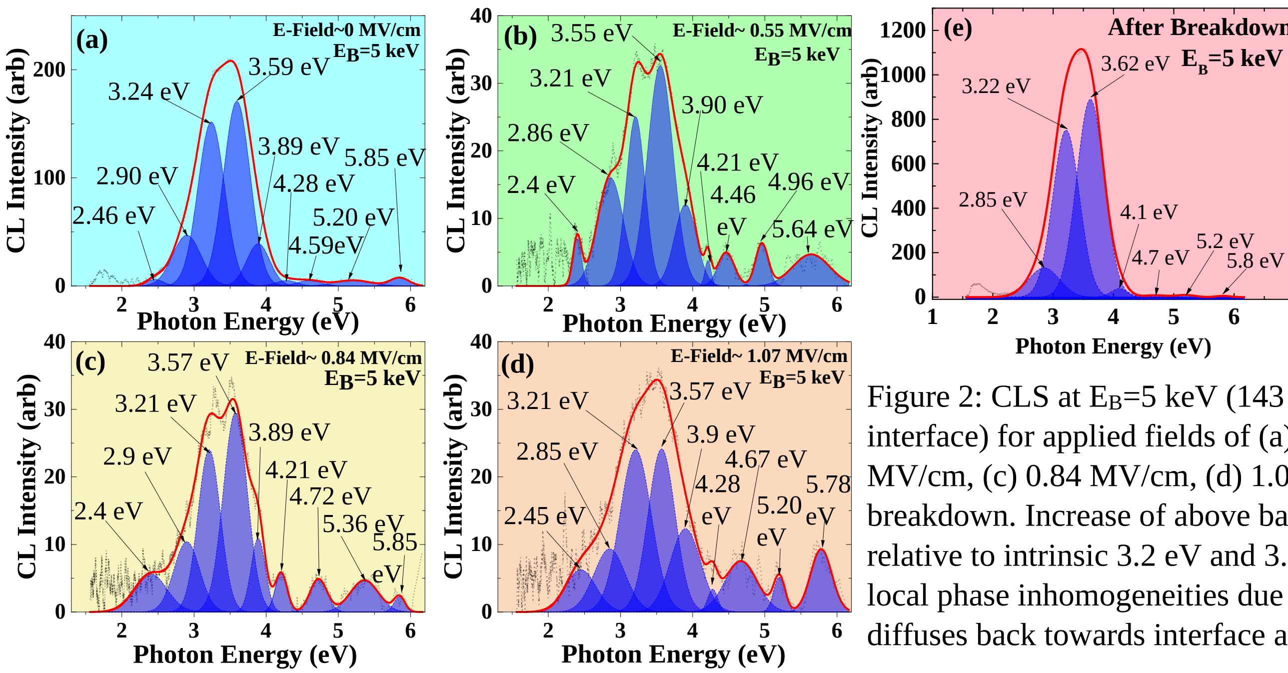

Figure 2: CLS at E_B=5 keV (143 nm below M-S interface) for applied fields of (a) 0 MV/cm, (b) 0.55 MV/cm, (c) 0.84 MV/cm, (d) 1.07 MV/cm & (e) after breakdown. Increase of above band gap emissions relative to intrinsic 3.2 eV and 3.6 eV emissions indicate local phase inhomogeneities due to Ni diffusion, which diffuses back towards interface after breakdown.

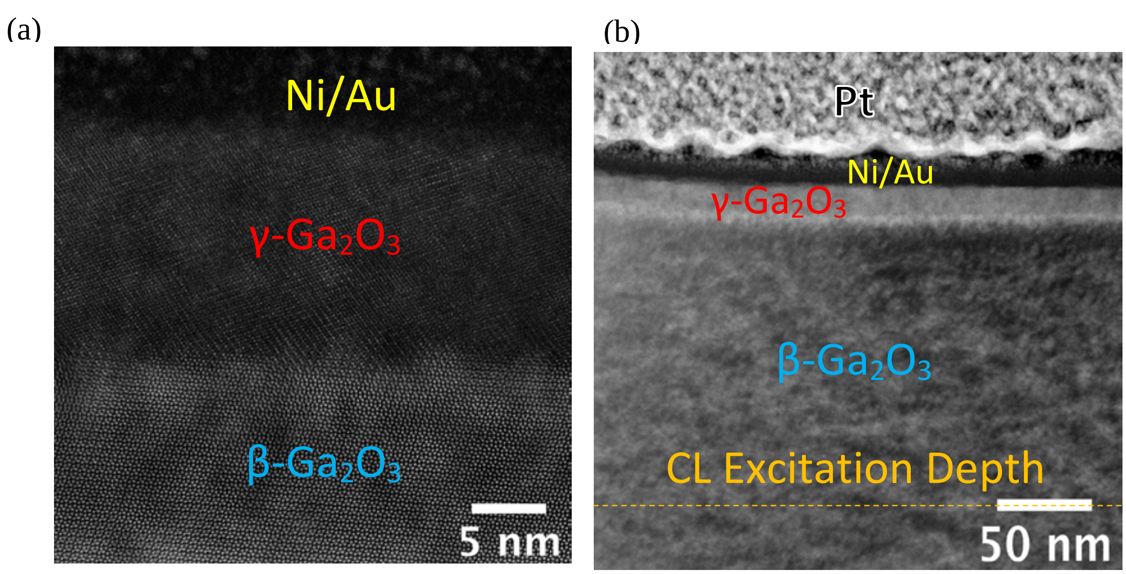

Figure 3: (a) HAADF image of near-interfacial region revealing that the γ phase became thicker after breakdown along with (b) LAADF image revealing that the phase 143 nm below M-S interface is homogenous after breakdown, indicating Ni diffusion back towards the Ni/Ga_2O_3 interface as breakdown

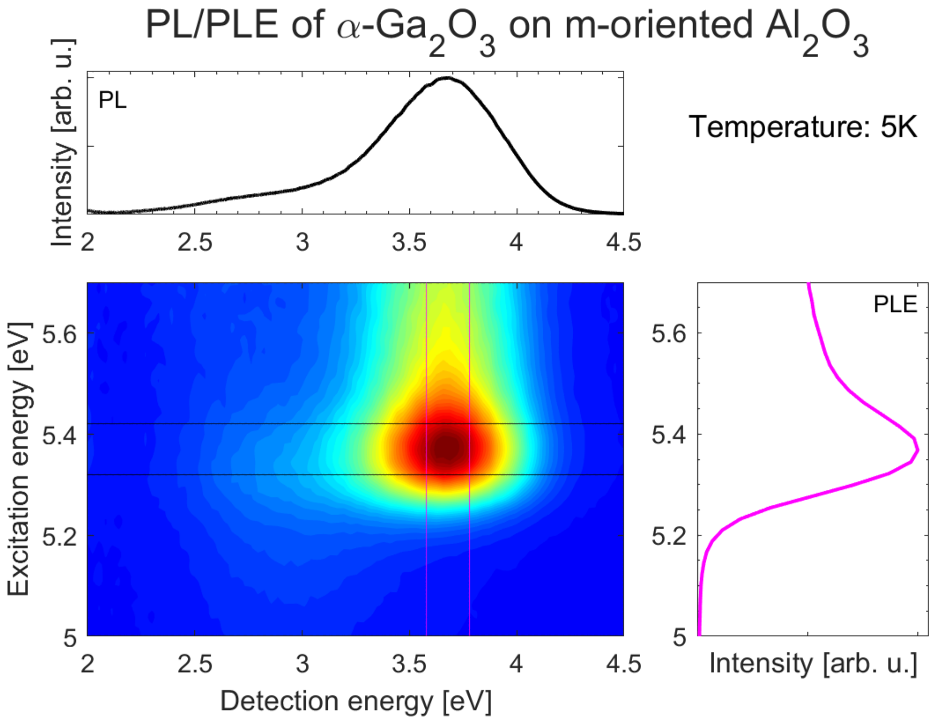

Fig. 1: Temperature-dependent UV photoluminescence excitation (PLE) and PL spectroscopy (here shown at 5K for α-Ga_2O_3).

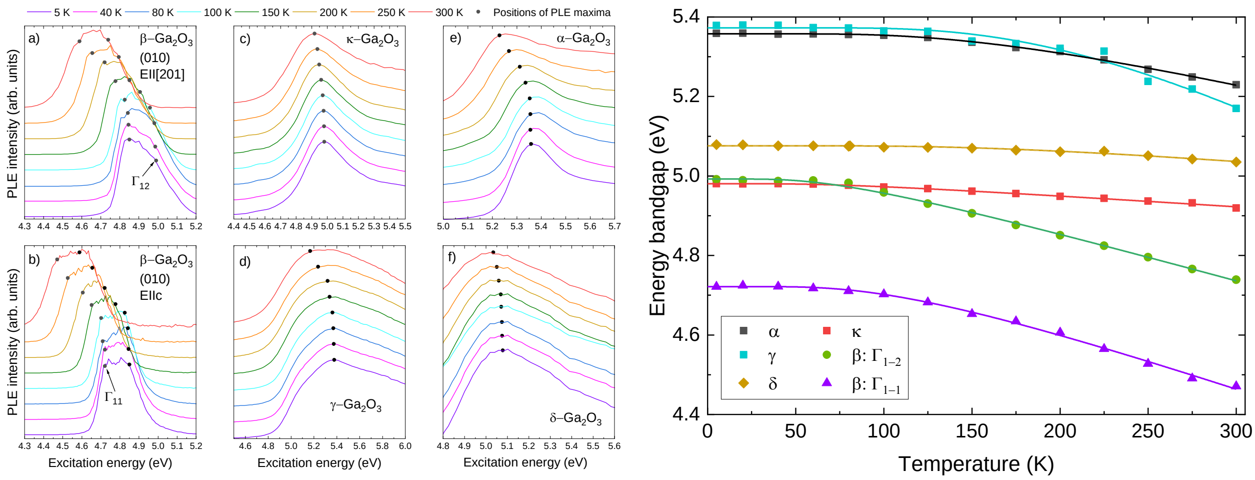

Fig. 2: (left) Temperature-resolved photoluminescence excitation spectra of Ga_2O_3 polymorphs illustrated in the temperature range between 5 K and 300 K. Spectra are normalized for each temperature step and vertically offset for better comparison. (right) Bandgap energies as a function of temperature shown for different Ga_2O_3 polymorphs.

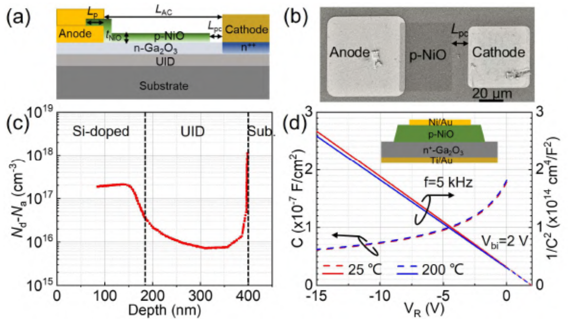

Fig. 1. (a) Schematic diagram and (b) top-view SEM image of the RESURF Ga_2O_3 SBD. (c) The N_d-N_a depth profile of the Ga_2O_3 epi layers. (d) C-V and $1/C^2$-V characteristics of the vertical NiO/Ga_2O_3 diode at 25°C and 200°C.

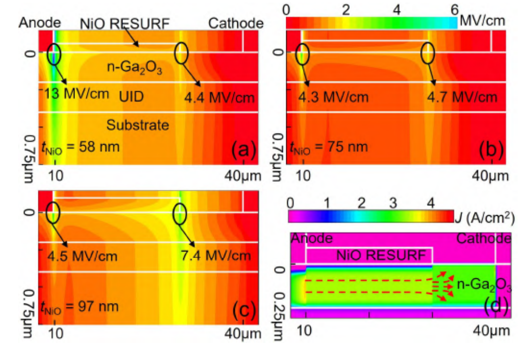

Fig. 2. Simulated E-field contour of Ga_2O_3 RESURF SBDs with t_{NiO} of (a) 58nm, (b) 75nm, and (c) 97nm, at V_R=4kV. (d) Simulated current density contour of the 75-nm-RESURF SBD at 2V.

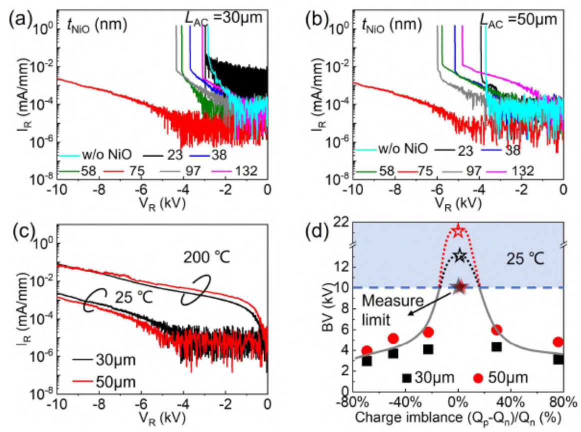

Fig. 3. Reverse I-V characteristics of the SBDs and RESURF SBDs with L_{AC} of (a) 30 and (b)50µm, both with various t_{NiO}. (c) Reverse I-V characteristics of the 75-nm-RESURF SBDs with two L_{AC} at 25°C and 200°C. (d) *BV* as a function of the charge imbalance percentage. The hollow symbols show the projected *BV* of the 75-nm-RESURF SBDs.

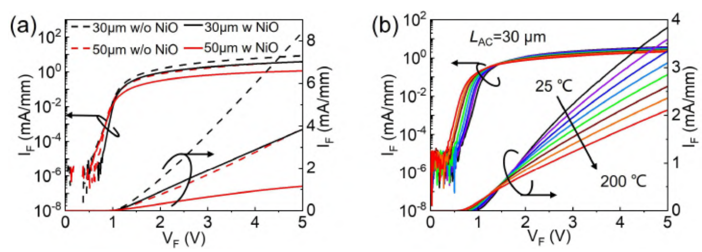

Fig. 4. (a) Forward I-V characteristics of the SBDs and RESURF SBDs, both with L_{AC}=30 and 50 µm. (b) Forward I-V characteristics of the RESURF SBD with L_{AC}=30µm at temperatures of 25°C to 200°C at a step of 25°C.

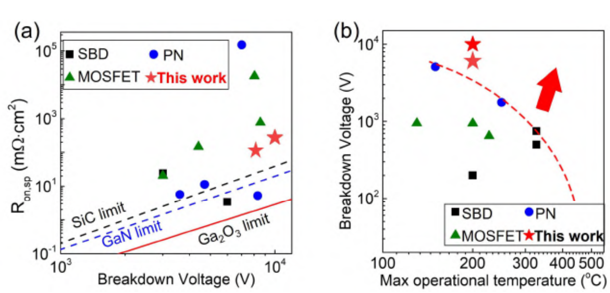

Fig. 5. (a) Benchmark of the differential $R_{on,sp}$ *vs.* *BV* for our device and the reported Ga_2O_3 devices with *BV* >3kV. (b) The *BV* *vs.* max operational temperature benchmark for our device and the reported high-temperature Ga_2O_3 devices with *BV* >100V.

Advances in the MOCVD Growth of β-Ga_2O_3 and Related Heterostructures

Andrei Osinsky and Fikadu Alema

Agnitron Technology, Inc, Chanhassen, MN 55317, U.S.A

β-Ga_2O_3 has attracted extensive interest in power electronic applications owing to its large bandgap of ~ 4.9 eV, estimated high breakdown field of ~ 8 MV/cm, and availability of melt grown high quality β-Ga_2O_3 substrates. The growth of high-quality epitaxial films with low dislocation density and background impurity is critical to realize the projected device performances. Available epitaxial methods to grow β-Ga_2O_3 thin films include MBE, HVPE, and MOCVD. But, despite coming late to the field, the MOCVD method has proven to be suitable for producing high-quality epitaxial β-Ga_2O_3 films at a fast growth rate with uniform and controllable doping [1]. The highest purity β-Ga_2O_3 films have been reported from MOCVD with record low-temperature electron mobility exceeding 23,000 cm^2/Vs and low~10^{13} cm^{-3} compensating acceptors [2]. Also, a recent record-breaking result for lateral Ga_2O_3 MESFETs with a lateral figure of merit (LFOM) of 355 MW/cm^2 and a breakdown voltage of ~2.5 kV [3], and a record low specific contact resistance ~10^{-7} Ωcm^2 [4] were reported based on MOCVD grown epitaxial Ga_2O_3 films.

This presentation will discuss recent progress in the growth of high-quality β-Ga_2O_3 thin films and related materials using MOCVD. The use of Ga precursors, including triethylgallium (TEGa) and trimethylgallium (TMGa), for the growth of Ga_2O_3 will be presented. Their advantages and disadvantages in realizing high-purity, carbon-free, epitaxial Ga_2O_3 films will be discussed. Critical process conditions and MOCVD reactor geometries on achieving high purity β-Ga_2O_3 films with high electron mobility and low background carrier concentration, including doping control in this range, will be discussed. This paper will also discuss the MOCVD growth of high Al composition (up to 30%) high quality strained β-$(AlGa)_2O_3$/Ga_2O_3 heterostructures and superlattices on various orientations of β-Ga_2O_3 substrates. The MOCVD growth of heavily doped (>10^{20} 1/cm^3), highly conductive β-Ga_2O_3, and strained β-$(Al_xGa_{1-x})_2O_3$/β-Ga_2O_3 heterostructures will be presented. We will also present the demonstration of record low resistance Ohmic contacts on heavily Si doped epitaxial β-Ga_2O_3 and strained β-$(Al_xGa_{1-x})_2O_3$ epilayers with varying Al composition. A recent in-situ non-destructive etching of Ga_2O_3 in MOCVD followed by a regrowth process will also be discussed.

[1] F. Alema *et al.*, Journal of Crystal Growth 475 (2017) 77-82.

[2] G. Seryogin *et al.,* Applied Physics Letters 117 (2020) 262101.

[3] A. Bhattacharyya *et al.*, IEEE Electron Device Letters 42 (2021) 1272-1275.

[4] F. Alema *et al.,* EEE Electron Device Letters 43 (2022) 1649-1652.

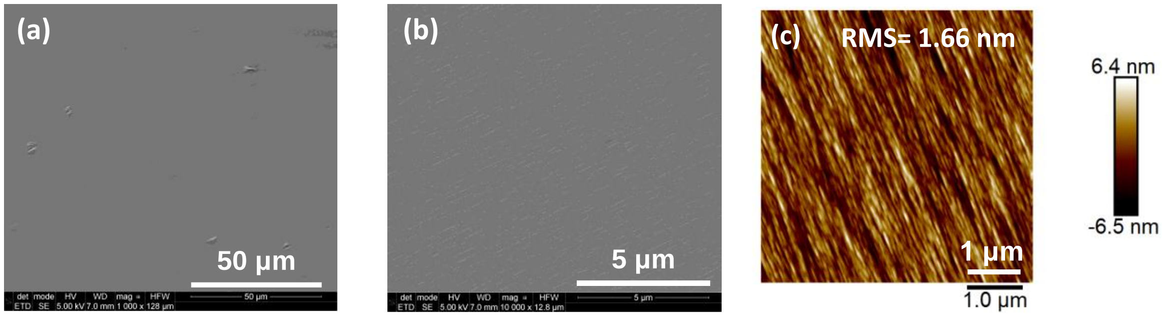

Figure 1. Top view FESEM images of MOCVD grown (010) β-Ga_2O_3 thin film with growth rate of 3 µm/hr and room temperature mobility of 190 cm^2/Vs: (a) large field of view; and (b) high magnification. (c) The corresponding AFM image of the same β-Ga_2O_3 sample (RMS: 1.66 nm).

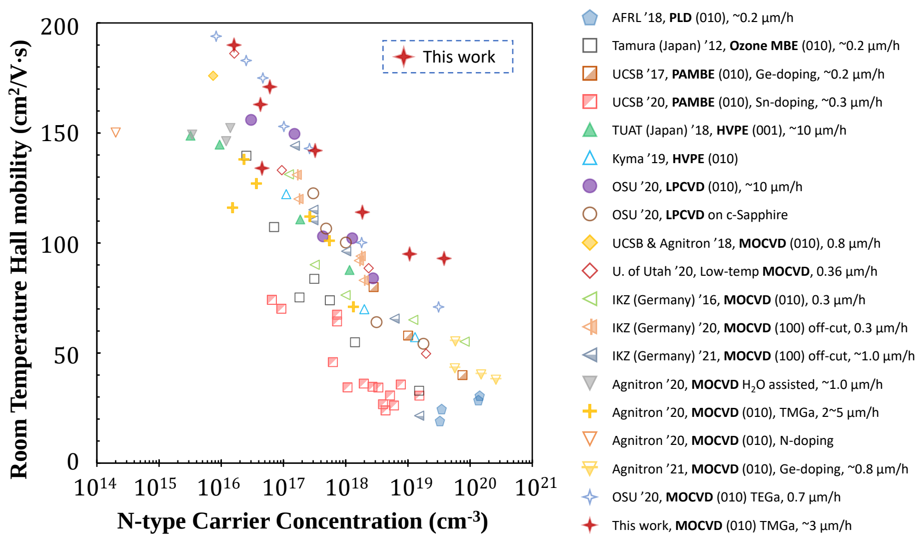

Figure 2. Room temperature electron mobility data of (010) β-Ga_2O_3 homoepitaxial thin films from this work (GR: 3µm/h) as compared to representative data from literature: room temperature electron mobility vs. electron concentration of β-Ga_2O_3 films grown by different growth techniques. The corresponding growth rates are listed.

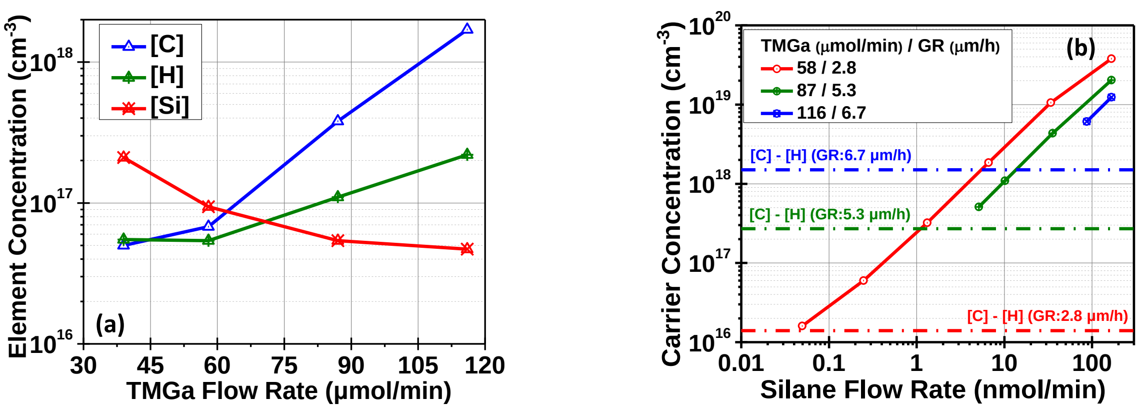

Figure 3. (a) The extracted C, H and Si incorporation concentrations as a function of the TMGa molar flow rate from quantitative SIMS measurements. (b) Measured free electron carrier concentration as a function of the silane molar flow rate for three different sets of samples varying the TMGa molar flow rate/growth rate. The dash-dotted lines indicate the net compensation levels ([C]-[H]) for the three sets of samples grown at different growth rate of MOCVD Ga_2O_3.

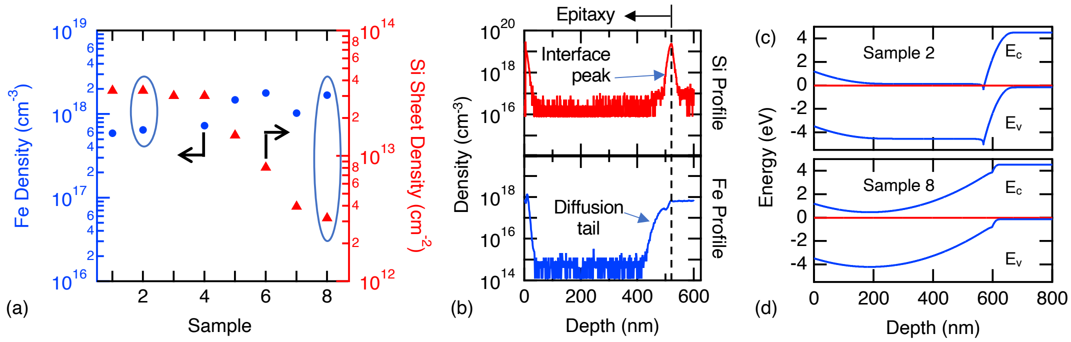

Fig. 1 (a) The average Fe density within the substrate for 8 different samples is shown (blue circles) and the sheet density of the interfacial Si peak is plotted (red triangles) for 8 different samples. The circled samples (sample 2 and 8) are studied further in the following panels. (b) The Si and Fe SIMS profiles are shown for sample 2. (c) and (d) Show the simulated band diagram. Sample 2 is shown in (c) and sample 8 is shown in (d). The Si and Fe densities are such that in sample 2, the conduction band is pulled below the E_f, (c), while in sample 8 the conduction band remains above the E_f.

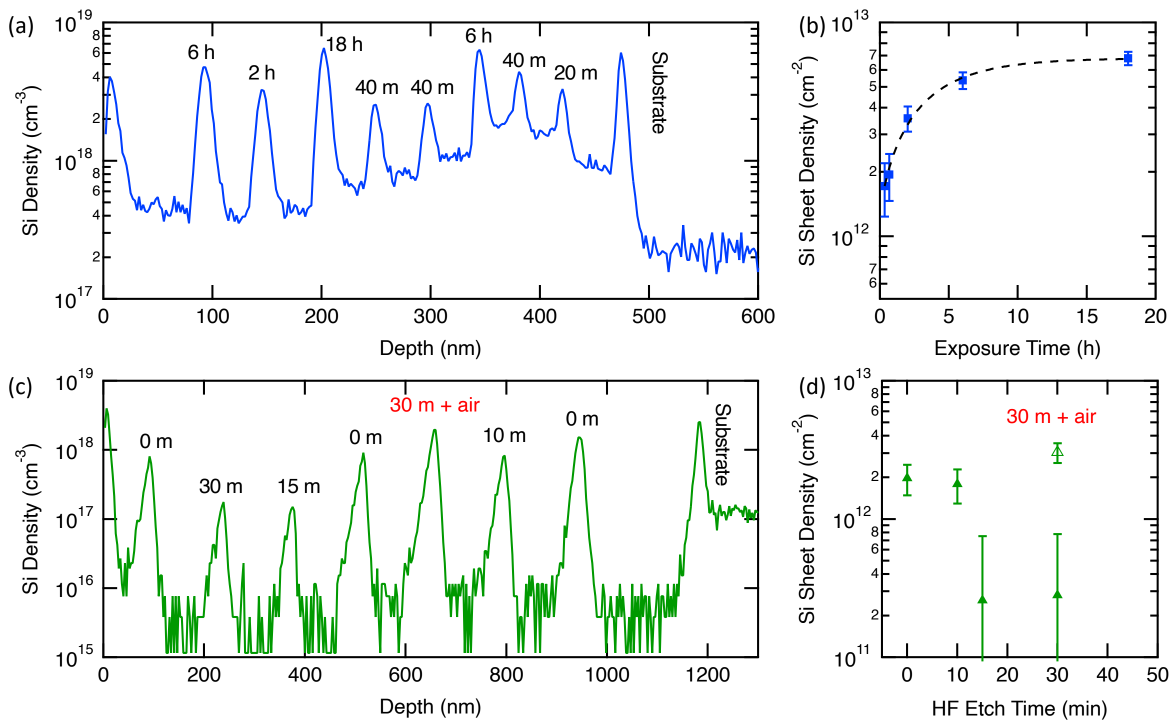

Fig. 2 (a) An unintentionally doped (UID) sample was grown by molecular beam epitaxy. The sample was removed and exposed to air for a predetermined amounts of time to allow Si to accumulate, and then the sample was returned to the growth chamber where another UID layer was grown to protect the previously exposed surface. This was repeated 8 times. The exposure time is listed above the peak and ranged from 20 minutes to 18 hours. (b) The Si peaks in (a) were integrated to determine a sheet density which is plotted as a function of the exposure time. After ~8 hours the Si sheet density begins to saturate to a value of ~7×10^{12}/cm^2. (c) and (d) show our efforts to remove the Si. UID layers were again grown, this time by metalorganic vapor-phase epitaxy. All layers within the stack were exposed to air for 2-hours (based on the results in panel (a)). Then the sample was etched in HF (49%). The etch time was varied from 10 minutes to 30 minutes, along with 3 control layers where no etching was performed. (d) shows the sheet density obtained by integrating the peaks shown in (c). After a 15-minute HF etch, the sheet density is reduced by ~ 1 order. Lastly, to understand how quicky Si re-accumulated on the surface, a 30-minute HF etch was performed after the initial 2-hour air exposure. After the HF etch, the sample was left in air for 10 minutes (open triangle with label). After 10-minutes, the Si has fully returned, indicating that the sample must be quickly moved to the growth chamber. Note, there is an additional 1.5 to 2 minutes for each step, as the sample is transferred to the growth chamber and pumped down.

Direct Approach to Diffusivity via Master Diffusion Equations

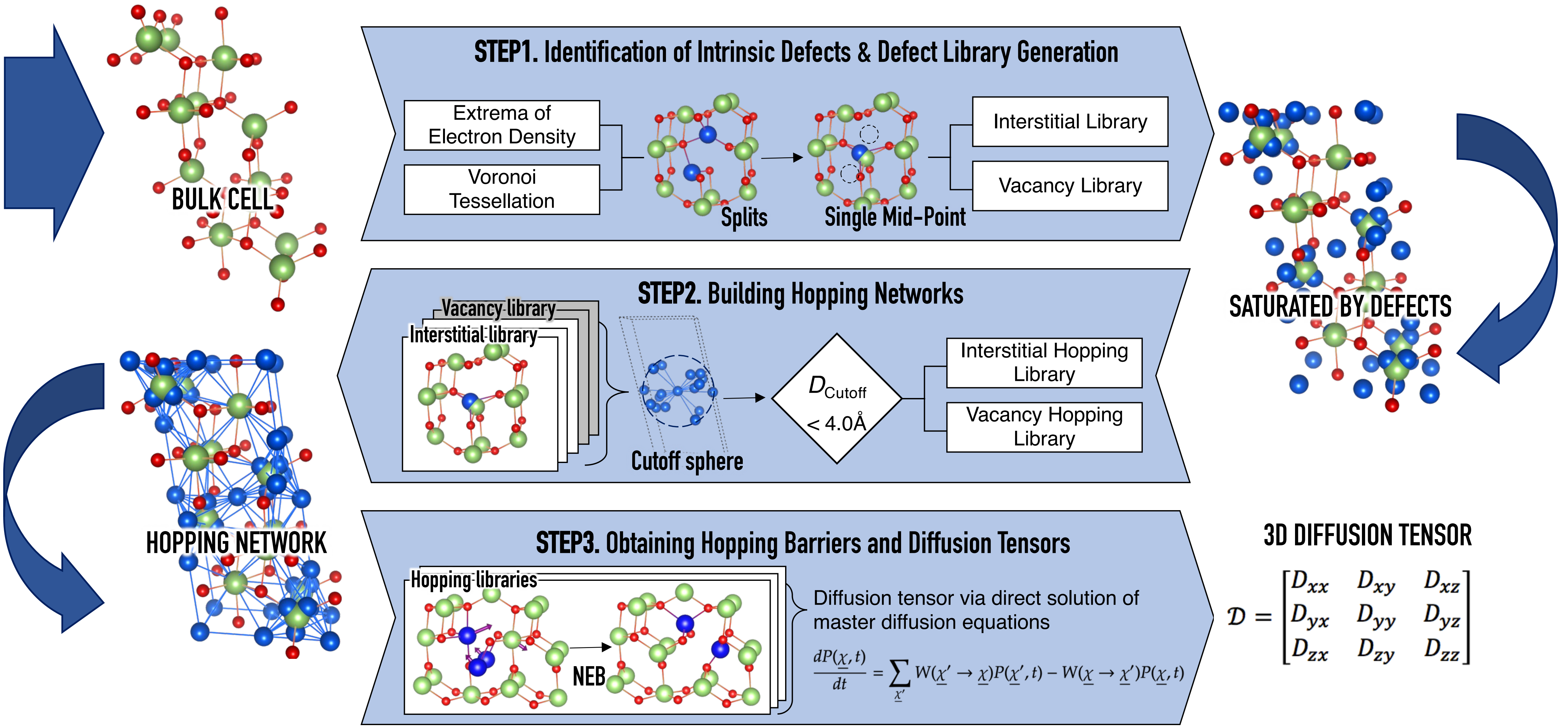

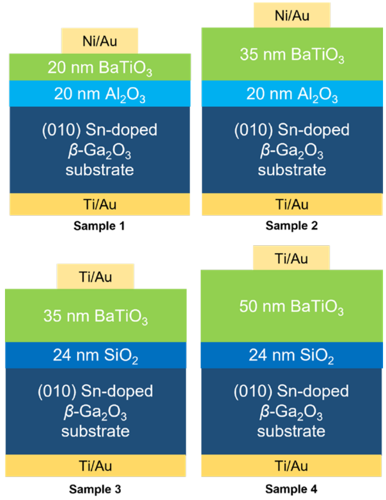

Fig. 1: Schematics of MOSCAPs studied in this work

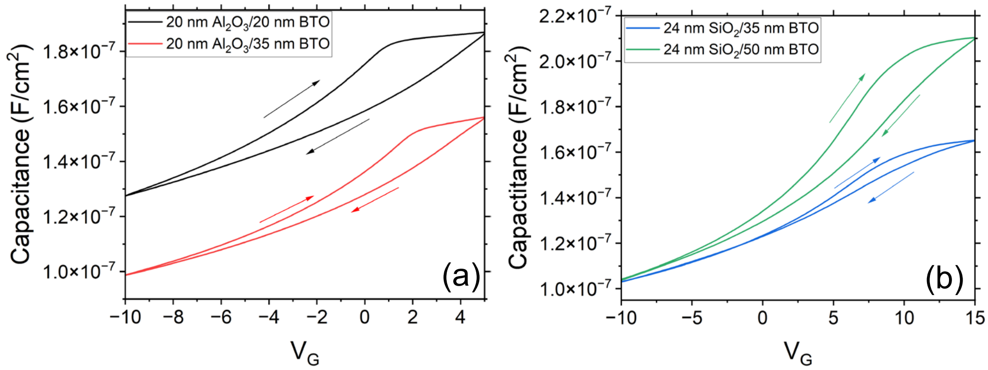

Fig. 2: Dual-sweep C-V characteristics at 1 MHz of (a) MOSCAPs with Al_2O_3 low-k layers and (b) MOSCAPs with SiO_2 low-k layer

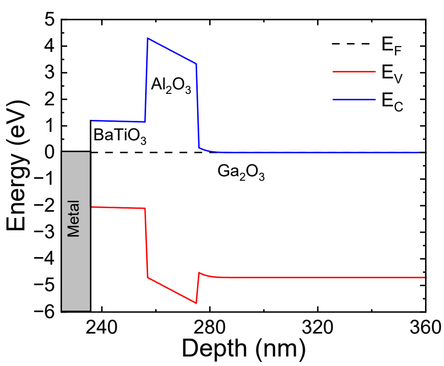

Fig. 3: Equilibrium energy band diagram of the sample with 20 nm $BaTiO_3$ and 20 nm Al_2O_3

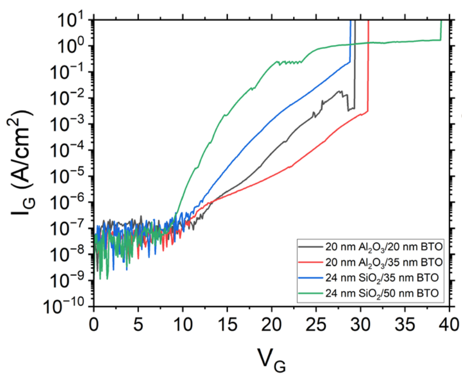

Fig. 4: Forward leakage characteristics of the four MOSCAPs

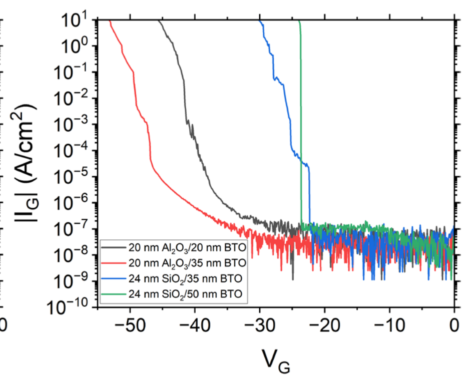

Fig. 5: Reverse leakage characteristics of the four MOSCAPs

Hybrid insulator Stack	Flat-band voltage	Net donor density from C-V	Insulator breakdown field under forward bias	Semiconductor breakdown field under reverse bias
20 nm Al_2O_3/20 nm $BaTiO_3$	0.8 V	4.4×10^{18} cm^{-3}	5.7 MV/cm	<u>6.8 MV/cm</u>
20 nm Al_2O_3/35 nm $BaTiO_3$	2 V	2.4×10^{18} cm^{-3}	4.7 MV/cm	5.9 MV/cm
24 nm SiO_2/35 nm $BaTiO_3$	7.9 V	5.5×10^{18} cm^{-3}	2.0 MV/cm	3.6 MV/cm
24 nm SiO_2/50 nm $BaTiO_3$	7.8 V	5.3×10^{18} cm^{-3}	0.9 MV/cm	3.5 MV/cm

Table 1: Summary of flat-band voltage, extracted doping density, forward breakdown field in oxide, and reverse breakdown field supported in Ga_2O_3 for all four samples

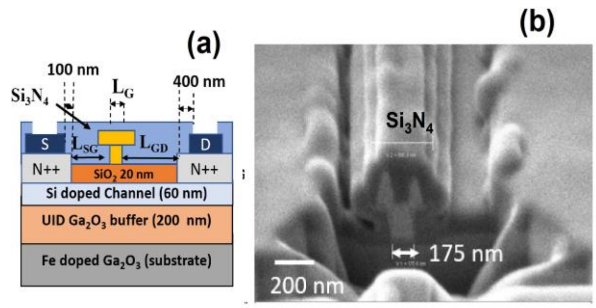

Figure 1(a): Cross section schematic of our fabricated device, (b) FIB cross-section SEM image of a passivated device

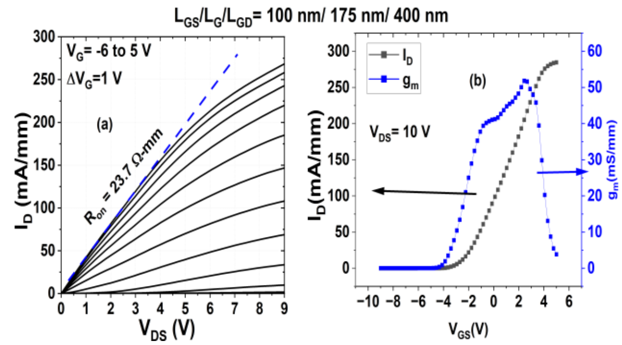

Figure 2 (a) Output and (b) transfer curve of a test device

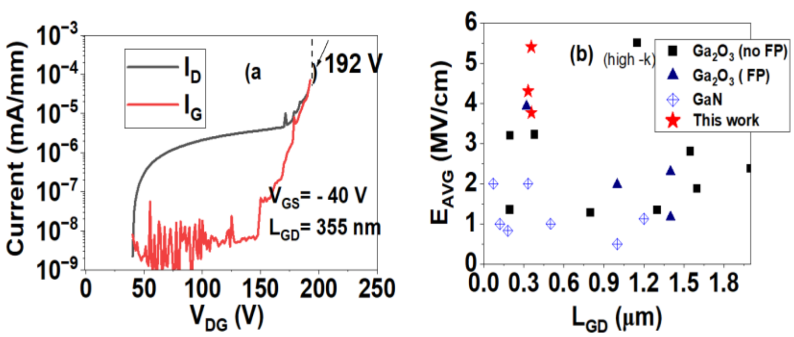

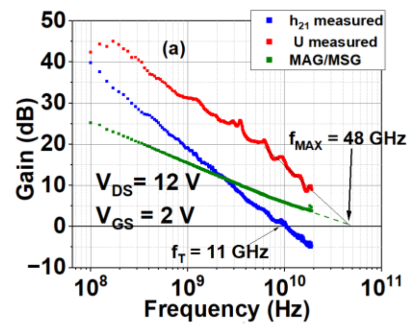

Figure 3 (a) 192 V breakdown voltage recorded for L_{GD}= 355 nm (b) Eavg vs Lgd benchmarking with other Gallium oxide and GaN HEMT devices

Figure 4: small signal analysis showing 48 GHz fmax

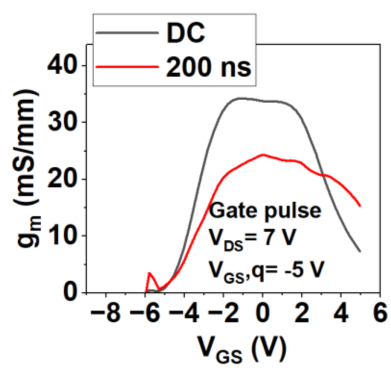

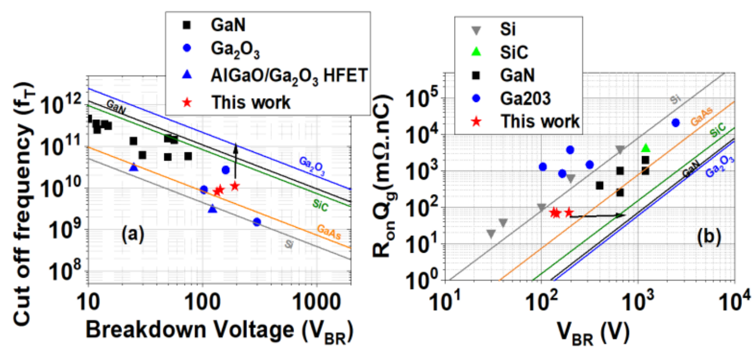

Figure 5: gm measured at 200 ns Showing current collapse for Gate pulse

Figure 6 (a) ft vs Vbr benchmarking of our device, (b) Huang's material figure of merit benchmarking (Ron Qg vs Vbr

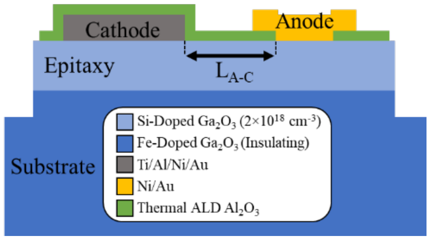

Fig. 1: Graphic depicting the cross-section of one Anode-Cathode pair

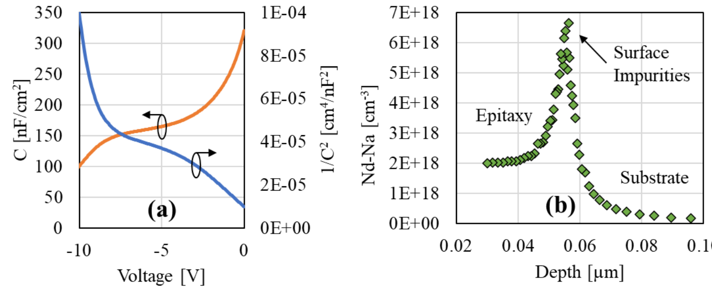

Fig. 2: (a) C-V test structure response and (b) extracted carrier concentration with respect to depth

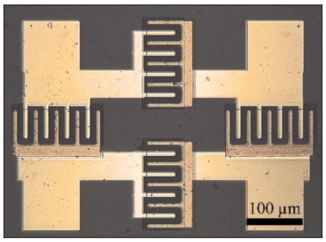

Fig. 3: Rectifier IC microscope image

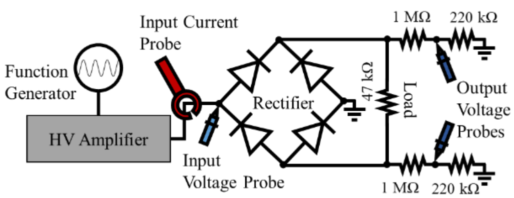

Fig 4: Rectifier IC test setup

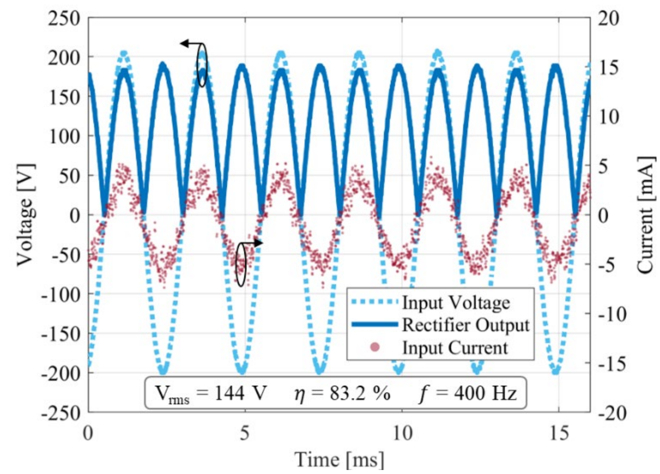

Fig 5: Rectifier IC input and output waveforms

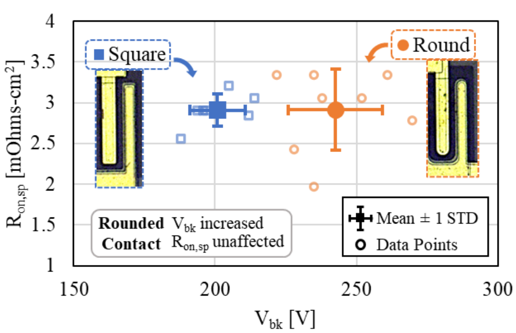

Fig 6: Analysis comparing the effect of contact geometries on $R_{on,sp}$ and V_{bk}

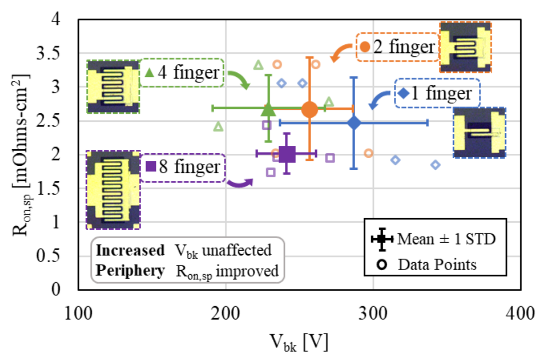

Fig 7: Analysis comparing the effect of additional anode-cathode pairs on $R_{on,sp}$ and V_{bk}

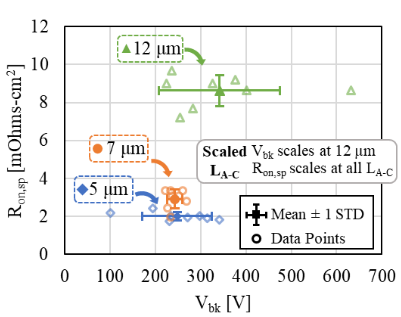

Fig 8: Analysis comparing the effect of L_{A-C} on $R_{on,sp}$ and V_{bk}

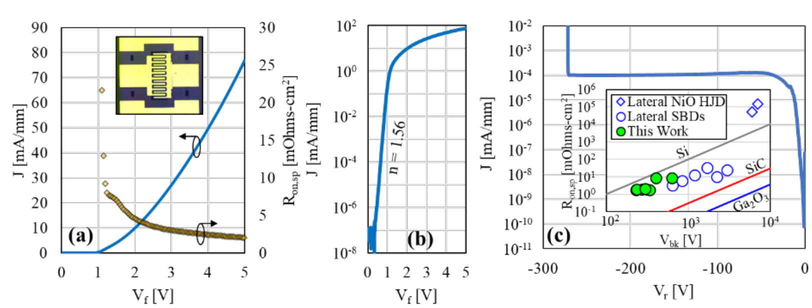

Fig 9: Forward (a-b) and reverse (c) J-V response of a select diode, with a comparison to published results inset to (c)

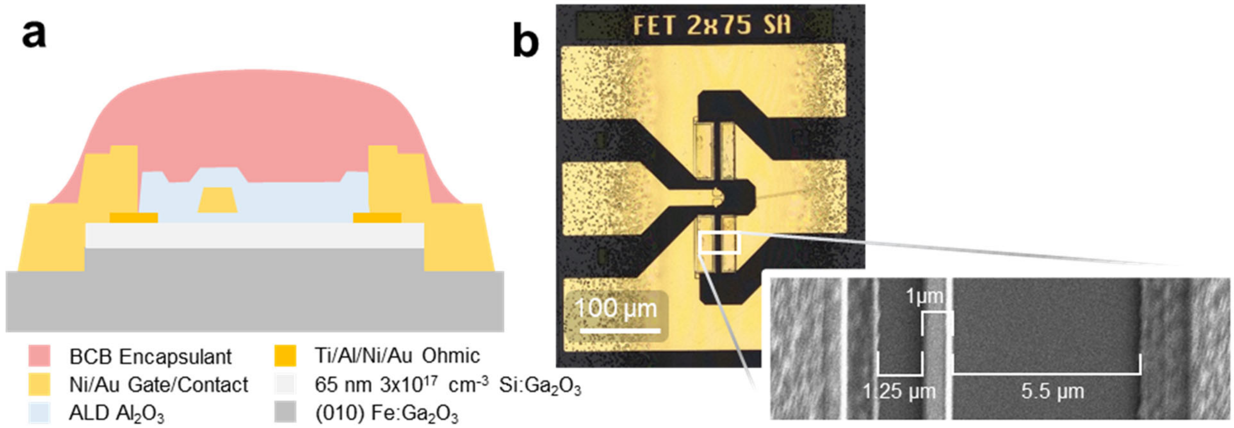

Figure 1 a) Schematic drawing of the MOSFET devices under test, showing the as-fabricated device as well as the encapsulant. b) Optical microscope image of a device after aerosol jet spray printing of the BCB encapsulant. Inset: scanning electron micrograph of the device active channel, including dimensions.

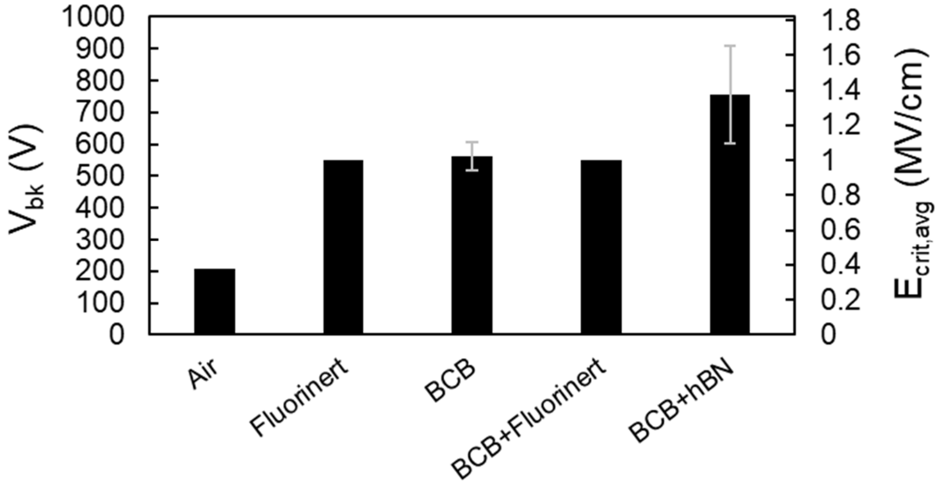

Figure 2 Breakdown voltage V_{bk} and associated average electric field $E_{crit,avg}$ for devices without encapsulation tested in air and Fluorinert, respectively; devices with BCB encapsulation tested in air and Fluorinert, respectively; and device tested with hBN-loaded BCB encapsulant.

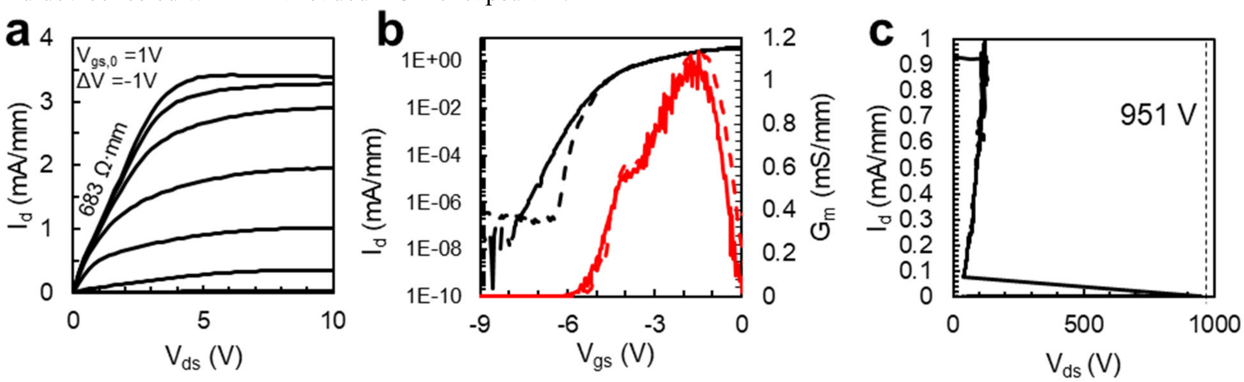

Figure 3 a) I_d-V_{ds} performance for a MOSFET prior to encapsulation; b) transfer curve I_d-V_{gs} and transconductance G_m for the same device before (dotted line) and after (solid) hBN-BCB encapsulation; c) breakdown voltage V_{bk} of the same device.

[1] Green et al., *APL Materials* 2022, doi:10.1063/5.0060327

[2] Dryden et al., *IEEE Electron Device Lett.* 2022, doi: 10.1109/LED.2022.3182575

[3] Sharma et al., *IEEE Electron Device Lett.* 2022, doi: 10.1109/LED/2022/3218749

[4] Burdeaux et al., *J. Electron. Mat.* 1990, doi: 1.1007/BF02662825

[5] Yao et al., *IEEE Trans. Compon., Packag. Manufact. Technol.* 2015, doi: 10.1109/TCPMT.2014.2337300

[6] Li and Cheng, *IEEE Electrical Insulation Magazine* 2020, DOI:10.1109/MEI.2020.9070113

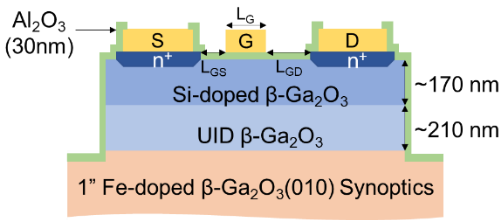

Fig.1: β-Ga_2O_3 MOSFET device schematic

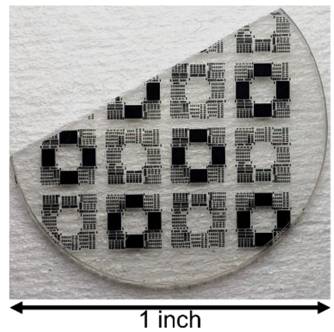

Fig. 2: MOSFETs on 1in. Synoptics (010) β- Ga_2O_3 wafer

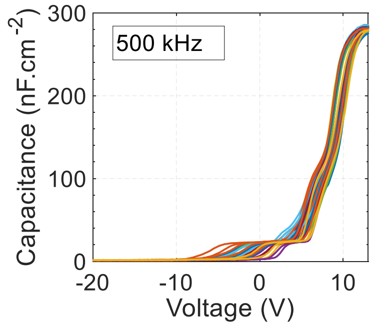

Fig. 3: Wafer-scale MOSCAP CV characterization

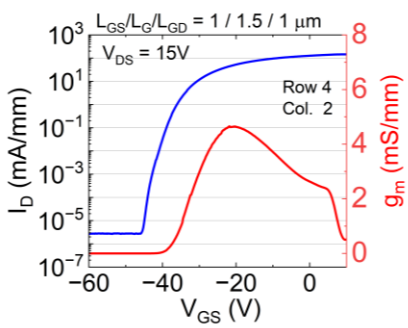

Fig. 4: Transfer Characteristics

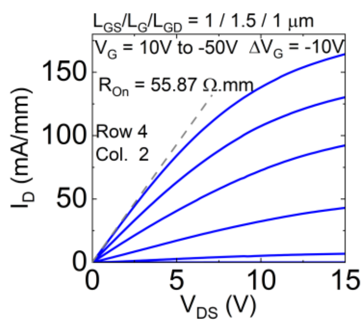

Fig. 5: Output Characteristics

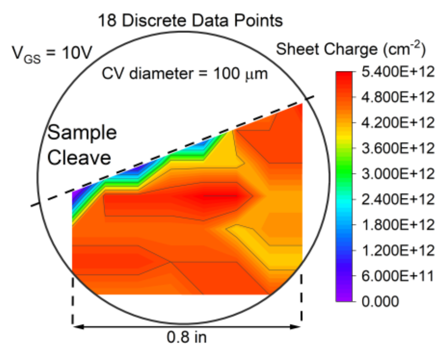

Fig. 6: Sheet charge map across the wafer at +10V V_{GS} from CV measurements

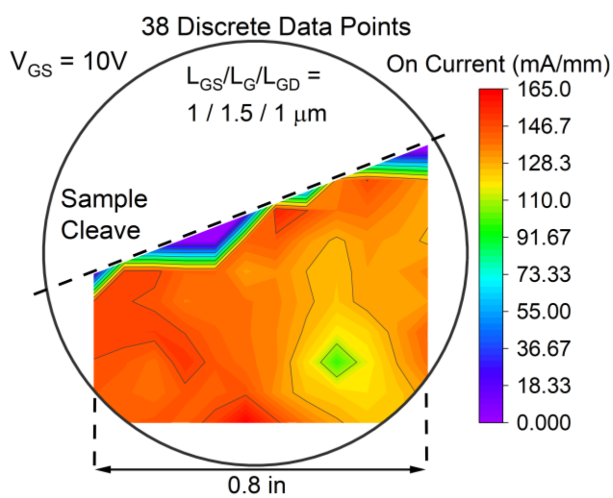

Fig. 7: On-current (I_D) map across the wafer at V_{GS} = +10 V, V_{DS} = 15 V showing uniform current levels across the wafer

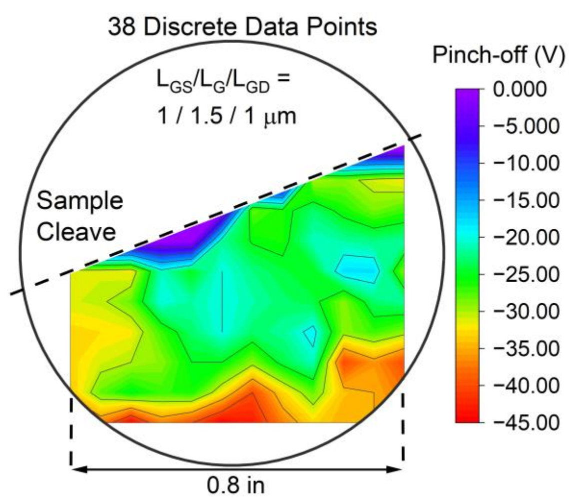

Fig. 8: Pinch-off Voltage Map (extracted from transfer curves) across the wafer

Reference

[1]. M.H. Wong; et al., Japanese Journal of Applied Physics 55, no. 12: 1202B (2016)
[2]. S Rafique; et al., Applied Physics Letters 112, no. 5: 052104 (2018).
[3]. T. J. Asel; et al.; J. Vac. Sci. Technol., A 38, 043403 (2020).
[4]. K. Tetzner, et al.; Microelectronics Reliability 114, 113951 (2020)
[5]. S. Kumar; et al.; Applied Physics Letters 117(19): 193502. (2020)
[6]. H. Doğan, et al; Physica B: Condensed Matter 457, 48 (2015).
[7]. A. Turut, er al; Materials Science in Semiconductor Processing 39, 400 (2015).
[8]. M. Yun, et al, Appl. Phys. Lett. 89 [1], 013506 (2006).

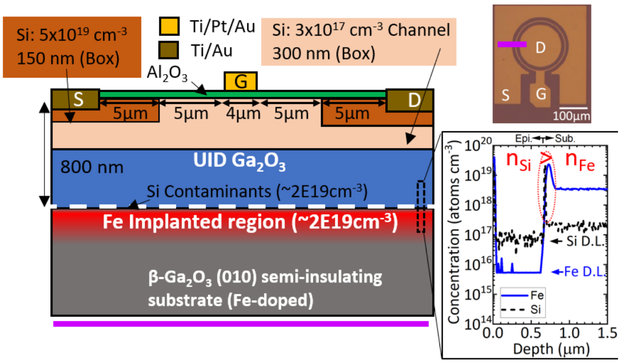

Fig. 1. Device schematic. The SIMS profile shows the concentration of Si and Fe in the dash box vertically.

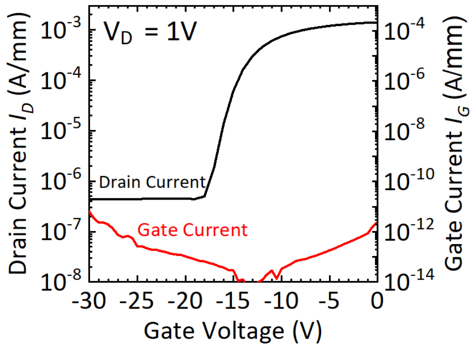

Fig. 2. The transfer characteristics at V_D =1V.

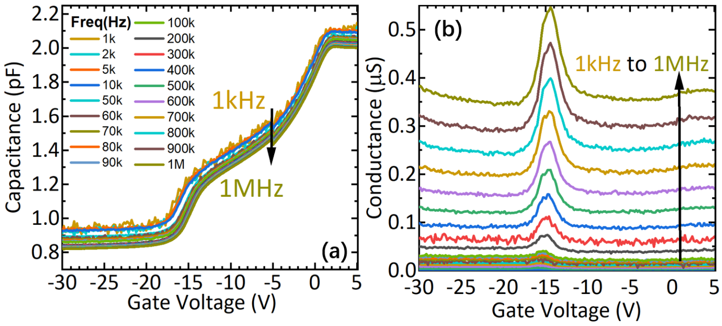

Fig. 3. (a) Gate-to-source capacitance and (b) corresponding equivalent conductance of the test devices at various frequency (1k-1MHz). The discontinuity of the capacitance around -5V is an artifact of the equipment.

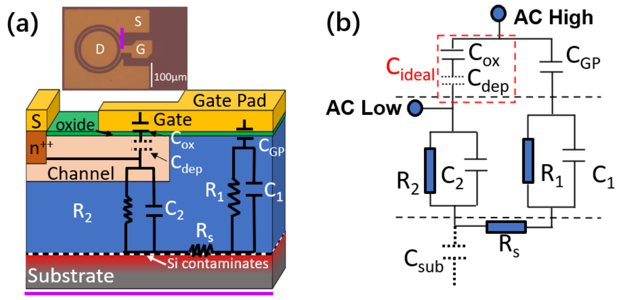

Fig. 4. (a) Schematic of coupling model when measuring gate-source impedance. (b) corresponding equivalent circuit.

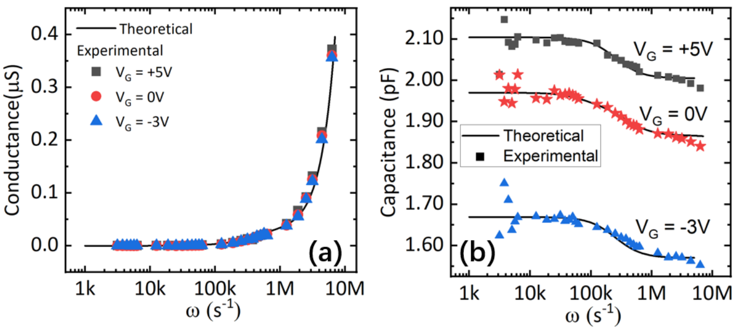

Fig. 5. (a) and (b) demonstrate the comparison of experimental results at V_G = +5V, 0V, and -3V and fit of models. The fitting parameters are listed in Table I.

Table I. The values of the elements obtained from the fitting

V_G(V)	+5	0	-3
C_{ideal} (F)	2.0E-12	1.9E-12	1.6E-12

C_{GP} (F)	R_1 (Ω)	C_1 (F)	R_2(Ω)	C_2(F)	R_s(Ω)
8.6E-12	4.0E7	2.2E-12	7.0E4	1.1E-13	5.5E3

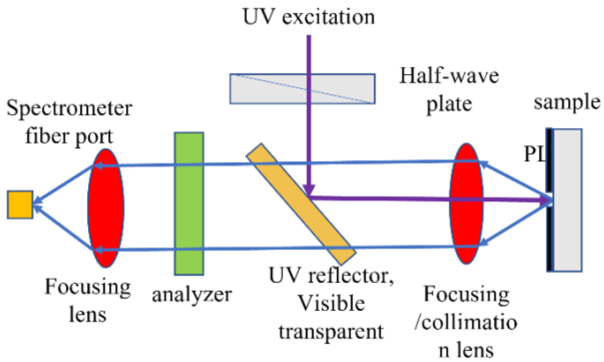

Fig. 1. Schematic of measurement of polarized PL.

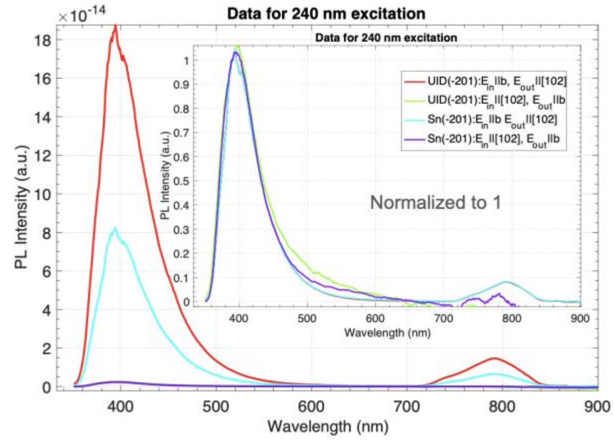

Fig. 2. Polarized PL of ($\bar{2}$01) bulk UID β-Ga_2O_3 and Sn-doped at β-Ga_2O_3 240 nm excitation wavelength. Insert is of the same data normalized. Excitation and emission polarizations chosen in the data come from the min and max PL intensities.

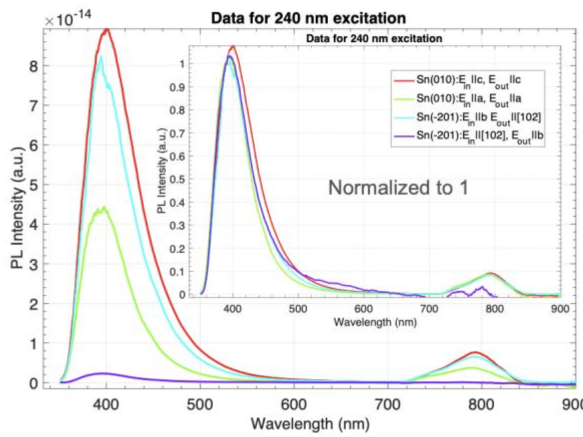

Fig. 3. Polarized PL of ($\bar{2}$01) bulk Sn-doped β-Ga_2O_3 and (010) Sn-doped β-Ga_2O_3 at 240 nm excitation wavelength. Insert is of the same data normalized. Excitation and emission polarizations chosen in the data come from the min and max PL intensities.

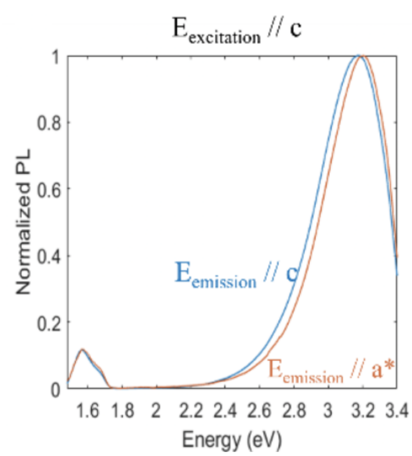

Fig. 4. Polarized PL of (010) bulk Sn-doped β-Ga_2O_3 at 240 nm excitation wavelength. The PL spectra for excitation polarization along c-axis.

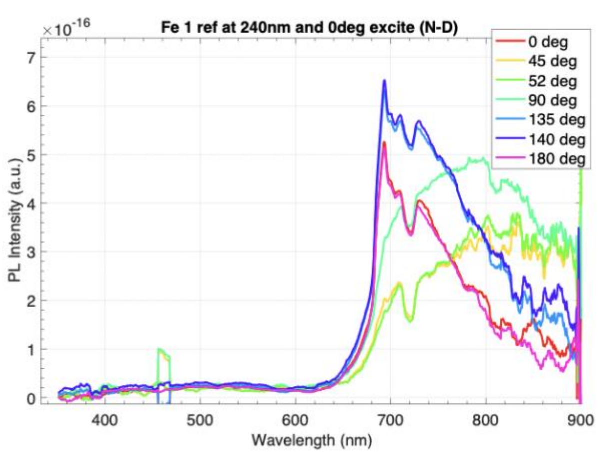

Fig. 5. Polarized PL of (010) bulk Fe-doped β-Ga_2O_3 at 240 nm excitation wavelength. Insert is of the same data normalized. We observe a different spectral shape as the emission is measured along different orientations.

Abstract Photo. SMI's tool development for oxide growth. These tools are delivered to several institutes including IKZ, Germany (the world leader in Ga_2O_3 growth), CMU, PSU, ANL, and Parma.

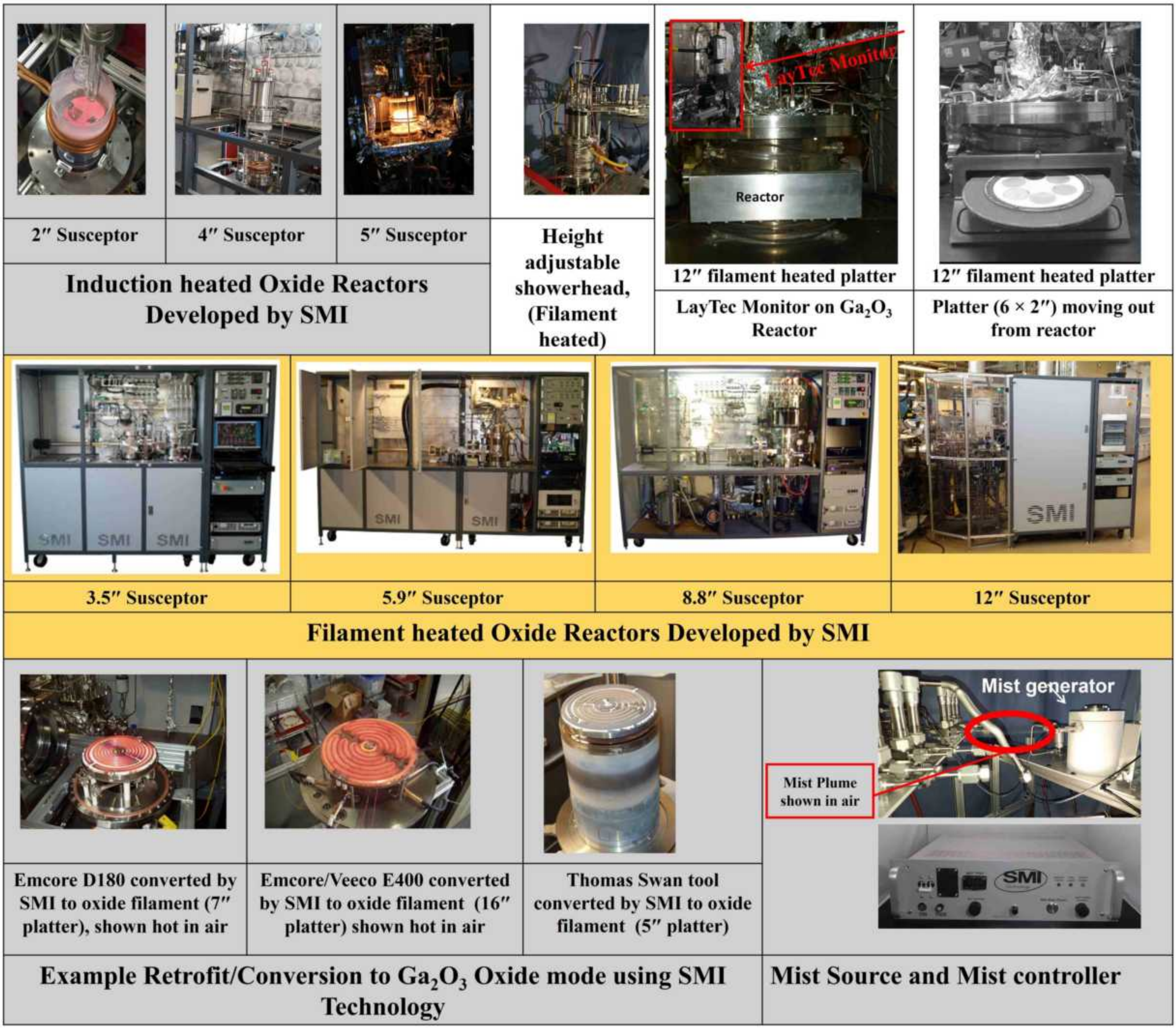

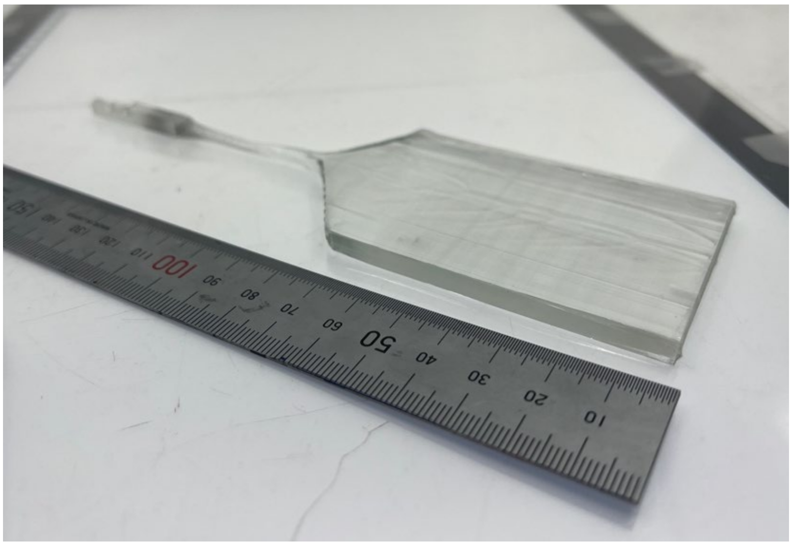

The typical bulk β-Ga_2O_3 single crystal ribbon grown by EFG method. The growth direction and the principal surface were set to be the [010] direction and the (001) plane for this β-Ga_2O_3 crystal, respectively. The ingot's body height and thickness are about 80mm and 4mm, respectively. The growth rate for this ingot is about 15mm/h.

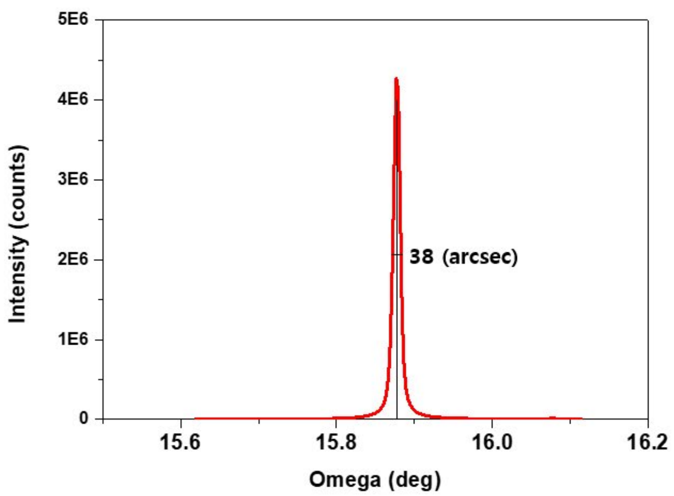

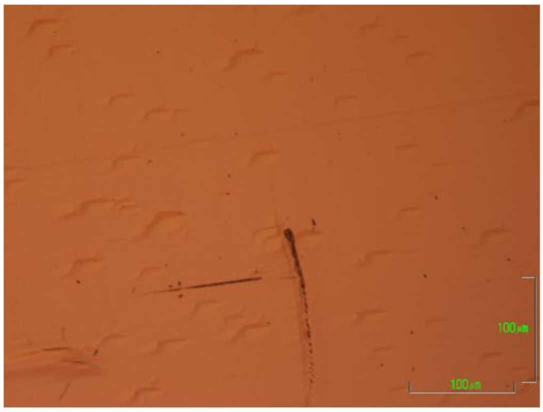

X-ray rocking curve and etched surface of the typical bulk β-Ga_2O_3 single crystal ribbon grown by EFG method.

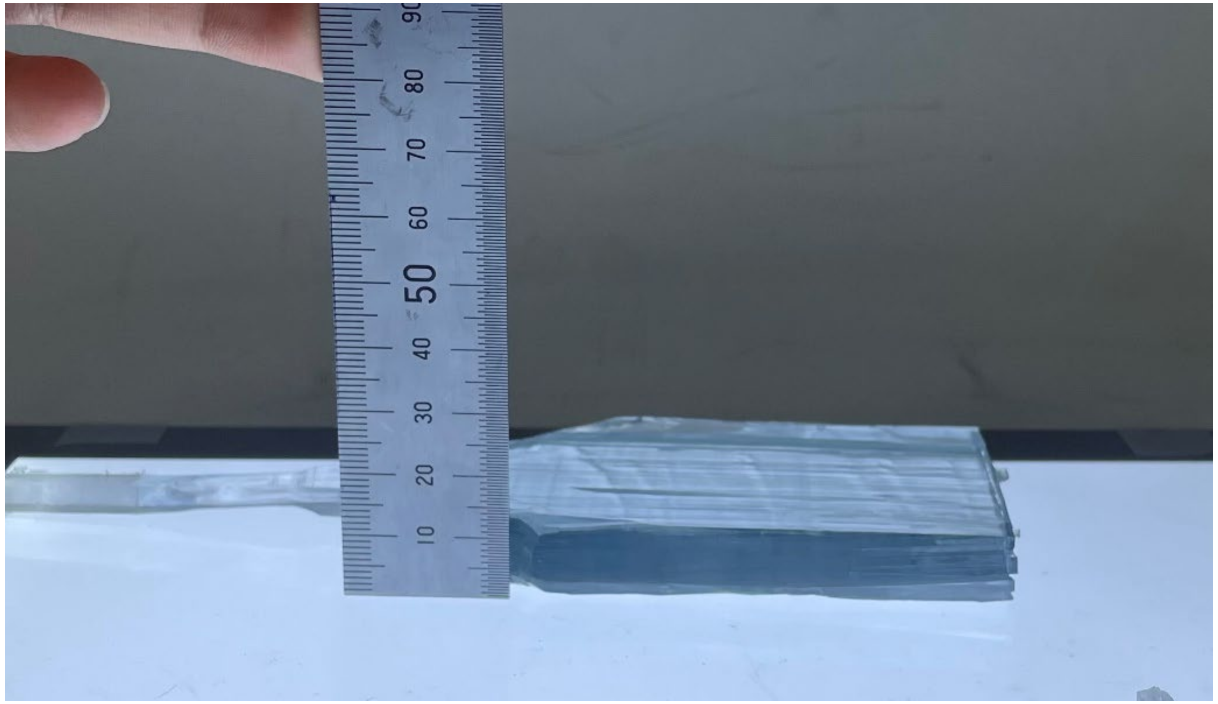

The typical bulk Ga_2O_3 single crystal ribbon grown by EFG method.
The growth direction and the principal surface were set to be the [010] direction and the (001) plane for this β-Ga_2O_3 crystal, respectively.
The ingot's body height and thickness are about 80mm and 10mm, respectively.
The growth rate for this ingot is about 12mm/h.

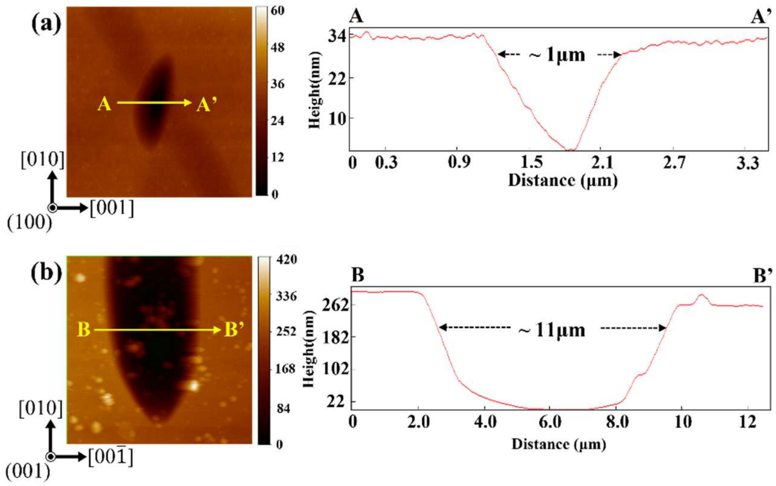

Figure 1. AFM images and cross-sectional height profile of etch pits observed on the (100) and (001) β-Ga_2O_3 surface. Etch pit on the (a) (100) plane with a width of ~1 μm and a depth of ~34 nm and (b) (001) plane with a width of ~10 μm and a depth of ~200 nm.

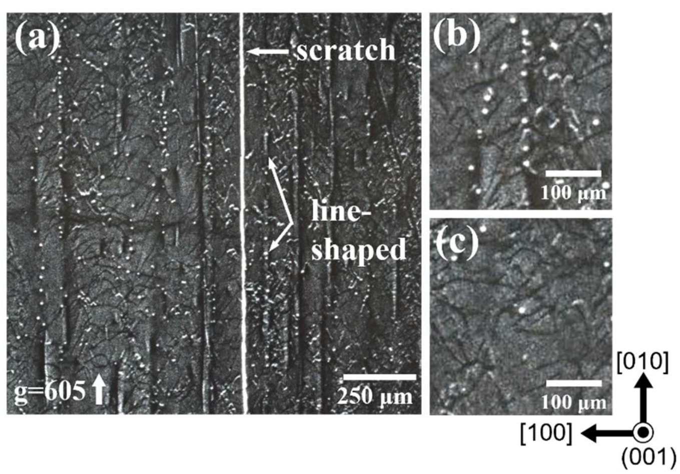

Figure 2. (a) X-ray topography image of (a) the (001)-oriented Ga_2O_3 crystal with ***g***=605, where defects related to (b) dots and (c) curved lines.

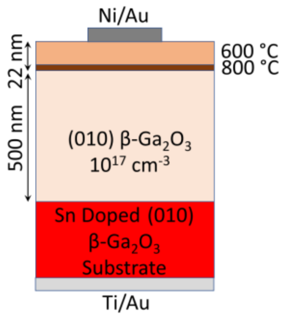

Fig. 1: Schematic Diagram of the hybrid dielectric

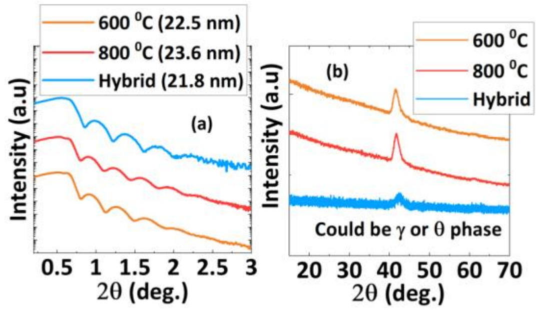

Fig. 2: (a) X-ray reflectivity (XRR) and (b) Grazing Incident X-ray diffraction (GIXRD) plot of the deposited dielectric films

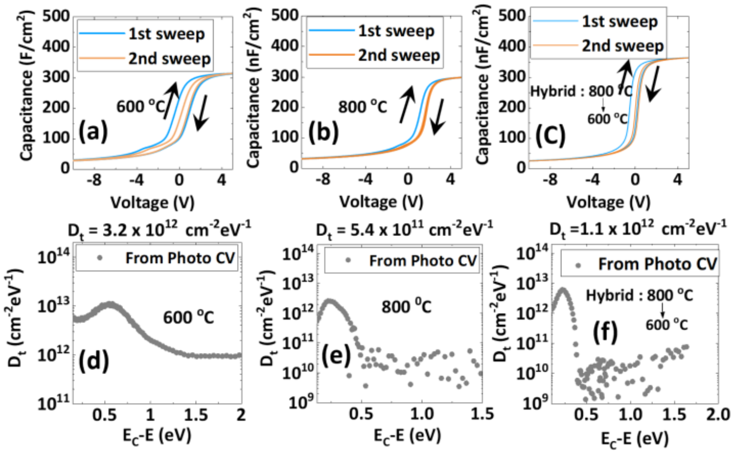

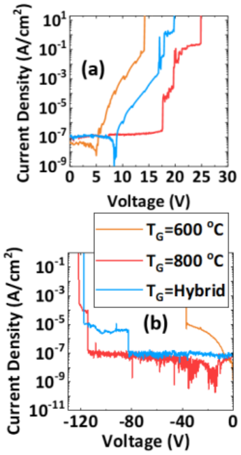

Fig. 3: CV Hysteresis and average trap density plot of (a)(d) 600 °C (b)(e) 800 °C & (c) (f) hybrid dielectric based MOS structure.

Fig. 4: IV characteristics of the three dielectrics in (a) forward and (b) reverse direction.

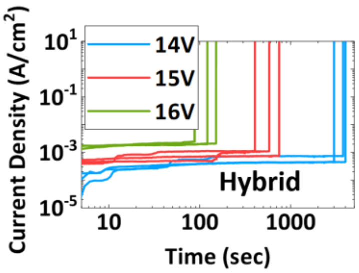

Fig. 5: Representative TDDB plot of the hybrid dielectric

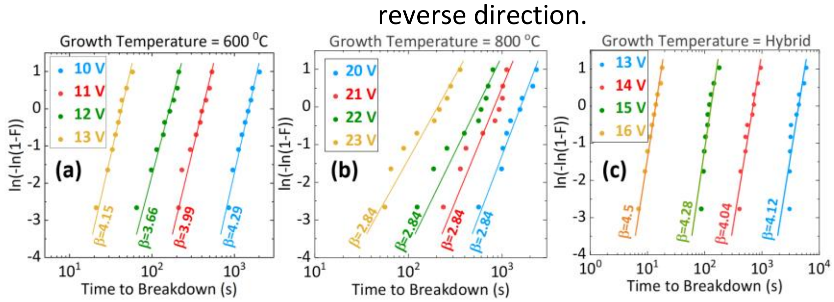

Fig. 6: TDDB Weibull distribution of the (a) 600 °C, (b) 800 °C & (c) Hybrid dielectric.

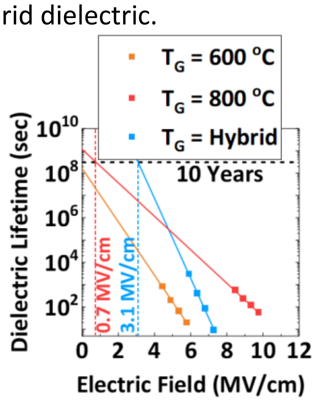

Fig. 7: Lifeime projection of the three dielectrics based on E-model

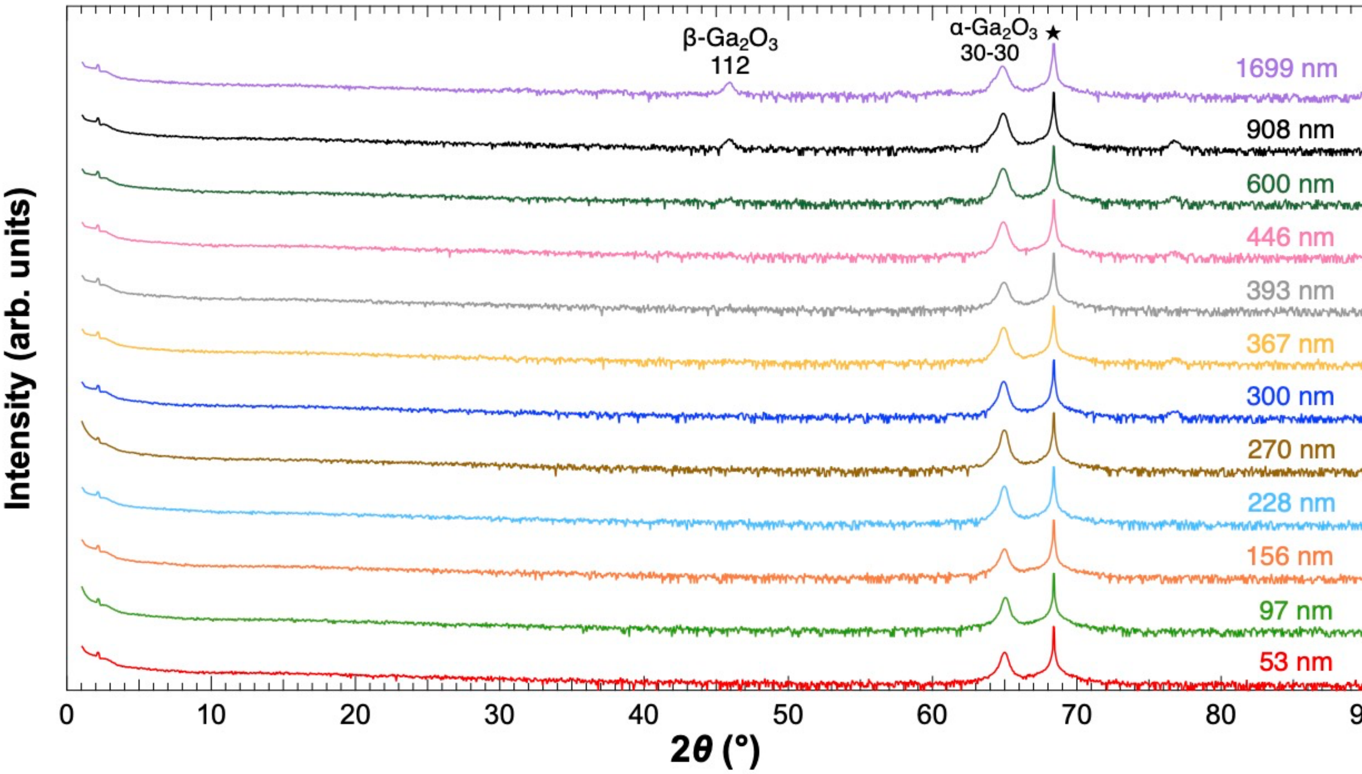

Figure 1: XRD θ-2θ scans for the α-Ga_2O_3 thin films with varying thicknesses grown on m-plane sapphire substrates using MOCVD. The heteroepitaxy of Ga_2O_3 films on m-plane sapphire substrates was performed at a reactor pressure of 15 Torr at a growth temperature of 600℃ (and 625℃ for the three Ga_2O_3 films with thicknesses of 270 nm, 446 nm, and 600 nm). We demonstrated that a single-phase α-Ga_2O_3 thin film with thickness 393 nm can be achieved on m-plane sapphire substrates via MOCVD.

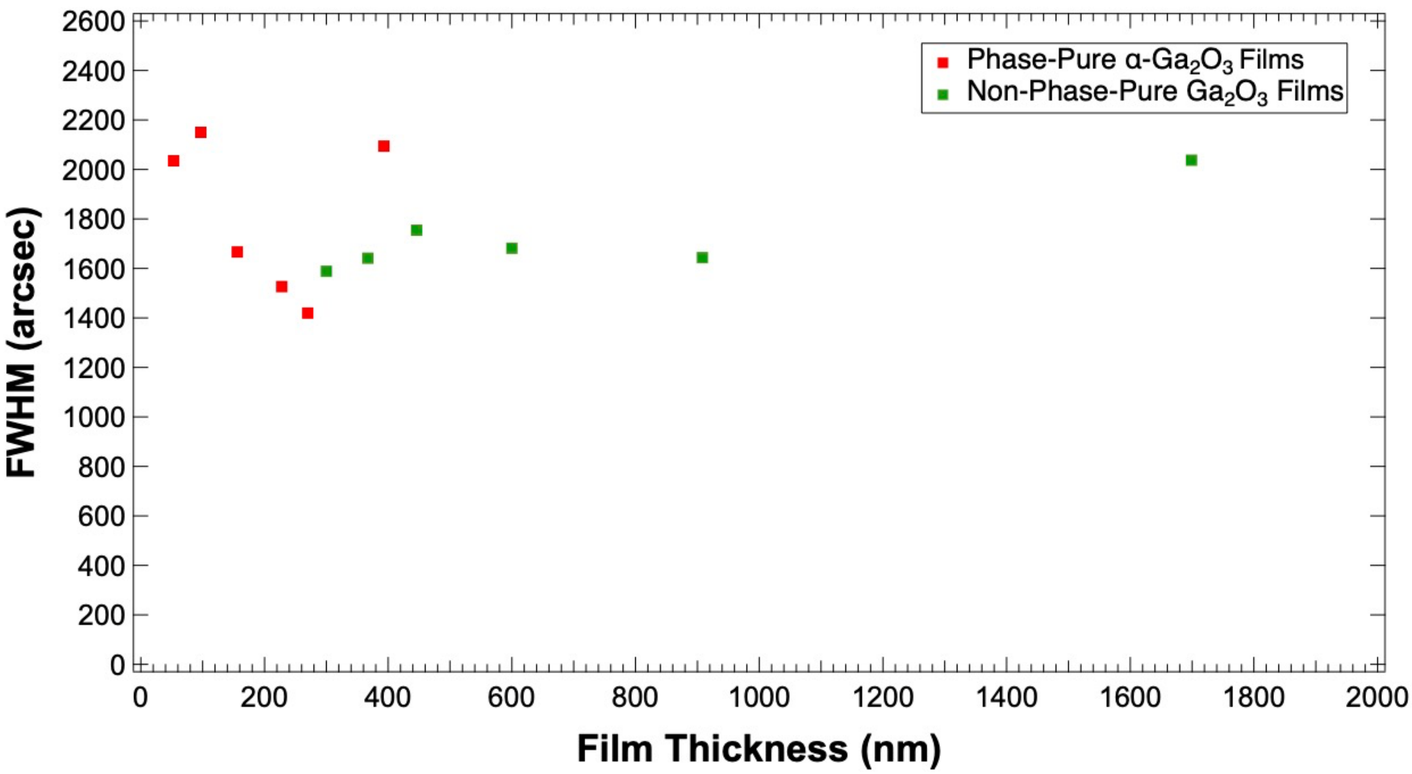

Figure 2: XRD rocking curve Full-Width-at Half-Maximum (FWHM) of Ga_2O_3 thin films grown on m-plane sapphire substrate using MOCVD as a function of film thickness. Single-phase α-Ga_2O_3 thin films are indicated by the red markers on the plot.

Supporting

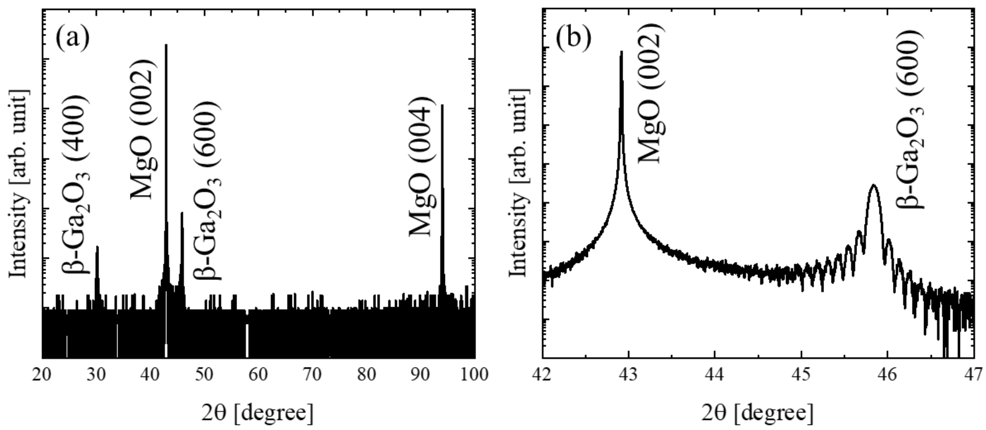

Figure 1. (a) XRD pattern of β-Ga_2O_3 film grown on MgO (001) substrate and (b) expansion of the region corresponding to diffraction from β-Ga_2O_3 (600). The presence of γ-Ga_2O_3 (400) would generate a diffraction peak at 2θ=43.93°, which was not observed.

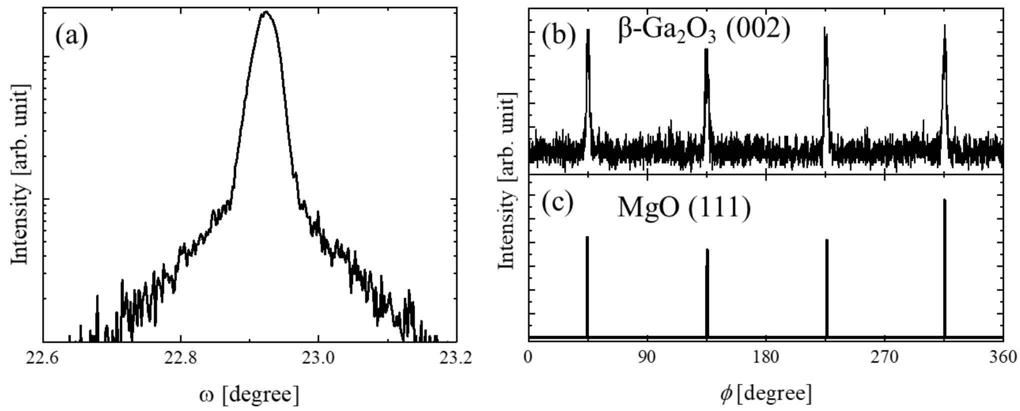

Figure 2. (a) The ω-rocking curve of the β-Ga_2O_3 (600) reflection. The full width at half maximum was 145 arcsec. (b) ϕ-scan profiles of β-Ga_2O_3 (002) film and (c) MgO(111) substrate.

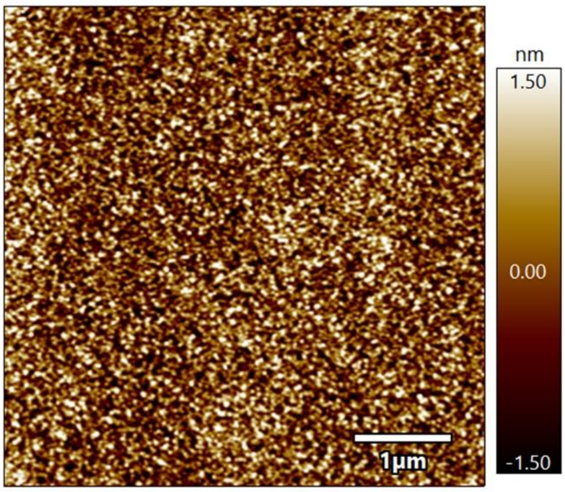

Figure 3. AFM image of β-Ga_2O_3 film grown on MgO(001) substrate showing 0.74 nm RMS roughness.

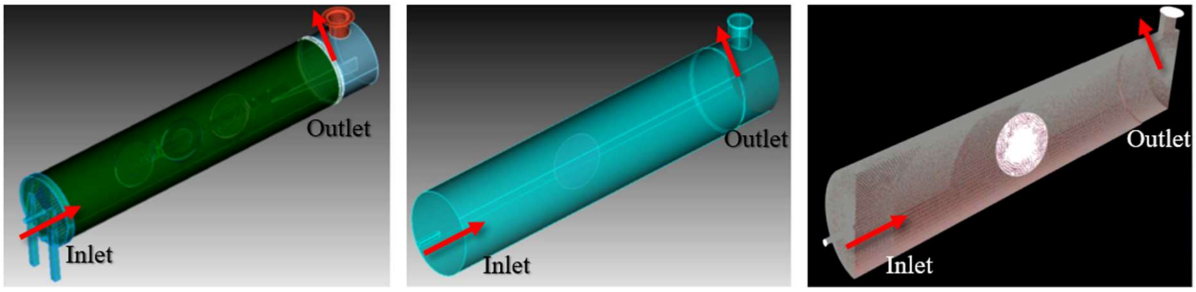

(a) (b) (c)

Figure 1. Chamber modeling process for fluid dynamics analysis. (a) Simplified MIST-CVD chamber shape (b) Flow analysis area extraction (c) Hexahedral mesh structure design for simulation

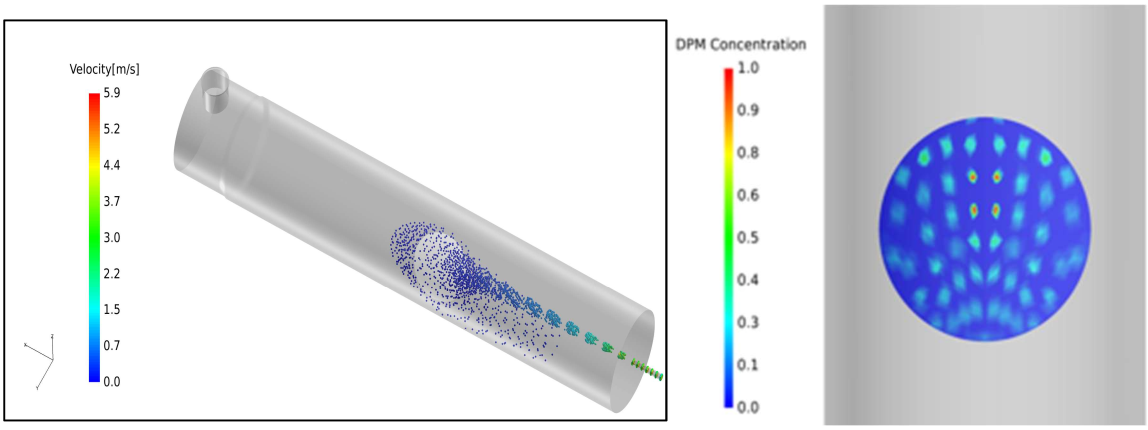

(a) (b)

Figure 2. (a) Fluid analysis example of the Horizontal MIST-CVD Chamber (b) Cross-sectional image of the mist Concentration in a 4inch wafer

Ga Beam Flux = 1 × 10^{-7} Torr "Gallium Rich" Regime

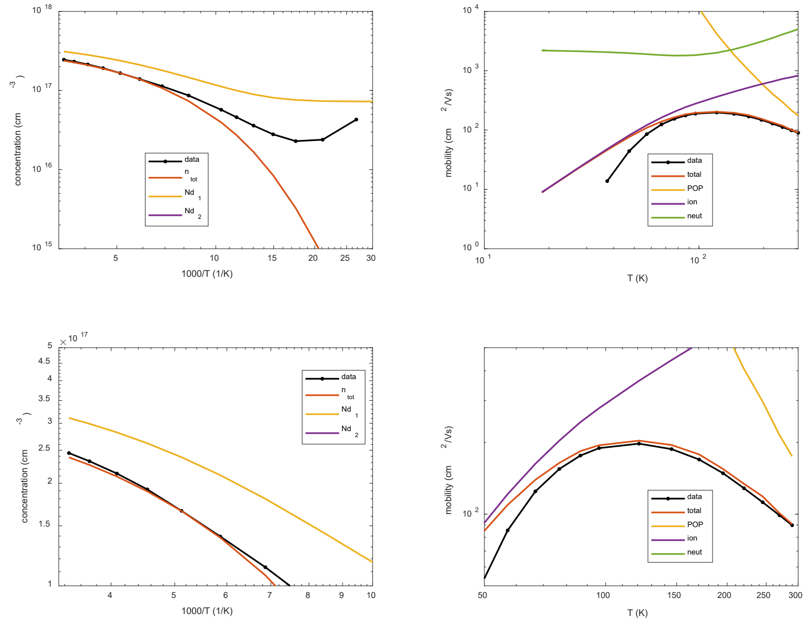

Figure 1: Transport of a gallium rich film and the fits to quantify defects and donors. A donor at 27 meV shows a concentration of 4.25 × 10^{17} cm^{-3} and an acceptor of 7.26 × 10^{16} cm^{-3}.

Ga Beam Flux = 6 × 10^{-8} Torr "Oxygen Rich" Regime

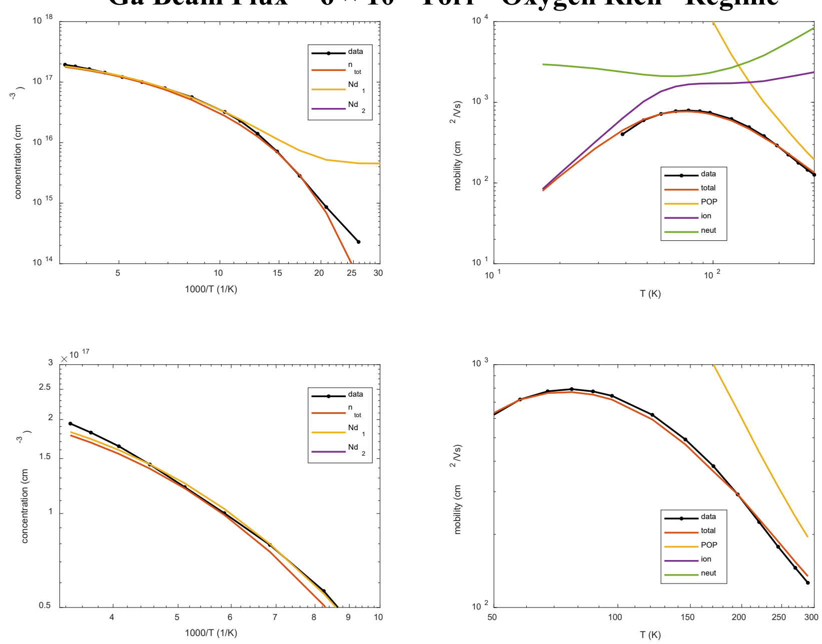

Figure 2: Transport of a gallium rich film and the fits to quantify defects and donors. A donor at 38 meV shows a concentration of 2.6 × 10^{17} cm^{-3} and an acceptor of 4.5 × 10^{15} cm^{-3}.

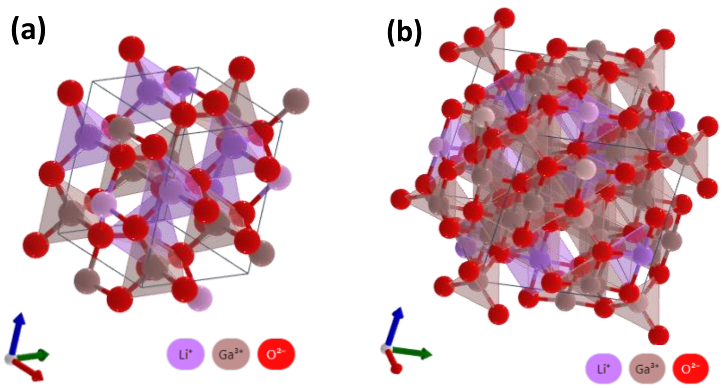

Figure 1. Structural illustrations of (a) β-$LiGaO_2$ with orthorhombic $Pna2_1$ crystal structure; and (b) $LiGa_5O_8$ with spinel cubic P4_33$\bar{2}$ crystal structure.

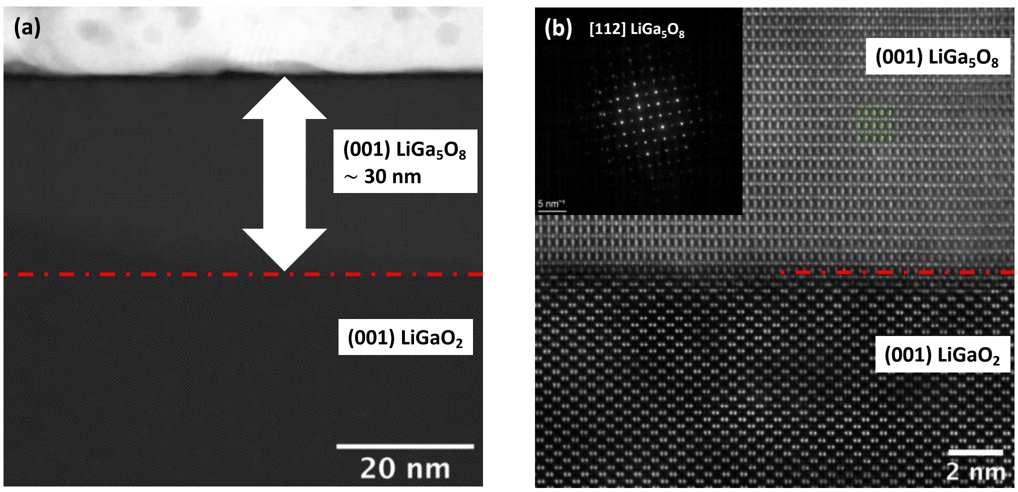

Figure 2. (a) Cross-sectional STEM image and (b) atomic resolution HAADF image and diffract pattern of $LiGa_5O_8$ thin film grown on (001) $LiGaO_2$ substrate. The interface is marked by a red dash-dotted line.

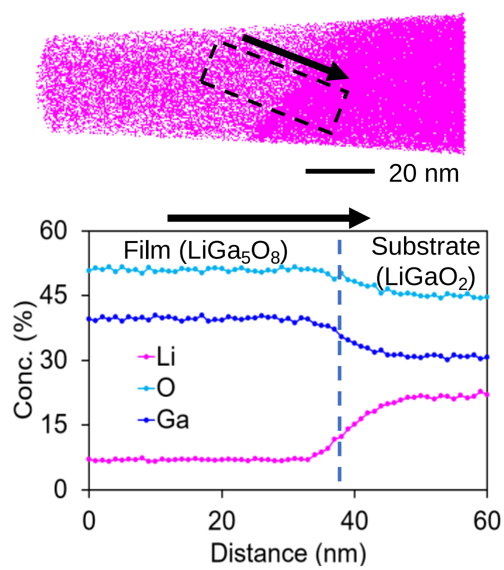

Figure 3. Reconstructed atom map of the $LiGa_5O_8$ film grown on (001) $LiGaO_2$ substrate as well as the atomic concentration for Li, Ga and O along the marked direction across the substrate/epi-layer interface. Only the Li atoms are shown in the upper figure with pink dots.

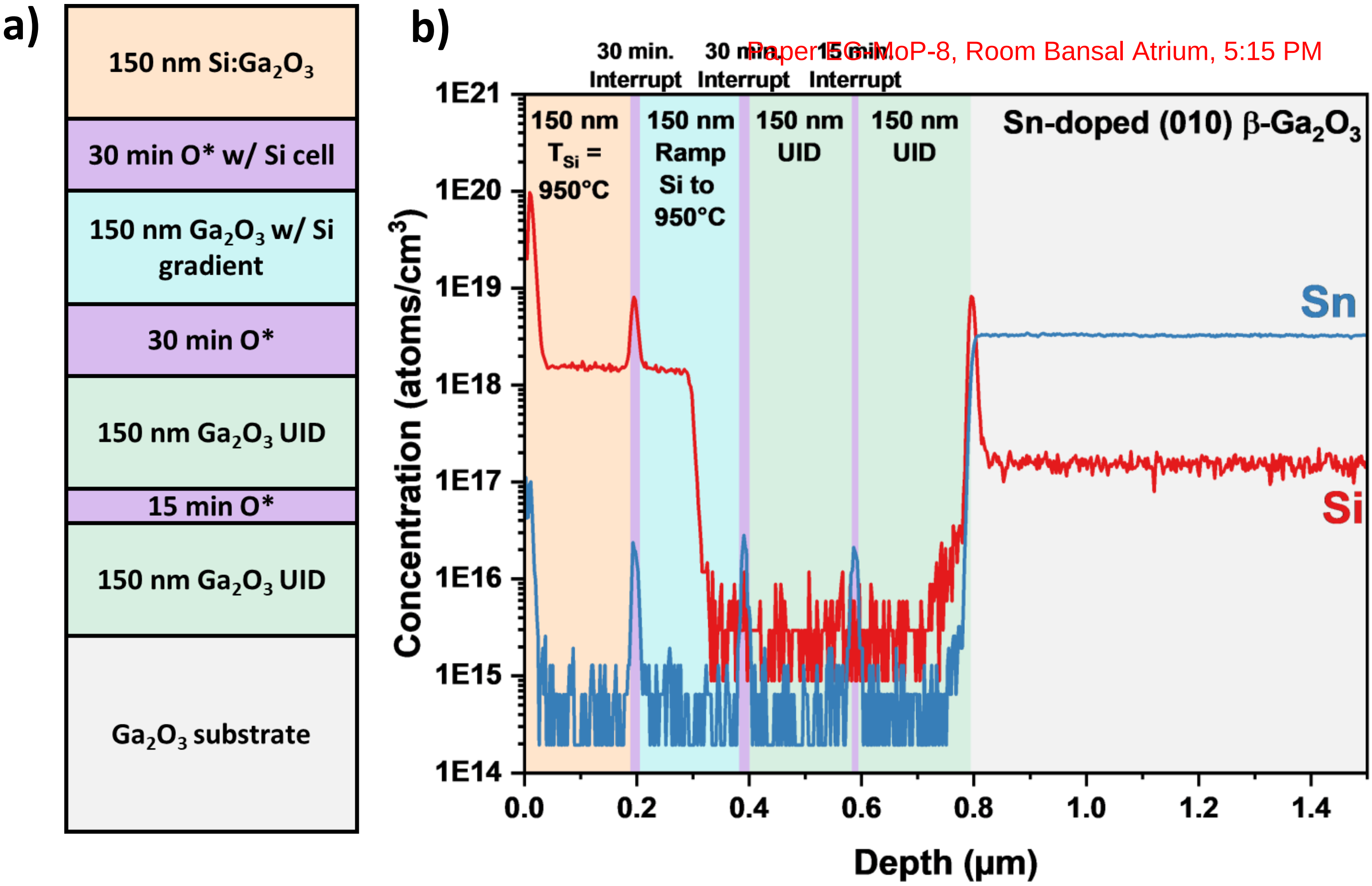

Figure 1 – a) Schematic of test structure to study impacts of plasma bulbs and Si dopant source during growth interrupts. b) TOF-SIMS depth profile showing Si only accumulates at the sample surface during growth interrupts while the Si cell was hot enough to provide a Si flux while no Si accumulated regardless of exposure time to just the quartz plasma bulb with a 250W O plasma.

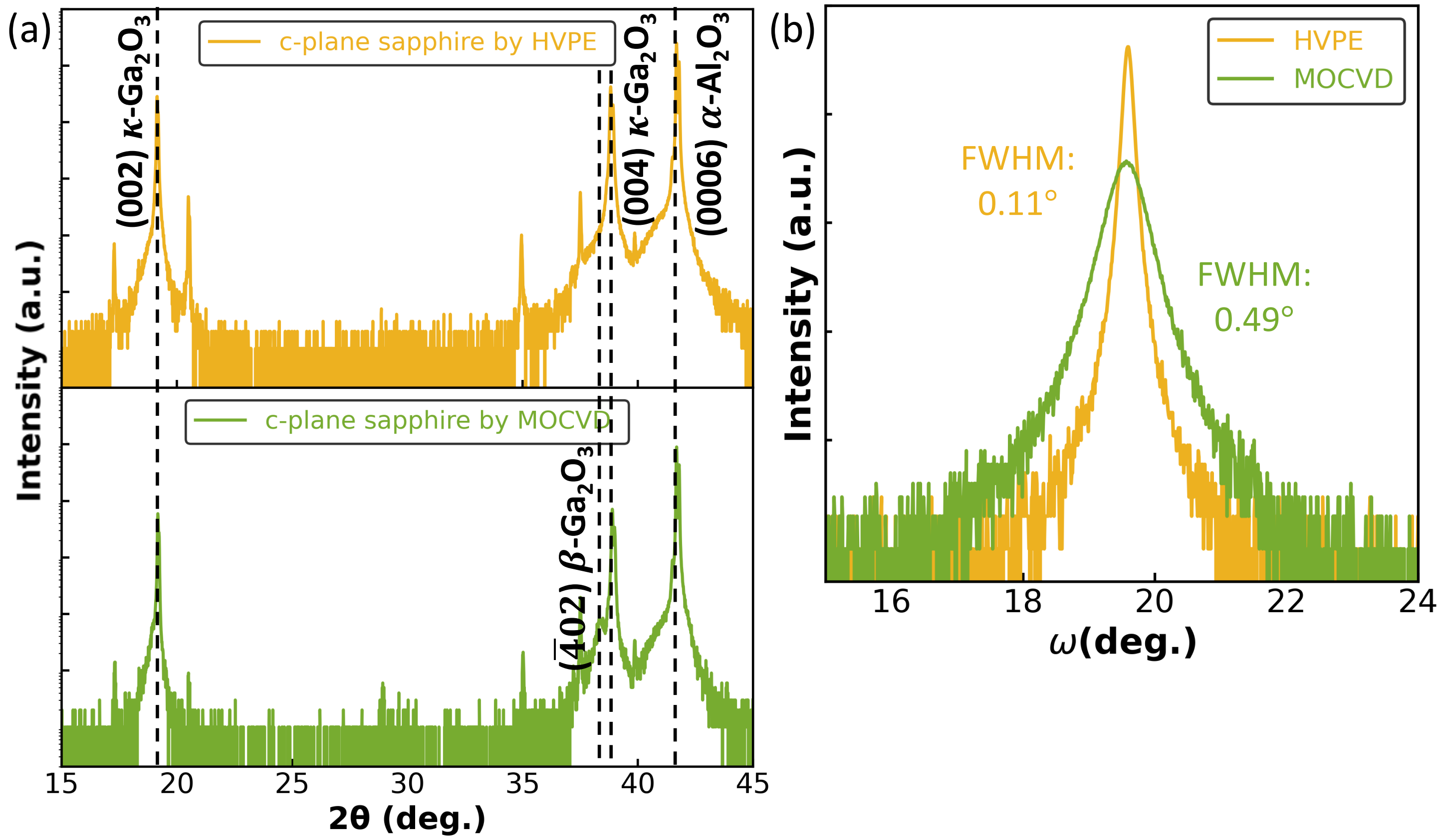

FIG. 1. (a) XRD patterns (log scale) for κ-Ga_2O_3 films grown on c-plane sapphire substrates by HVPE and MOCVD (b) Corresponding XRD rocking curves for the (004) symmetric diffraction peaks of κ-Ga_2O_3

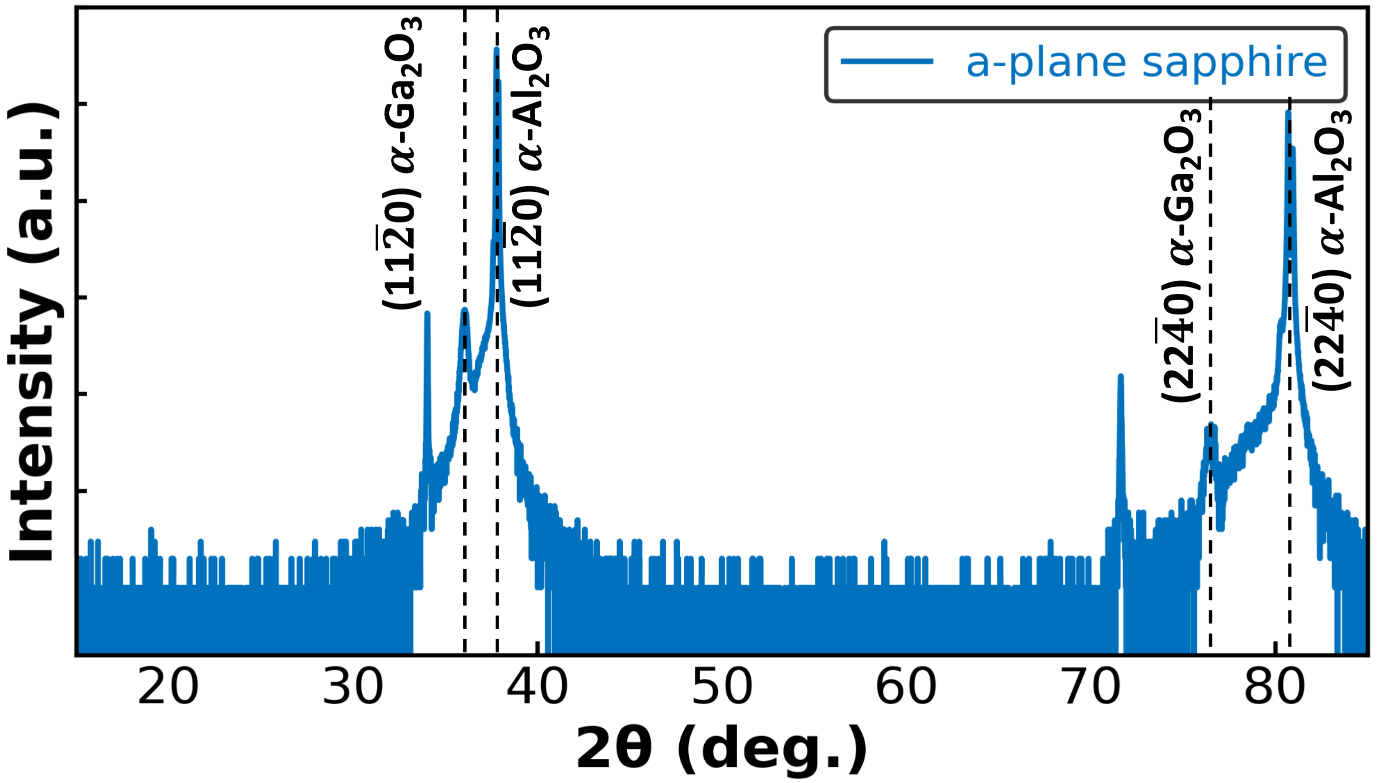

FIG. 2. XRD pattern (log scale) for α-Ga_2O_3 films grown on a-plane sapphire substrate by HVPE

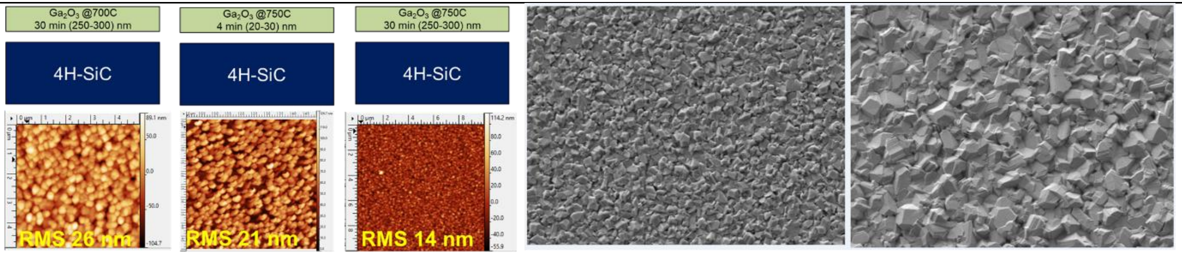

Fig. 1 AFM and FEGSEM surface morphology of samples grown at different temperatures

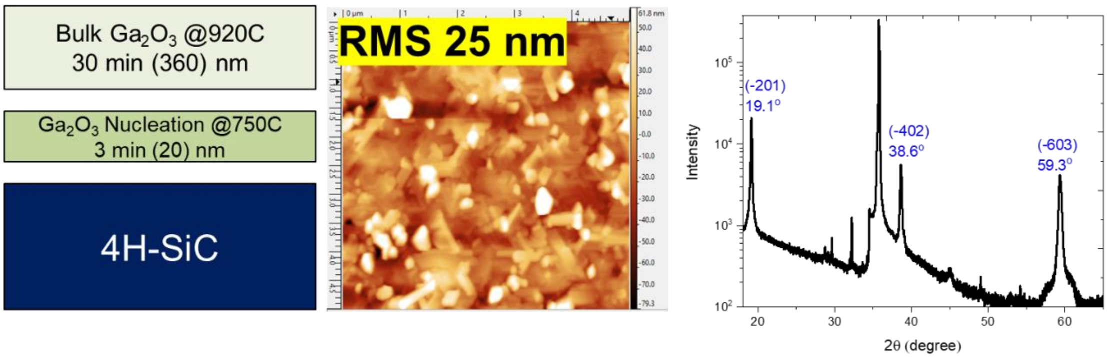

Fig. 2 Showing a schematic of S1 including AFM surface morphology and XRD 2θ-ω scan

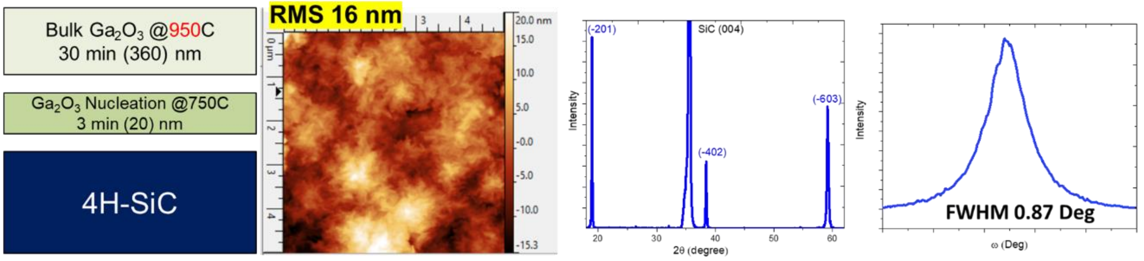

Fig. 3 Shows epitaxial layer schematic of S2 with AFM surface morphology, XRD 2θ-ω scan and FWHM from rocking curve

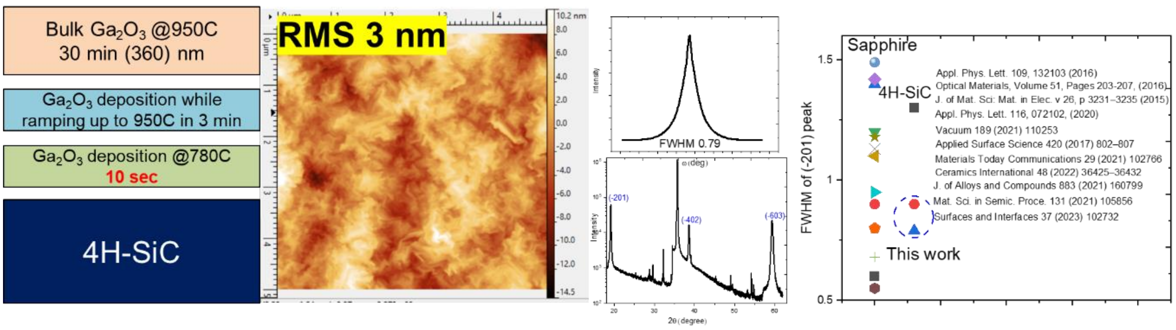

Fig. 4 shows schematic of S3 including with AFM and FEGSEM surface morphology, XRD 2θ-ω scan, FWHM from rocking curve and benchmarking of reported FWHM of MOCVD grown β-Ga_2O_3 on different substrates

200 W, RT	3 mTorr	5 mTorr	12.5 mTorr
2.5% O_2	Dep rate – 138 nm/hr Hg CV – N/A Resistivity – 9.3×10^3 Ω/sq	Dep rate – 111 nm/hr Hg CV – 4.22×10^{17} cm^{-3} Resistivity – 9.6×10^3 Ω/sq	Dep rate – 43 nm/hr Hg CV – 9.28×10^{17} cm^{-3} Resistivity – 7.9×10^3 Ω/sq
5% O_2	Dep rate – 118 nm/hr Hg CV – N/A Resistivity – 9.5×10^3 Ω/sq	Dep rate – 70 nm/hr Hg CV – 3.89×10^{17} cm^{-3} Resistivity – 7.0×10^3 Ω/sq	Dep rate – 34 nm/hr Hg CV – 1.32×10^{18} cm^{-3} Resistivity – 3.1×10^3 Ω/sq
10% O_2	Dep rate – 83 nm/hr Hg CV – N/A Resistivity – 1.0×10^4 Ω/sq	Dep rate – 59 nm/hr Hg CV – 1.24×10^{18} cm^{-3} Resistivity – 8.7×10^3 Ω/sq	Dep rate - 32 nm/hr Hg CV – 2.74×10^{18} cm^{-3} Resistivity – 6.4×10^3 Ω/sq

Table 1) Deposition rate, acceptor concentration, and resistivity of NiO thin films sputtered at various oxygen partial pressure and chamber pressure. The temperature and power were constant.

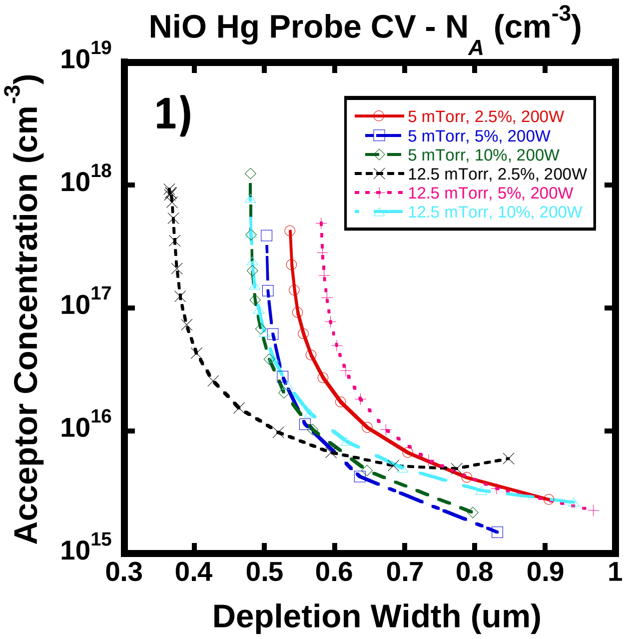

	Contact Res. (Ω*mm)	Sheet Res. (Ω/sq)	Specific Contact Res. (Ω*cm^2)
Ni/Au	1079	3.8×10^5	3×10^{-2}
PtOx/Au	259	2.3×10^5	2.8×10^{-3}

Table 2) Data extracted from the linear transmission line measurements of Ni/Au and PtOx/Au contacts to NiO including contact resistance, sheet resistance, and specific contact resistance.

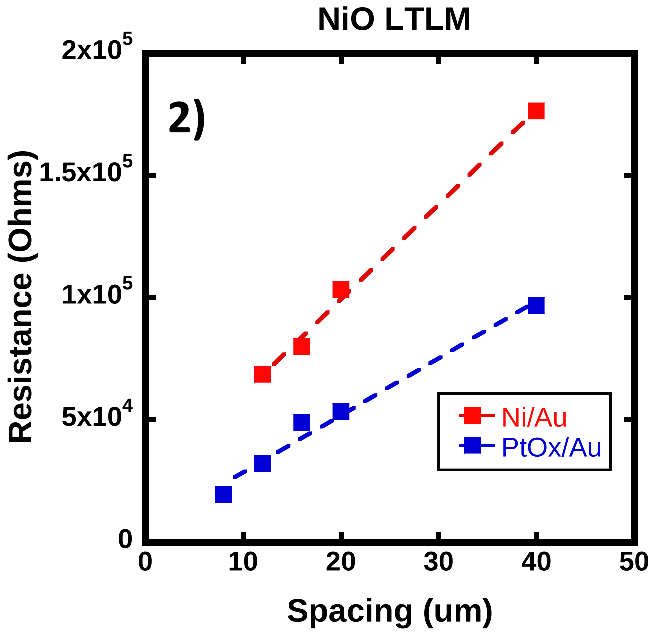

Fig. 1) NiO acceptor concentration as a function of depletion width for six various sputtering recipes. Data was extracted from mercury (Hg) probe capacitance-voltage measurements. **Fig. 2)** Resistance as a function of contact spacing for the Ni/Au and PtOx/Au contacts to NiO films.

Abstract References:

[1] Spencer, J.A., et al. *Applied Physics Reviews*, 9.1 (2022): 011315 2022

[2] Kokubun, Y., et al. *Applied Physics Express* 9.9 (2016): 0911012

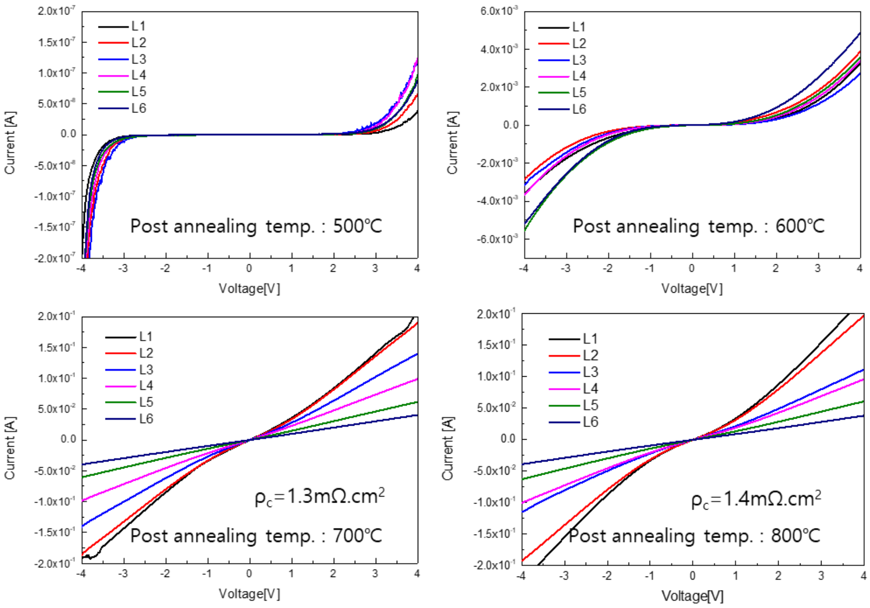

Fig 1. Ohmic contact characteristics of n-ITO/Ti/Au Multilayer on Ga_2O_3 epi. Layer as a function of post annealing temperatures

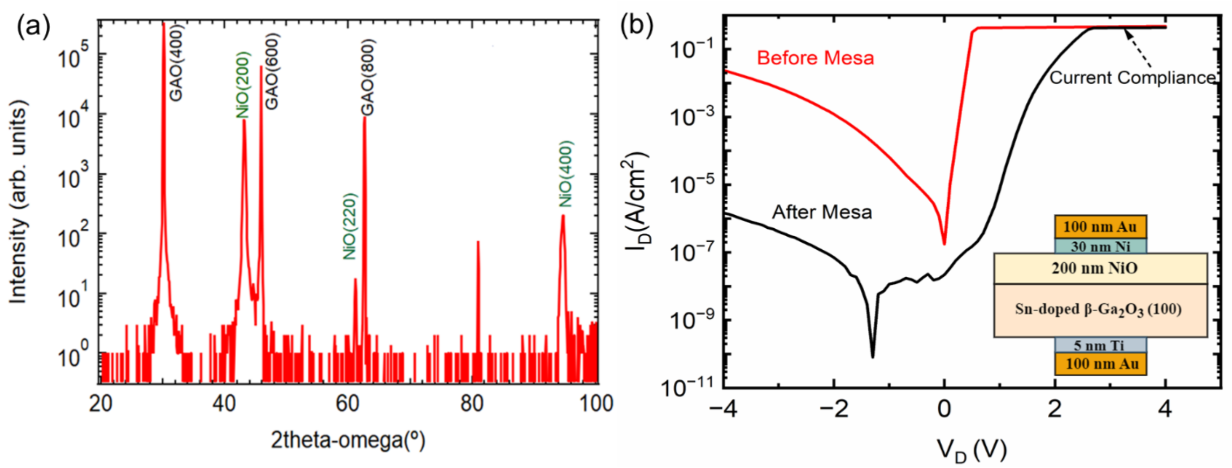

Figure 1: (a) Wide angle x-ray diffraction scan of ~200nm thick NiO thin film grown by pulsed laser deposition on Sn-doped Ga_2O_3(100) substrate, showing a polycrystalline layer with a preferential (100) orientation. (b) Room temperature I-V characteristics of NiO/β-Ga_2O_3 *p-n* diode on a 100 μm pad before(red) and after (black) NiO mesa isolation. The mesa etch is effective at reducing current spreading leading to improved leakage current. Inset shows a schematic of the device structure.

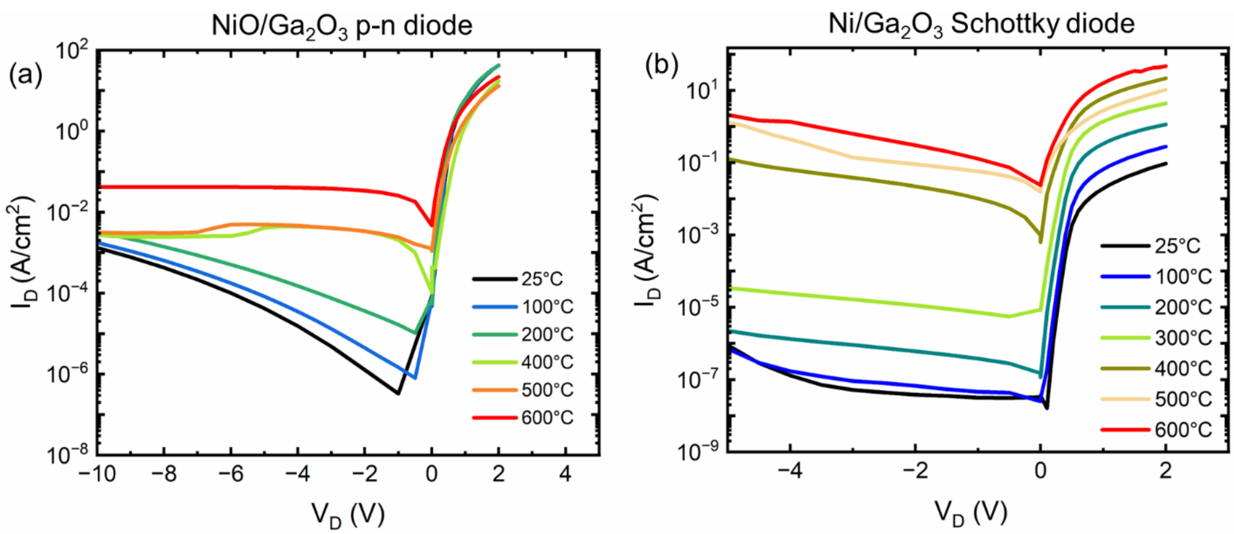

Figure 2: High temperature rectification characteristics of (a) NiO/β-Ga_2O_3 *p-n* diode and (b) Ni/β-Ga_2O_3 Schottky diode. The reverse leakage current of the *p-n* diode increases approximately 2 orders of magnitude from 300 °C to 600 °C, compared to about 5 orders of magnitude for the Schottky diode over the same temperature range.

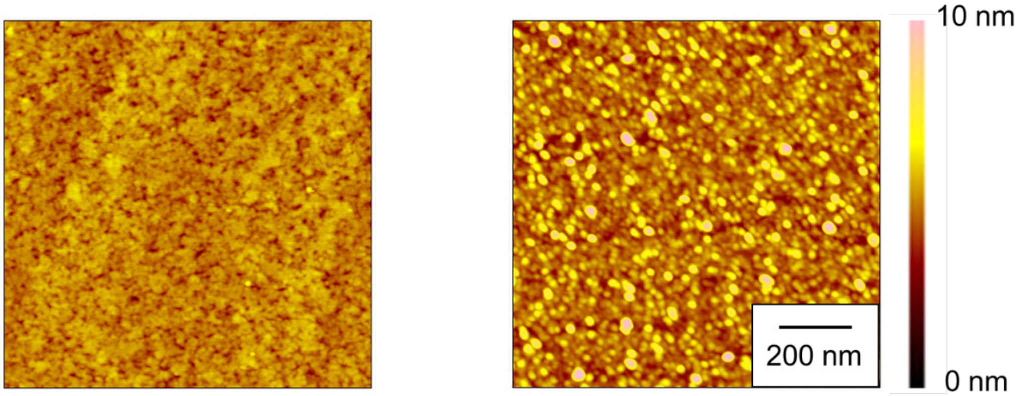

(a) (b)

Fig. 1 AFM images of Ga_2O_3 (a) (100) and (b) (010) surfaces after 120-min N radical irradiation.

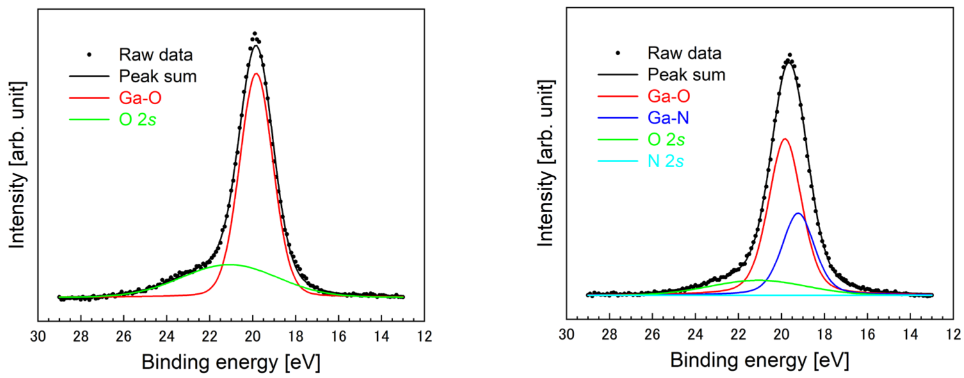

(a) (b)

Fig. 2 XPS spectra from Ga 3*d* core levels of Ga_2O_3 (100) surfaces

(a) without and (b) with 120-min N radical irradiation.

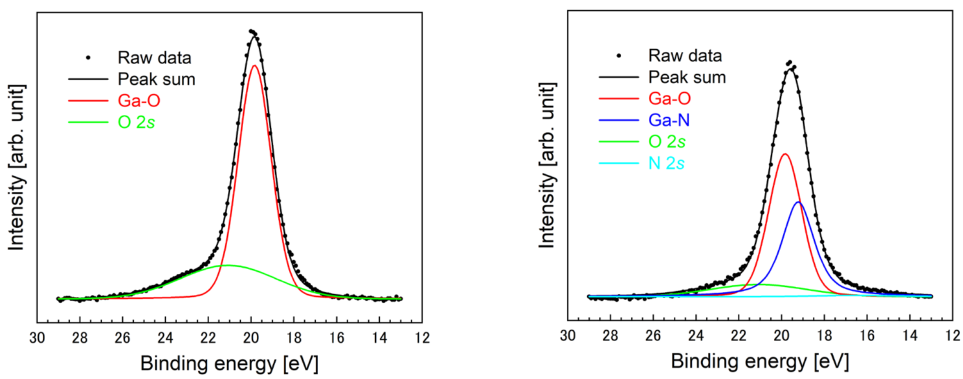

(a) (b)

Fig. 3 XPS spectra from Ga 3*d* core levels of Ga_2O_3 (010) surfaces

(a) without and (b) with 120-min N radical irradiation.

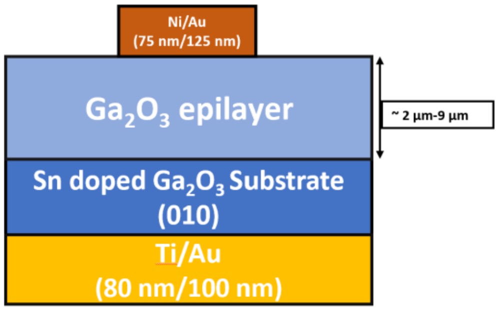

Table I. Growth conditions of β-Ga_2O_3 films on the Sn-doped β-Ga_2O_3 substrate

Sample No	Epilayer Thickness (µm)	Estimated Growth Rate	Target Doping (cm^{-3})
S1	9.5	3 µm/hr	2-3 × 10^{16}
S2	3	650 nm/hr	2 × 10^{16}
S3	2	650 nm/hr	7 × 10^{16}

Fig. 1. Schematic cross-section of the vertical Schottky diode structures

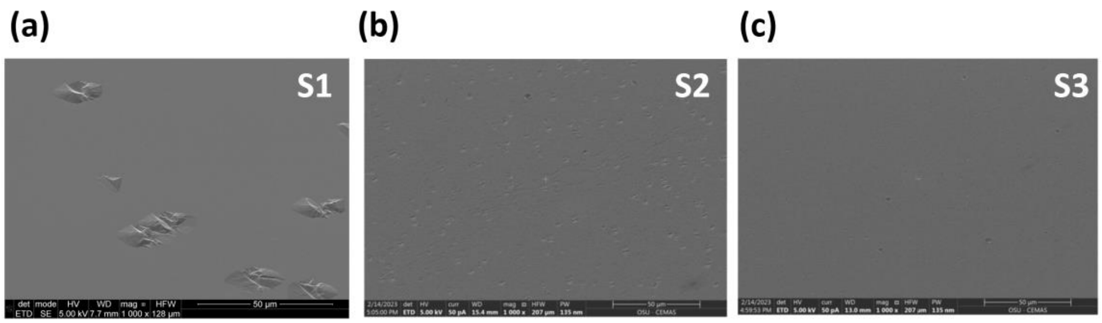

Fig. 2. FESEM images of MOCVD grown β-Ga_2O_3 films on Sn-doped β-Ga_2O_3 substrates for all the Schottky diodes associated with this study. The figure below also shows that S3 has the smoothest surface than the other two samples.

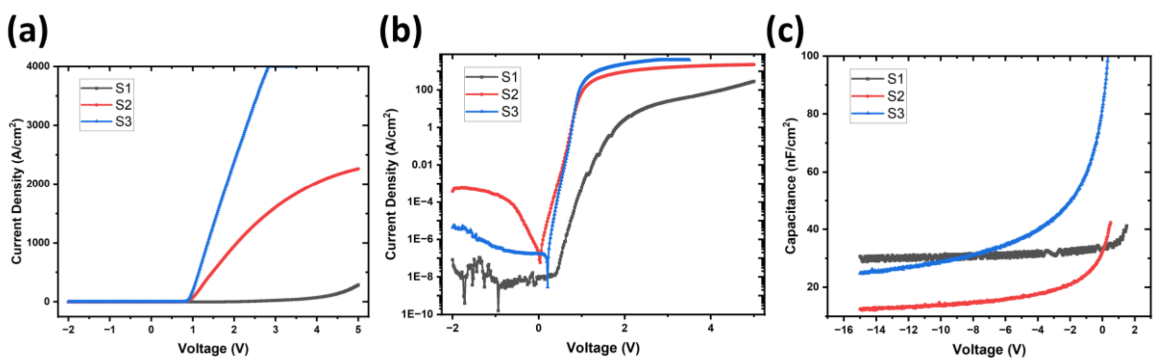

Fig. 3. (a) Room temperature current density (*J*) vs. voltage (*V*) characteristics for S1, S2, and S3 Schottky barrier diodes. (b) Semi-logarithmic *J*-*V* characteristics for S1, S2, and S3 Schottky barrier diodes. (c) Room temperature reverse bias capacitance (C)-voltage (V) data for S1, S2, and S3 Schottky barrier diodes.

Table II. Extracted electrical properties at room temperature for S1, S2, and S3.

Sample No	Ideality Factor	Barrier Height (eV)	$R_{on,sp}$ (mΩ.cm^2)	ON-OFF Ratio	Average Doping (cm^{-3})
S1	2.17	1.42	17.36	>10^9	2.02 × 10^{16}
S2	1.73	1.18	1.87	>10^7	1.73 × 10^{16}
S3	1.31	1.0	0.707	>10^8	6.08 × 10^{16}

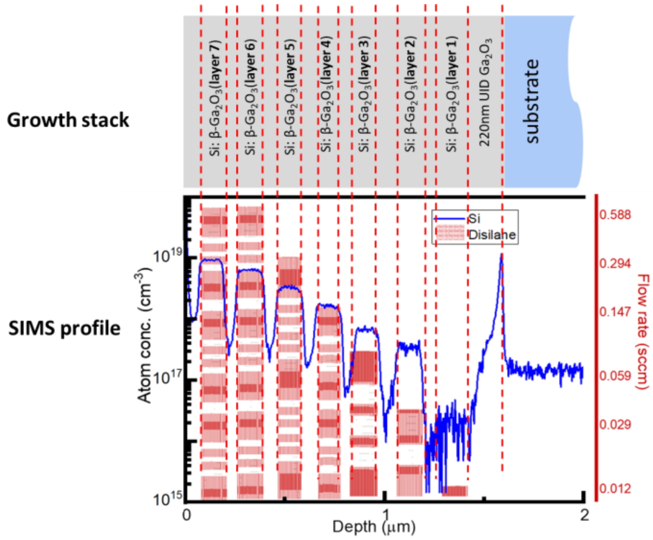

Figure 1. SIMS stack of Si doped Ga_2O_3 by suboxide source with different disilane flow rates. Si concentration of $3\times10^{16}cm^{-3}$ to $1\times10^{19}cm^{-3}$ has been achieved.

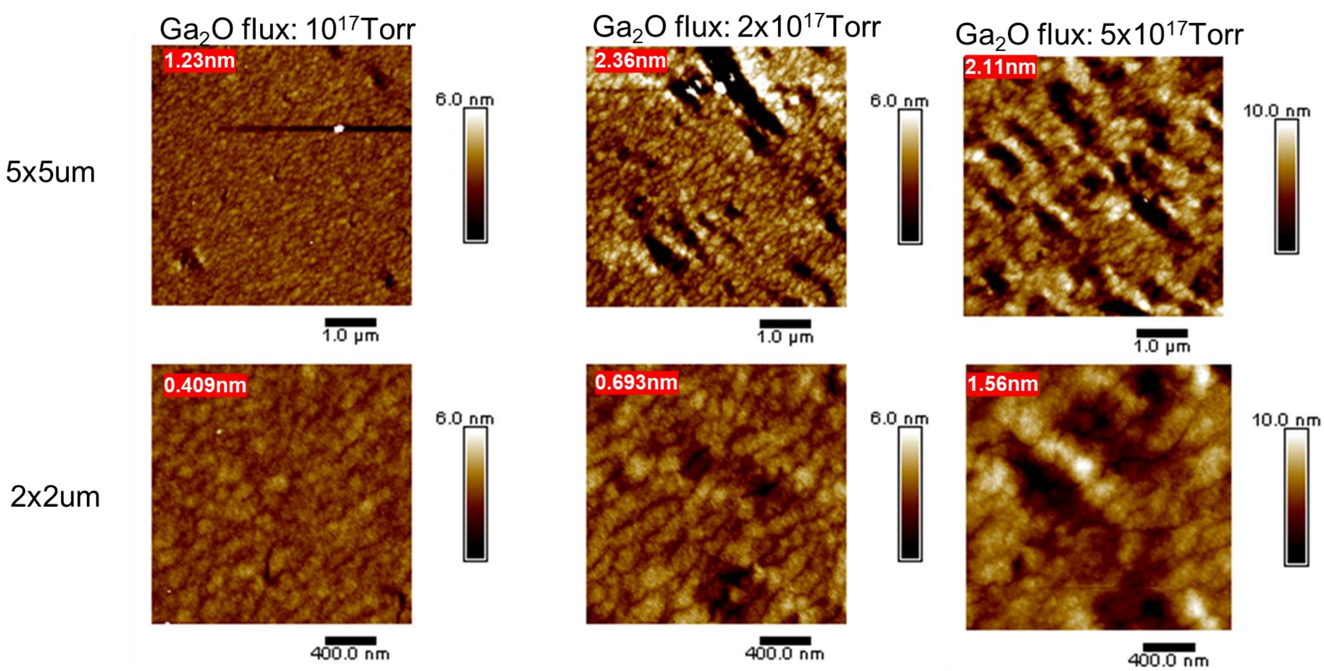

Figure 2. AFM images of Ga_2O_3 surface morphology growth by different sub-oxide fluxes.

Microscopic-scale Defect Analysis on Ga_2O_3 through Microscopy

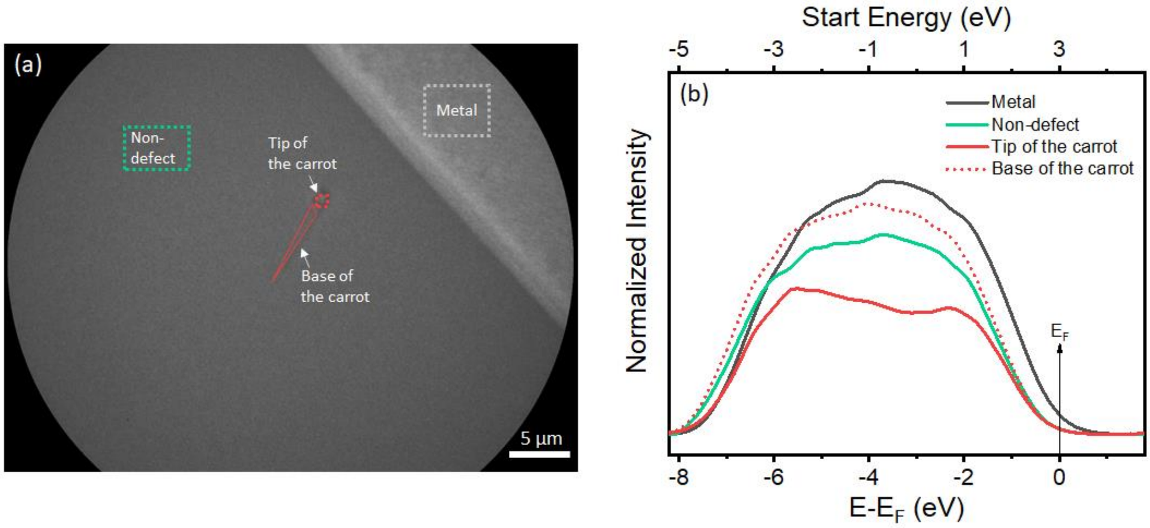

Fig. 1. (a) PEEM image of the carrot defect in Ga_2O_3 epi-layer grown with HVPE. The field of view is 50 µm. (b) Normalized photoelectron spectroscopy illuminated by 193 nm light on metal, non-defect and carrot defect.

References

[1] Das, H., Sunkari, S., & Naas, H. (2016). Characterization of Leakage Causing Visible Epitaxial Defects Nucleating from Crystal Defects in the Substrate. ECS Transactions, 75(12), 233.

[2] Meneghini, M., Bertin, M., Stocco, A., dal Santo, G., Marcon, D., Malinowski, P. E., ... & Zanoni, E. (2013). Degradation of AlGaN/GaN Schottky diodes on silicon: Role of defects at the AlGaN/GaN interface. Applied Physics Letters, 102(16), 163501.

[3] Benamara, M., Zhang, X., Skowronski, M., Ruterana, P., Nouet, G., Sumakeris, J. J., ... & O'Loughlin, M. J. (2005). Structure of the carrot defect in 4H-SiC epitaxial layers. Applied Physics Letters, 86(2), 021905.

Supplementary Material

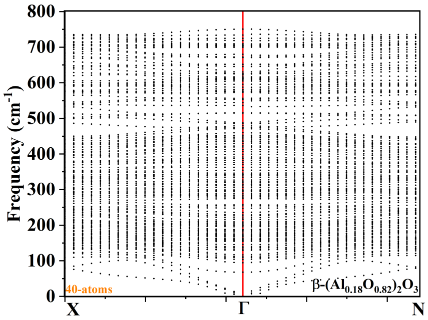

Figure 1: The full phonon dispersion for the 40-atom (120 phonon modes) supercell used to model the alloy disorder with 18% aluminum fraction

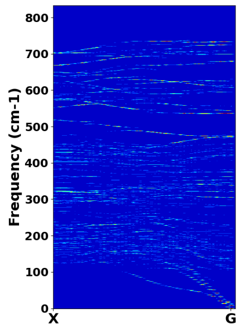

Figure 2: The effective phonon dispersion (30 phonon modes corresponding to 10atom primitive cell of GaO)in the $X - \Gamma$ direction with 18% aluminum fraction

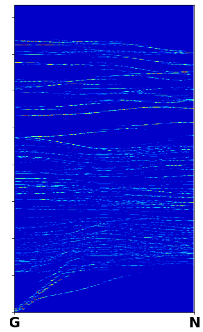

Figure 3: The effective phonon dispersion (30 phonon modes corresponding to 10atom primitive cell of GaO)in the $\Gamma - N$ direction with 18% aluminum fraction

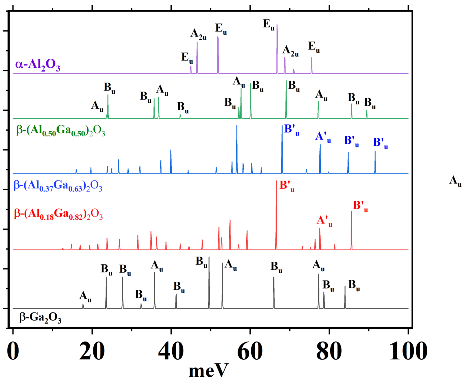

Figure 4: The comparison of the IR spectrum obtained for the alloy using the Brillouin zone unfolding scheme. Some of the modes that are labeled show a trend of moving to higher energies with increasing aluminum fraction in the AlGaO alloy

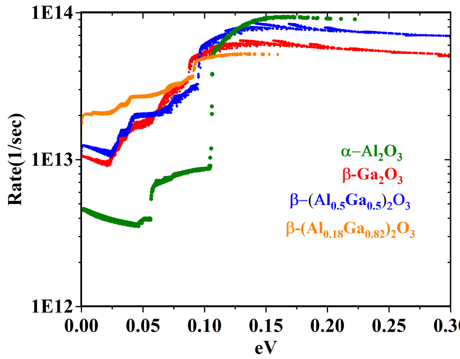

Figure 5: The polar optical phonon scattering rate for varying aluminum compositions calculated from first principles

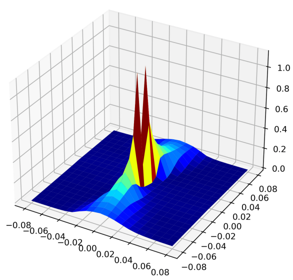

Figure 6: The polar electron-phonon interaction elements showing the $\frac{1}{|q|}$ dependence in $\beta - (Al_{0.18}Ga_{0.82})_2O_3$

1

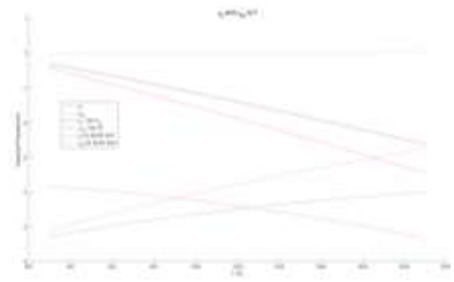

Fig. 1: Ga and O chemical potentials as functions of temperature calculated from thermochemical functions used for Ga-O binary phase diagram for various chemical environments such as: $pO_2 = 10^{-4}$ atm, $pO_2 = 1$ atm, and the equilibrium vapor pressure of Ga over liquid Ga. The non-constant values vs T influence the quantitative defect equilibrium.

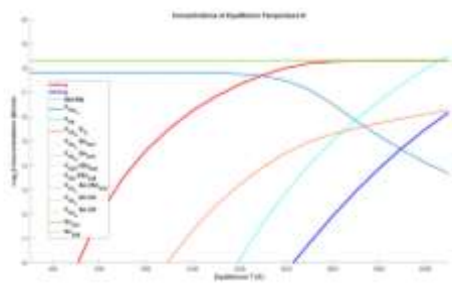

Fig. 2: Simplified results for full equilibrium calculation including >350 chargestates of various defects and complexes at different equilibrium temperatures, subject to the constraints that $[Sn_{GaII}] = 2x10^{18}$ /cm^3 but all other Sn-containing defects are set to zero. This illustrates the capability to execute calculations incorporating T-dependent E_c and E_v (which is primarily responsible for suppressing the V_{Ga}), T-dependent chemical potentials, and estimated vibrational entropy, as well as constraints on the concentrations of various defect types.

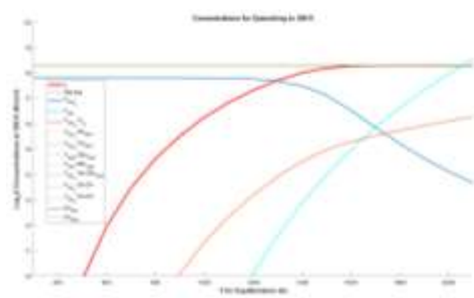

Fig. 3: Simplified results for quenching calculations from the indicated T to 300 K including >350 chargestates of various defects and complexes, subject to the constraints that $[Sn_{GaII}] = 2x10^{18}$ /cm^3 and all other Sn-containing defects set to zero. This illustrates the capability to execute quenching calculations including certain defects constrained to set values.

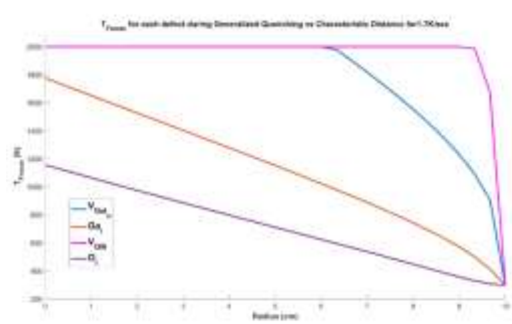

Fig. 3: Illustrative, simplified example of calculated freezing temperatures vs radius in a hypothetical Ga2O3 boule for O_i, Ga_i, relaxed V_{Ga}, and V_{OIII} arbitrarily assigned migration energies of 0.15, 0.2, 0.5, and 0.75 eV as shown.

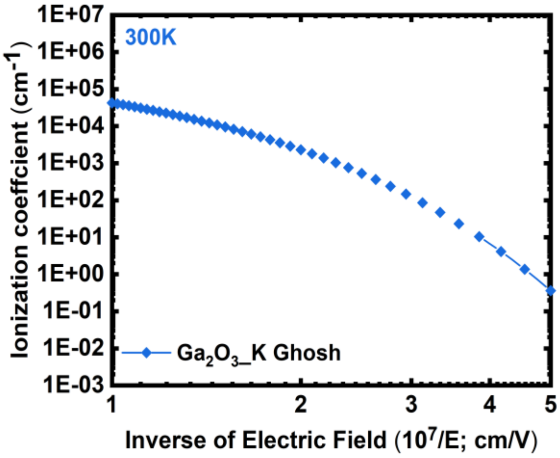

Figure 1: Ionization rate coefficient of electrons in β-Ga_2O_3 at room temperature [1]

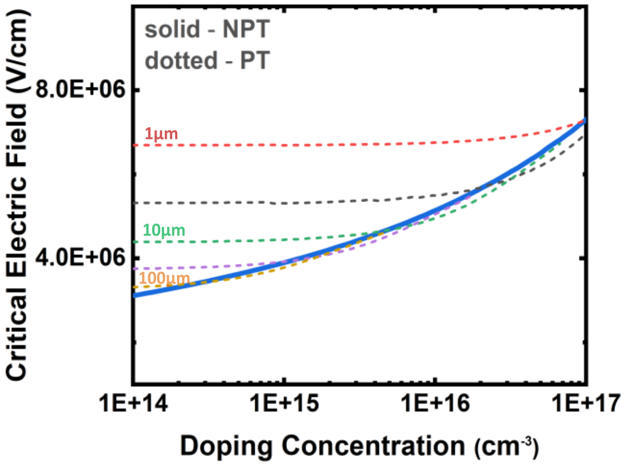

Figure 2: Critical electric field for avalanche breakdown in β-Ga_2O_3 for both NPT(solid) and PT(dotted with varied widths) structures

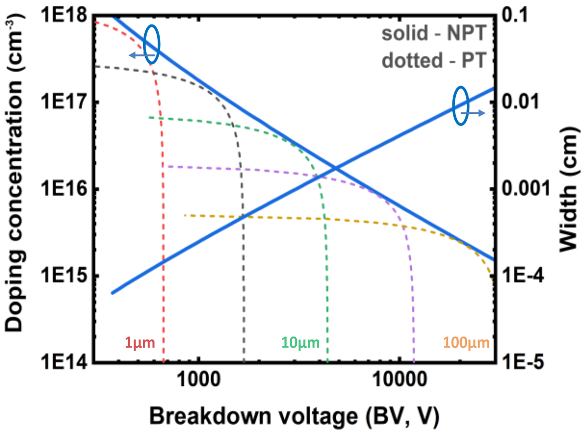

Figure 3: Doping concentration and width of the drift layer dependence on the breakdown voltage in β-Ga_2O_3 for NPT (solid) and PT (dotted with varied widths) structures

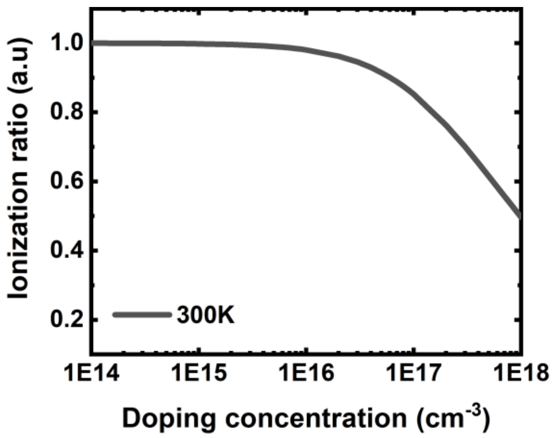

Figure 4: Ionization ratio of dopant extracted at room temperature in β-Ga_2O_3 with ionization energies reported in [2]

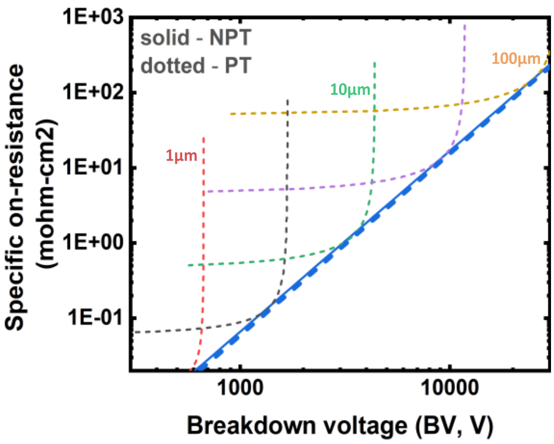

Figure 5: Trade-off relationship between the specific on-resistance of the drift layer and breakdown voltage in β-Ga_2O_3 unipolar devices for the NPT (solid) and PT (dotted with varied widths) structures

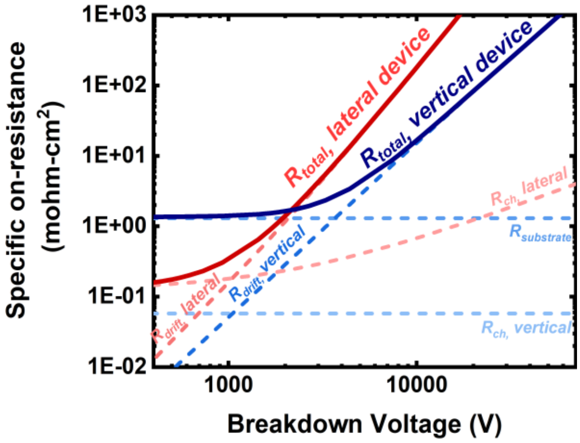

Figure 6: Trade-off relationship between the specific on-resistance and breakdown voltage in β-Ga_2O_3 for a lateral and vertical MOSFET. The resistance components (channel and drift) associated with the lateral device are represented in color red while the vertical device resistance components (channel, drift, and substrate) are represented in color blue

[1] K. Ghosh and U. Singisetti, "Impact ionization in β-Ga2O3," Journal of Applied Physics, vol. 124, no. 8, p. 085707, 2018, doi:10.1063/1.5034120.

[2] R. Sharma, M. E. Law, F. Ren, A. Y. Polyakov, and S. J. Pearton, "Diffusion of dopants and impurities in β-Ga2O3," Journal of Vacuum Science & Technology A, vol. 39, no. 6, p. 060801, Dec. 2021, doi: 10.1116/6.0001307.

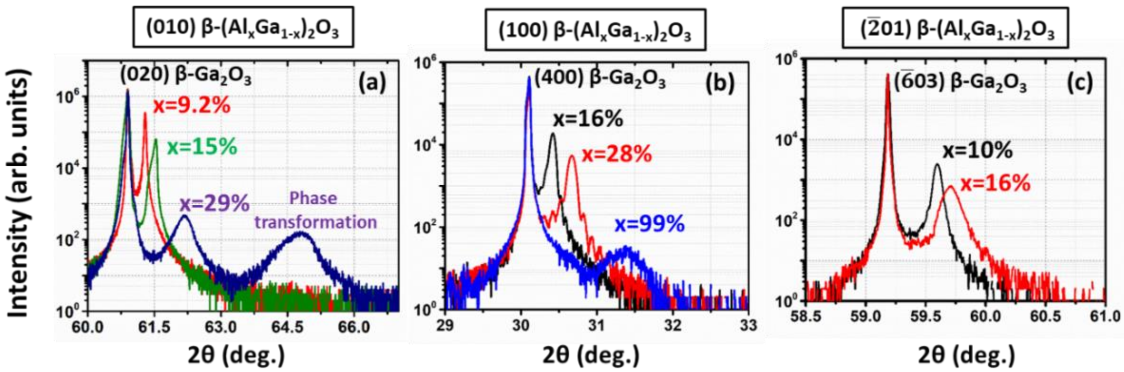

Figure 1. XRD ω-2θ scan profiles of the (a) (020), (b) (400), and (c) ($\bar{6}$03) reflections of MOCVD β-(Al_xGa_{1-x})$_2O_3$ films grown on (010), (100) and ($\bar{2}$01) β-Ga_2O_3 substrates with Al compositions up to 29%, 99% and 16%, respectively.

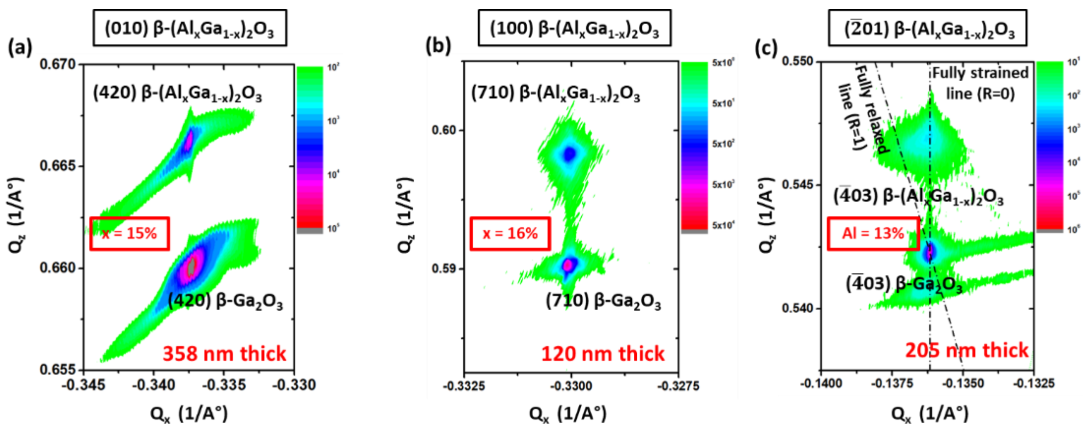

Figure 2. Asymmetric reciprocal space maps (RSMs) around (a) (420), (b) (710), and (c) ($\bar{4}$03) reflections of (010), (100) and ($\bar{2}$01) β-(Al_xGa_{1-x})$_2O_3$ films with x = 15%, 16%, and 13% respectively.

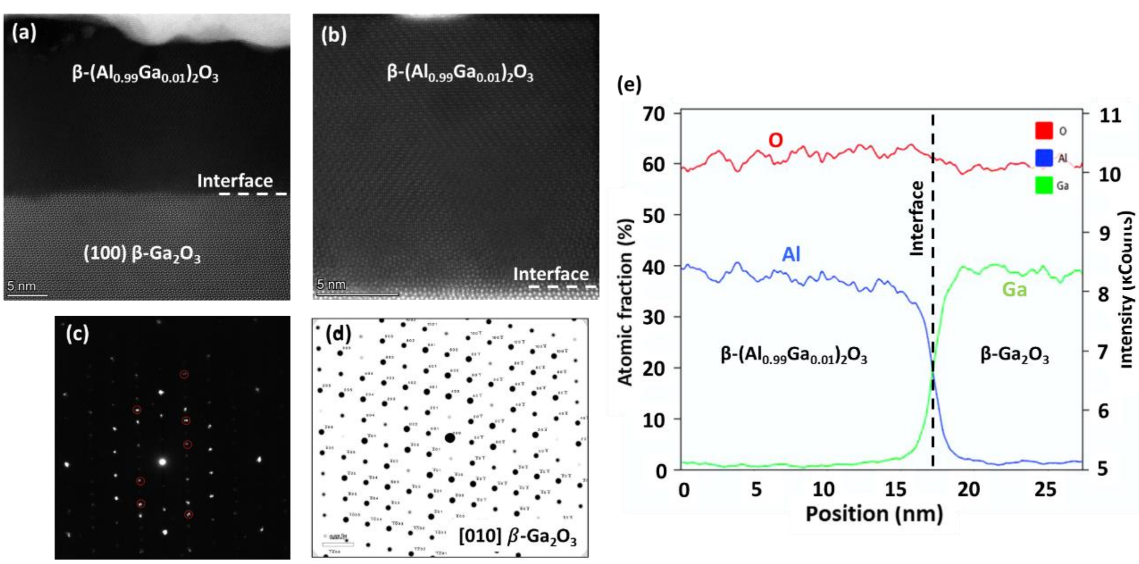

Figure 3. (a) High resolution HAADF-STEM images taken from the $[010]_m$ zone axis of (100) β-($Al_{0.99}Ga_{0.01}$)$_2O_3$ film grown on a 65 nm thick (100) β-Ga_2O_3 buffer layer on top of an on-axis (100) β-Ga_2O_3 substrate. (b) High magnification STEM images of the β-($Al_{0.99}Ga_{0.01}$)$_2O_3$ film. Electron nano-diffraction pattern obtained from the (c) β-($Al_{0.99}Ga_{0.01}$)$_2O_3$ film and (d) simulation. (e) STEM EDX atomic fraction elemental profile of β-($Al_{0.99}Ga_{0.01}$)$_2O_3$ film, confirming an average Al composition of ~99% in the epilayer.

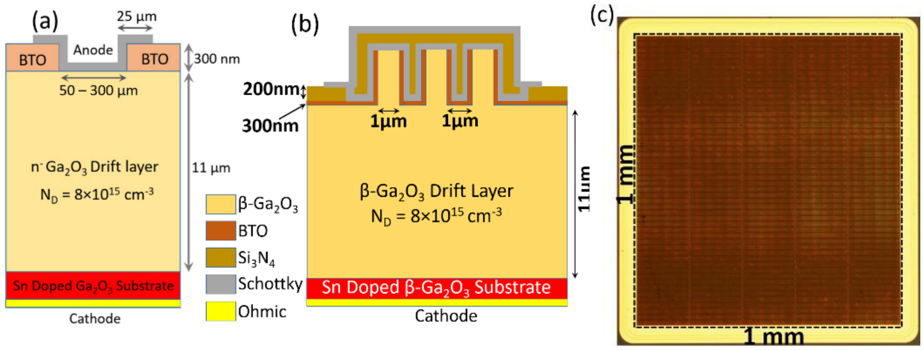

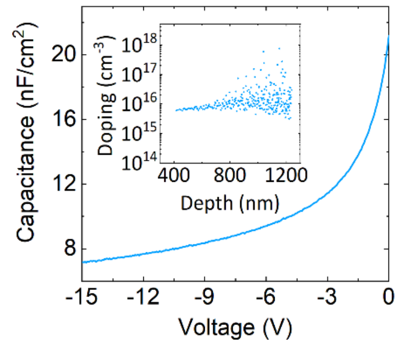

Fig. 1 Schematic diagram of (a) BTO field plated and (b)BTO RESURF trench Ga_2O_3 SBD, (c) Microscope image of the large area (1mm²) SBD.

Fig. 2 CV and doping profile of the HVPE epitaxial layer from a Pt/Ga_2O_3 (Bare Schottky) test structure.

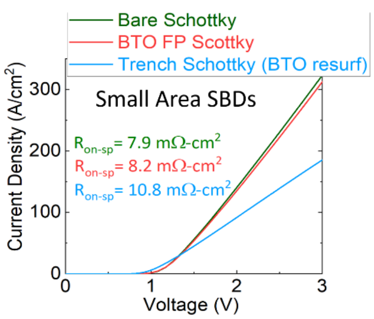

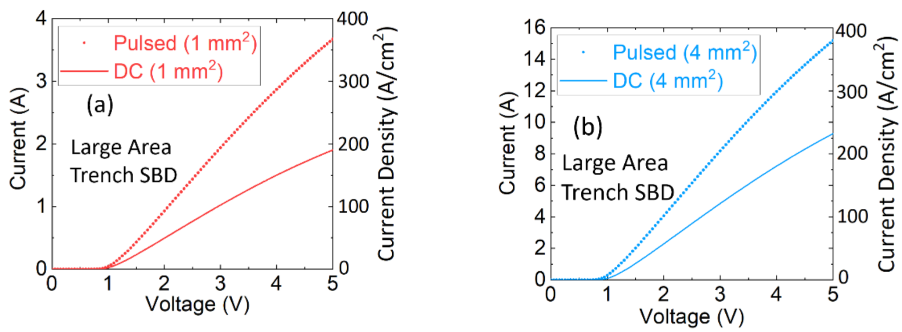

Fig. 3 IV characteristics of three types of SBDs (small area ~ 200x 200 µm²)

Fig. 4 DC and pulsed IV characteristics of (a) 1mm² and (b) 4 mm² large area SBD.

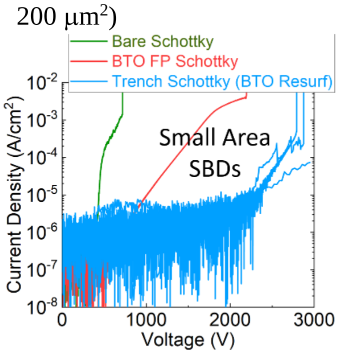

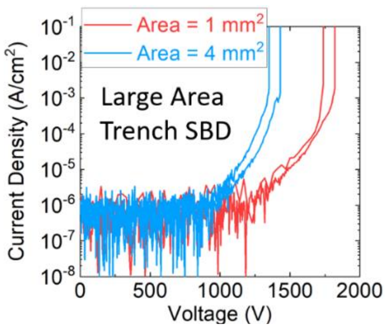

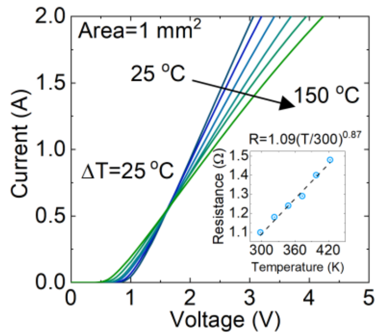

Fig. 5 Reverse IV and breakdown characteristics of the small area SBDs.

Fig. 6 Reverse IV and breakdown characteristics large area trench SBDs.

Fig. 7 Temperature Dependent IV Characteristics. The inset shows temperature dependence of the R_{on} and the power law fitting.

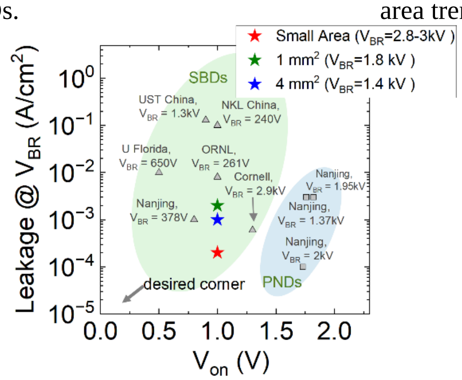

Fig. 8 Benchmark plots showing V_{on} vs $I_{Leakage}$ at breakdown for state-of-the-art β-Ga_2O_3 SBDs

Table I Summary of the performance parameters of high current (> 1 A) β-Ga_2O_3 SBDs

Device Type	Area (mm²)	Current @ (V_{on} + 2V) (A)	V_{on} (V)	V_{BR} (V)	$R_{on\text{-}sp}$ (mΩ-cm²)	$I_{Leakage}$@V_{Br} (A/cm²)
Normal SBD (U Florida) JVST. A 39, 013406 (2021).	115	45	0.7	240	-----	-----
FP SBD (Virginia Tech) IEEE Trans. Power Electron. 36, 8565 (2021).	9	20	0.8	700	6.75	-----
NiO JTE SBD (UST China) IEDM. 2022, 210 (2022).	0.78	3	0.9	1300	4.7	0.13
FP JBS (NKL China) IEEE Trans. Power Electron. 36, 6179 (2020).	1	1.7	1	700	7.6	0.005
This Work	**1**	**1 (DC) 2 (Pulsed)**	**1**	**~ 1800**	**~ 10.6**	**0.001**
This Work	**4**	**5 (DC) 9 (Pulsed)**	**1**	**~ 1400**	**~ 10.6**	**0.002**

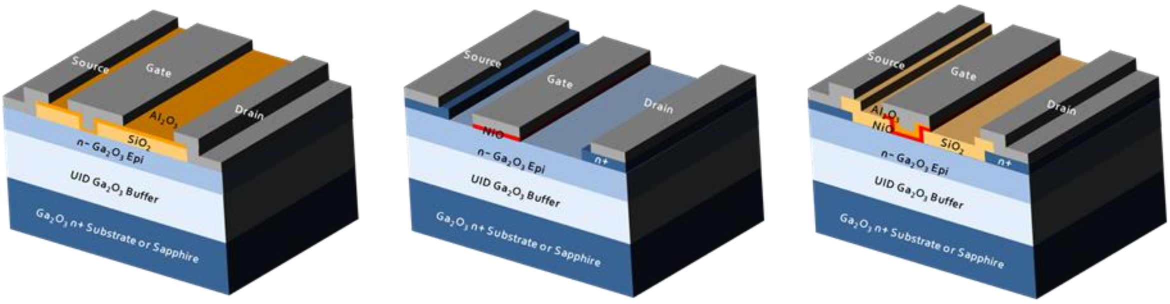

(a) Structure A (b) Structure B (c) Structure C

Fig. 1 Cross-sectional schematics of Ga_2O_3 MOSFETs

Table. 1 Electrical measurement results for each structure

	Structure A	Structure B	Structure C
Threshold Voltage	-50V	3V	30V ↑
Breakdown Voltage	201V (@Vgs -50V)	481V (@Vgs 0V)	613V (@Vgs 0V)

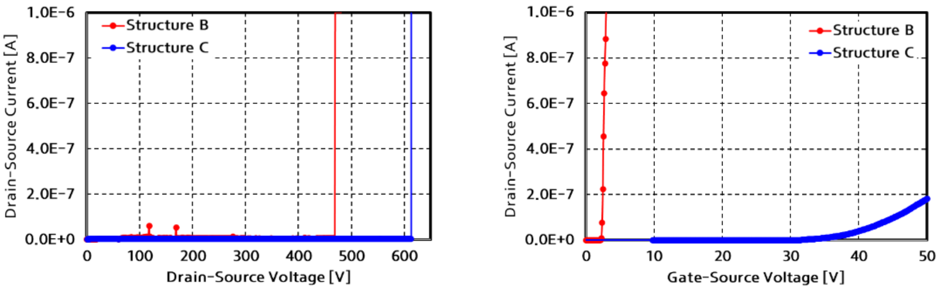

(a) Breakdown Voltage (b) Threshold Voltage

Fig. 2 Electrical measurement results

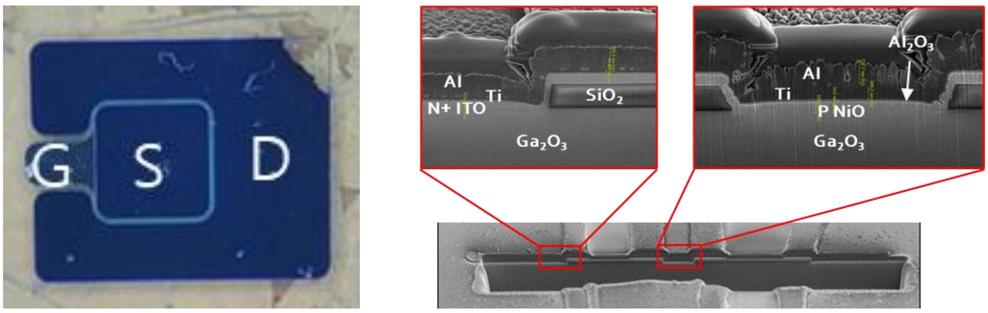

Fig. 3 Fabricated Ga_2O_3 MOSFET and cross section analysis result

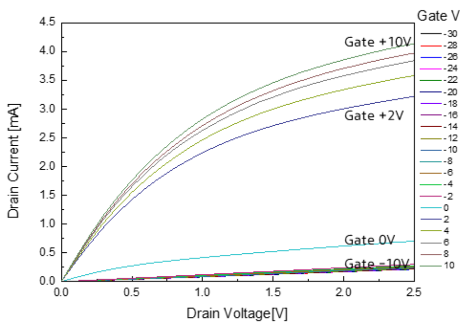

Fig. 4 $I_{DS} - V_{DS}$ curve

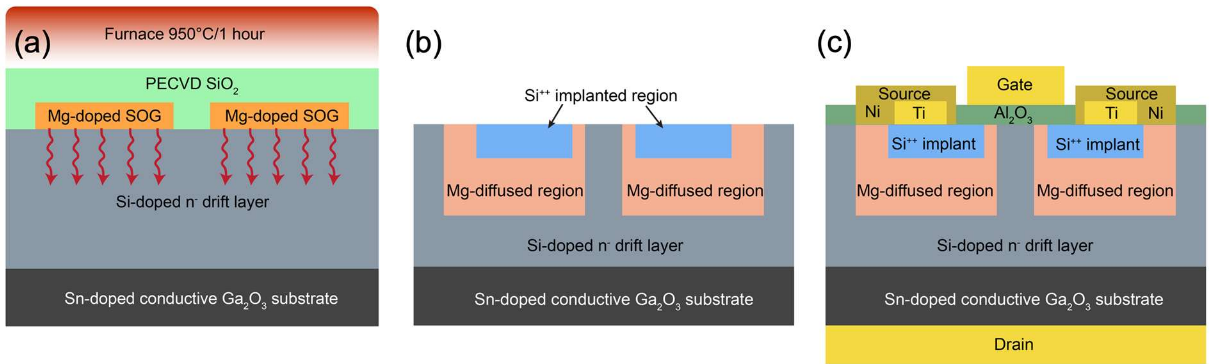

Fig. 1. Fabrication process flow of the β-Ga_2O_3 VDBFET. (a) shows the patterned Mg-SOG diffusion doping process; (b) shows the schematic after the source Si^+ ion implantation; (c) shows the cross-section schematic of the final fabricated device.

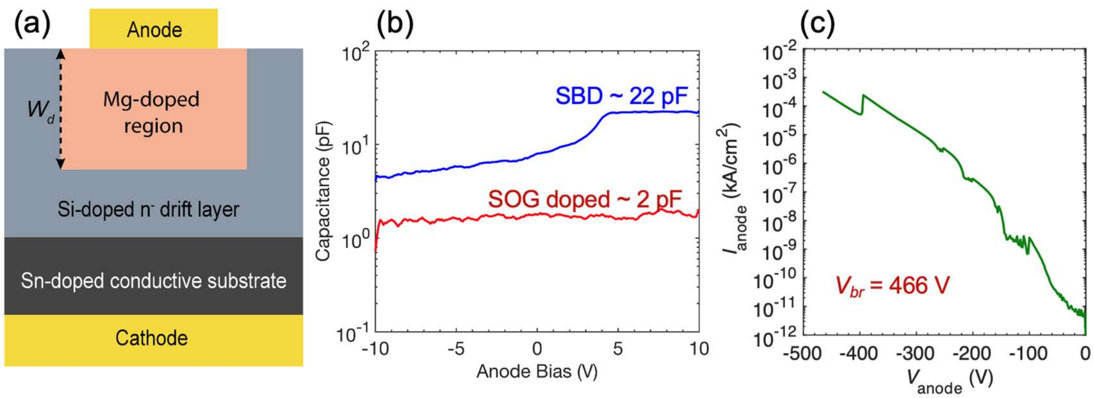

Fig. 2. (a) The metal-isolation-semiconductor (MIS) test structure used for CV analysis shown in (b) and the IV analysis shown in (c).

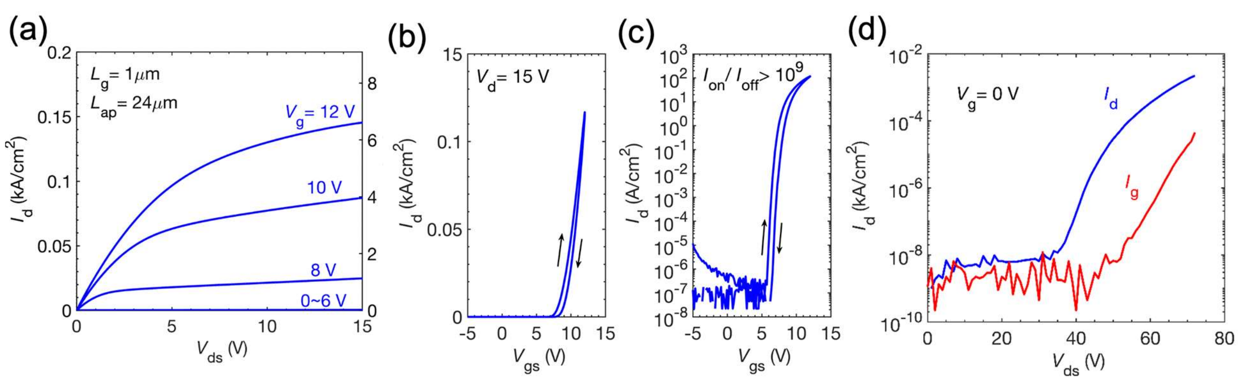

Fig. 3. Representative (a) output IV characteristic, transfer characteristic in (b) linear, (c) log scale and the breakdown characteristic of the fabricated Ga_2O_3 VDBFET.

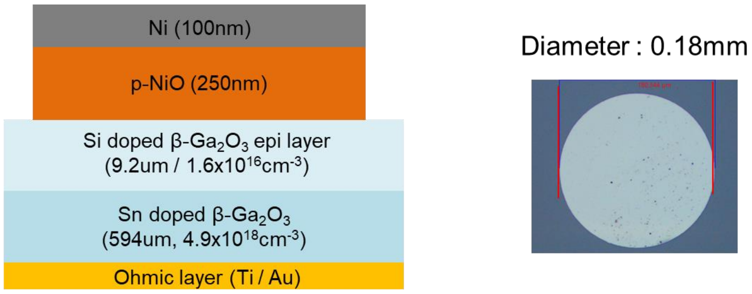

Fig.1. Schematics of vertical pn heterojunction diode

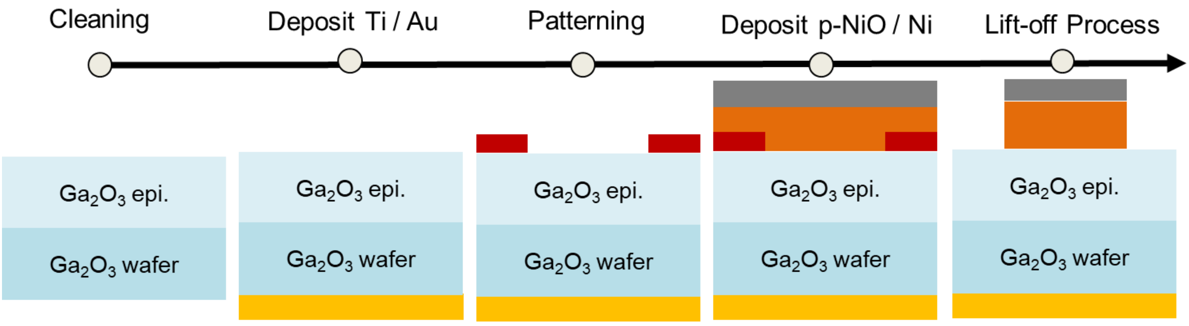

Fig.2. Vertical pn heterojunction diode fabrication process

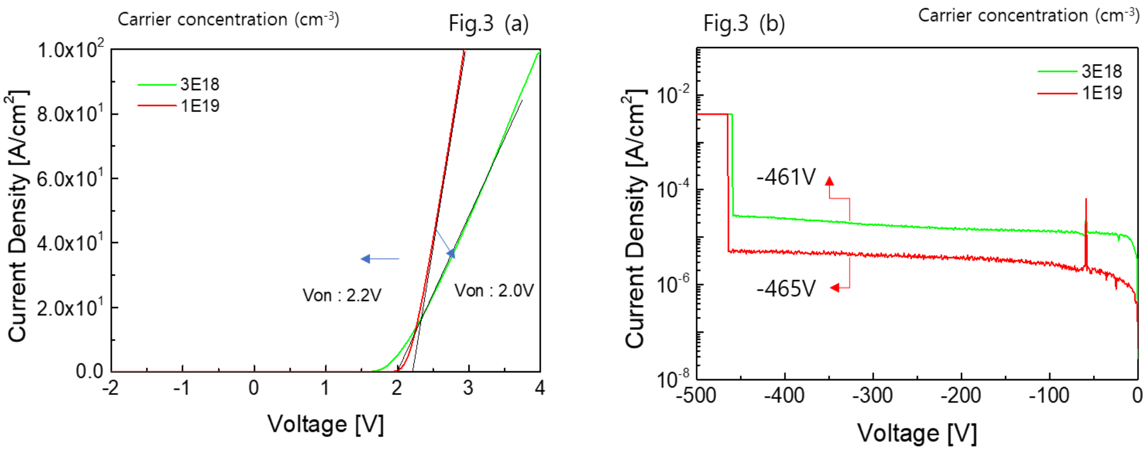

Fig.3(a) The J-V curve of pn diode as a function of carrier concentration

Fig.3(b) The Breakdown voltage of pn diode as a function of carrier concentration

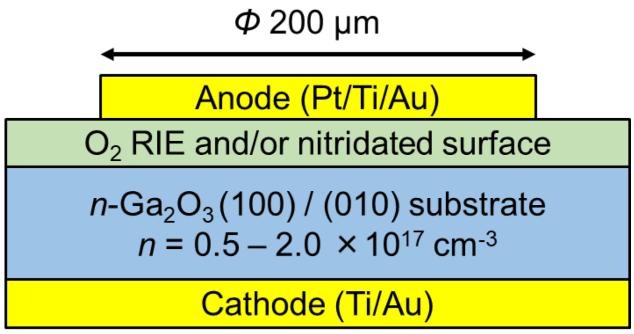

Figure 1 Cross-sectional schematic of β-Ga_2O_3 SBD structures.

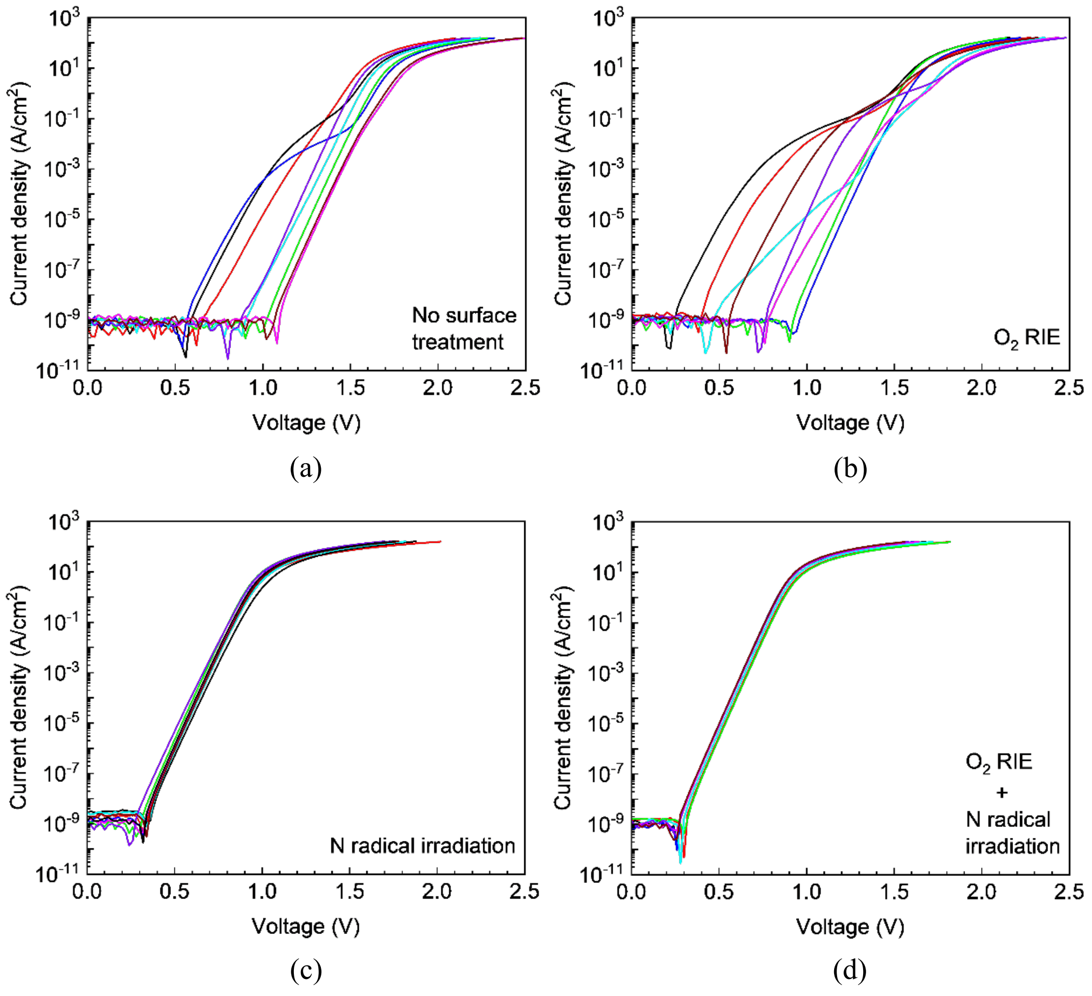

Figure 2 Forward *J*–*V* characteristics of β-Ga_2O_3 (100) SBDs fabricated on four different treated substrates: (a) no surface treatment, (b) O_2 RIE, (c) N radical irradiation, (d) O_2 RIE followed by N radical irradiation.

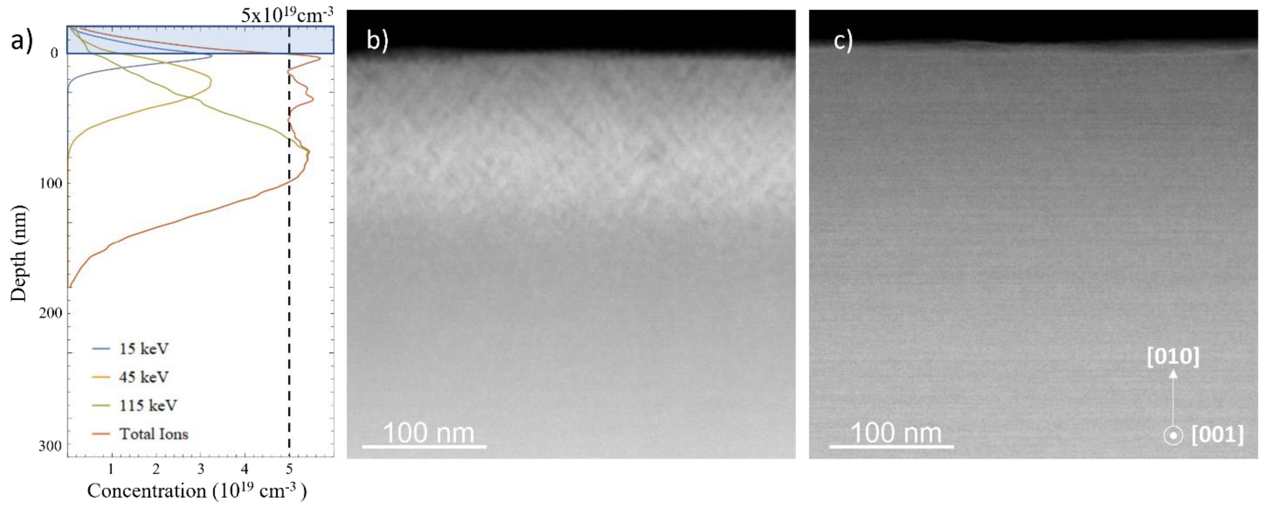

Figure 1: a) Implant conditions of room temperature control sample at Si concentration $5x10^{19}cm^{-3}$. b) HAADF STEM image of control sample showing region of visible damage from Si implantation. c) HAADF-STEM image of control sample after annealing at 950 °C for 20 minutes under high purity nitrogen showing full recovery of lattice with no visible damage remaining.

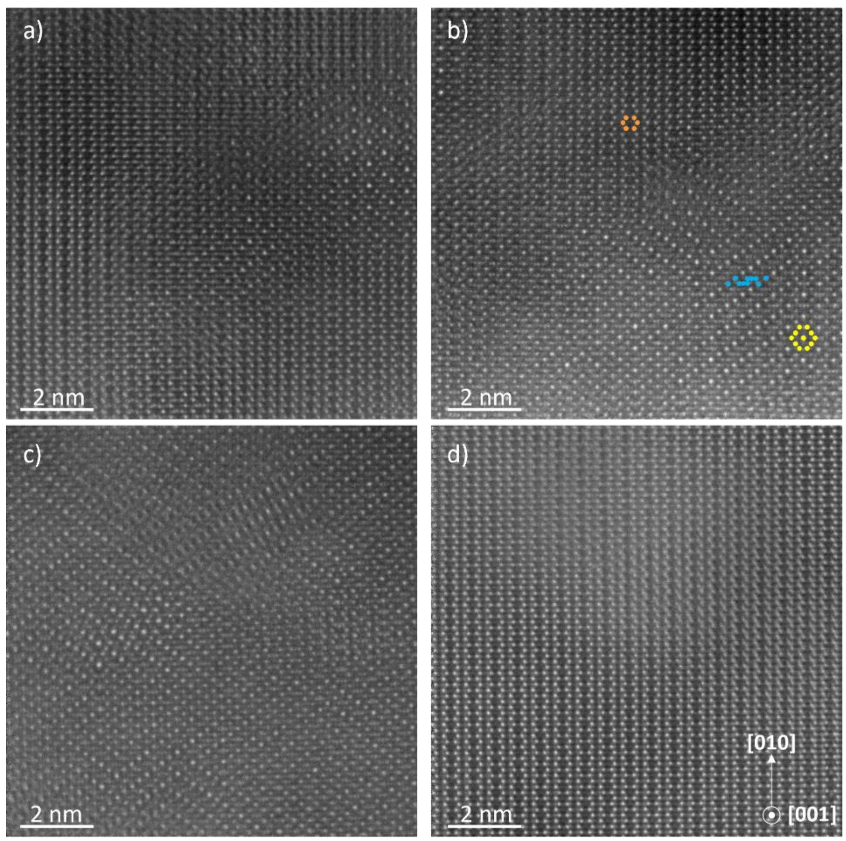

Figure 2: HAADF-STEM image of Si implanted β-Ga_2O_3 viewed along the [001] direction for various implant concentrations. a) Room temperature box to $5x10^{19}cm^{-3}$. b) Room temperature implant to $1x10^{20}cm^{-3}$. c) Implant at 77K to $5x10^{19}cm^{-3}$. a) Heated implant at 600 °C to $1x10^{20}cm^{-3}$. a)-c) shows mixture of β phase and γ phase. The β phase projection is overlayed in orange, γ phase in yellow, and overlapping γ phase sheets in blue. All images taken within the first 50 nm from sample surface, except d) taken within the first 100nm.

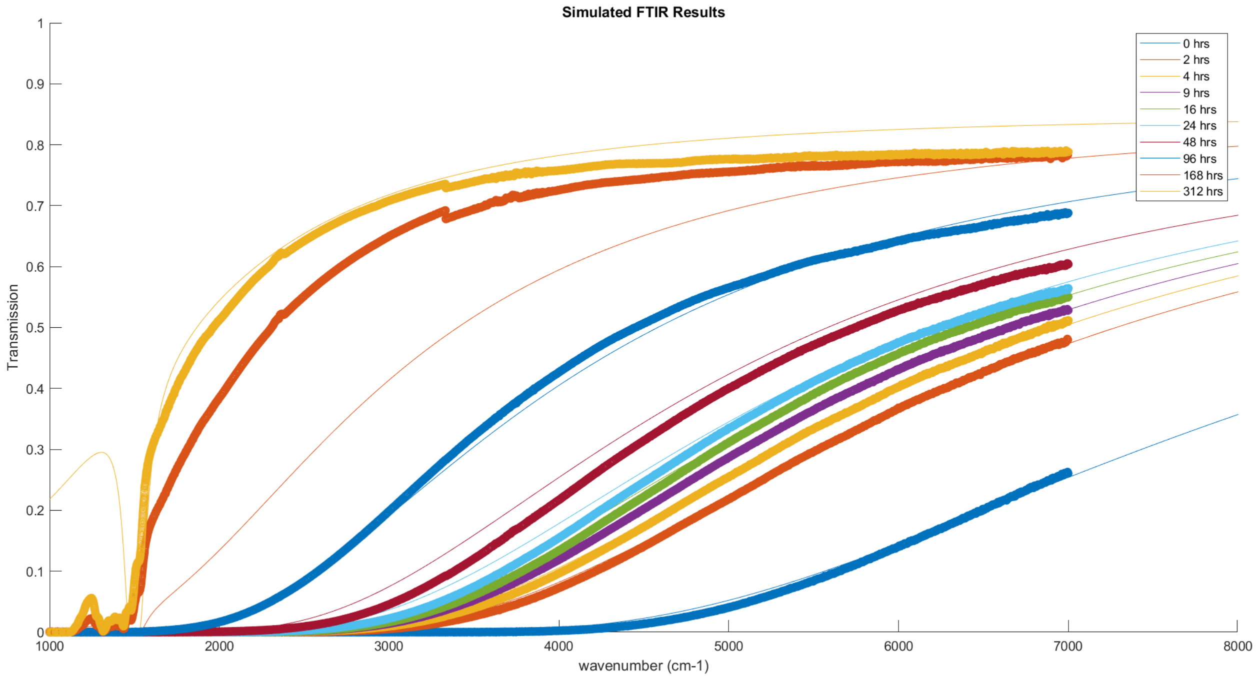

Measured (thick) and simulated (thin) FTIR transmission through Sn-doped Ga_2O_3 sample annealed at 1000 °C for the indicated times assuming a particular combination of fast-but-limited and slow compensating defect introduction process.

Case 1.

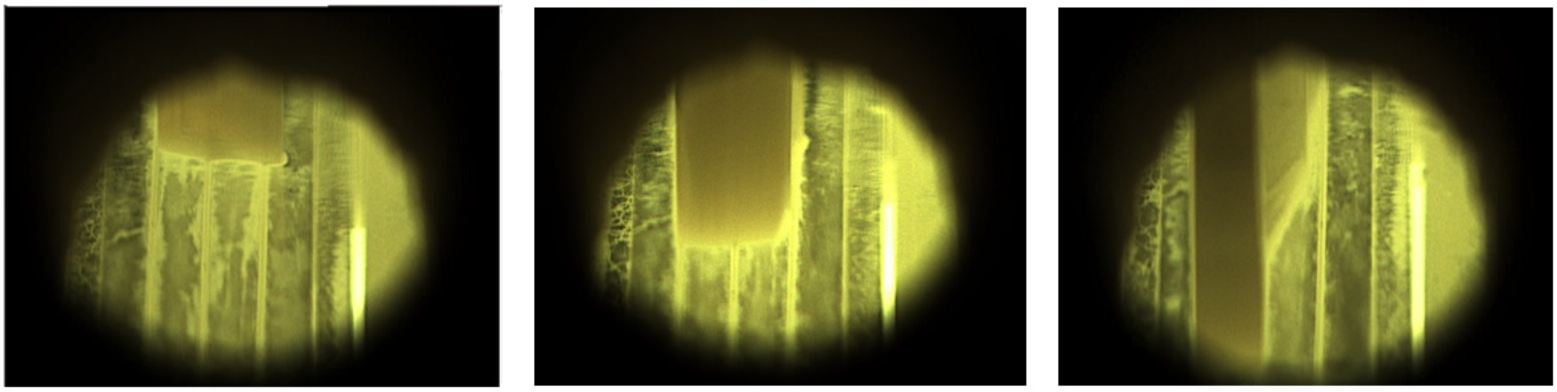

Case 2.

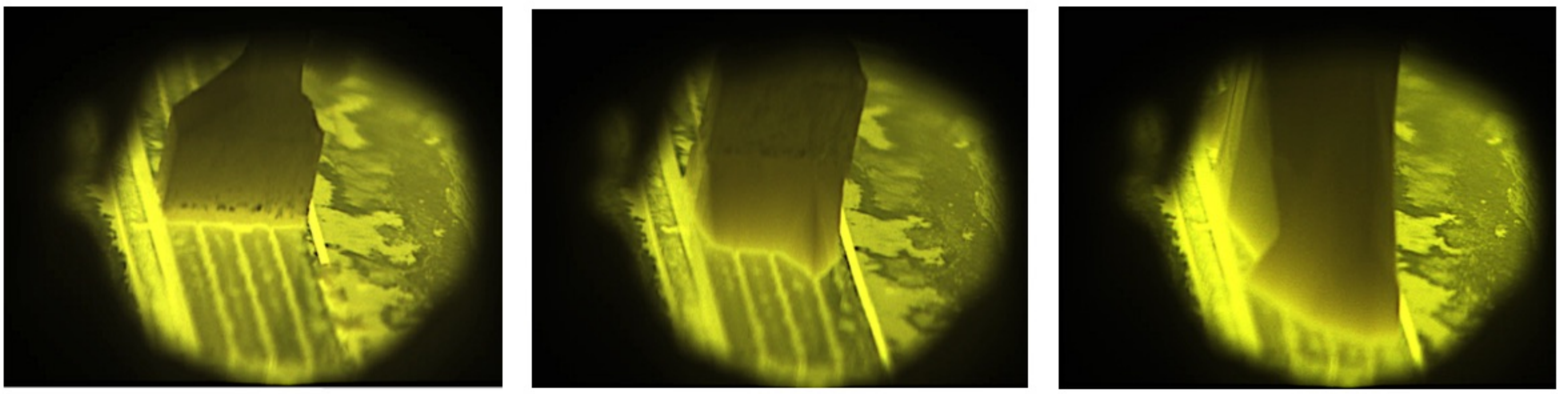

Case 3.

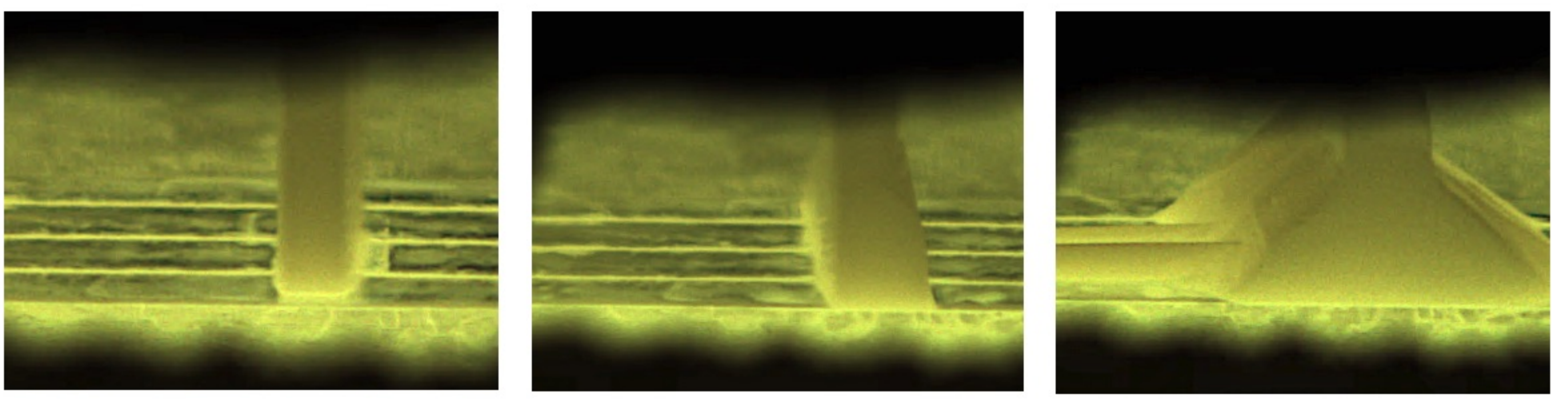

Case 4.

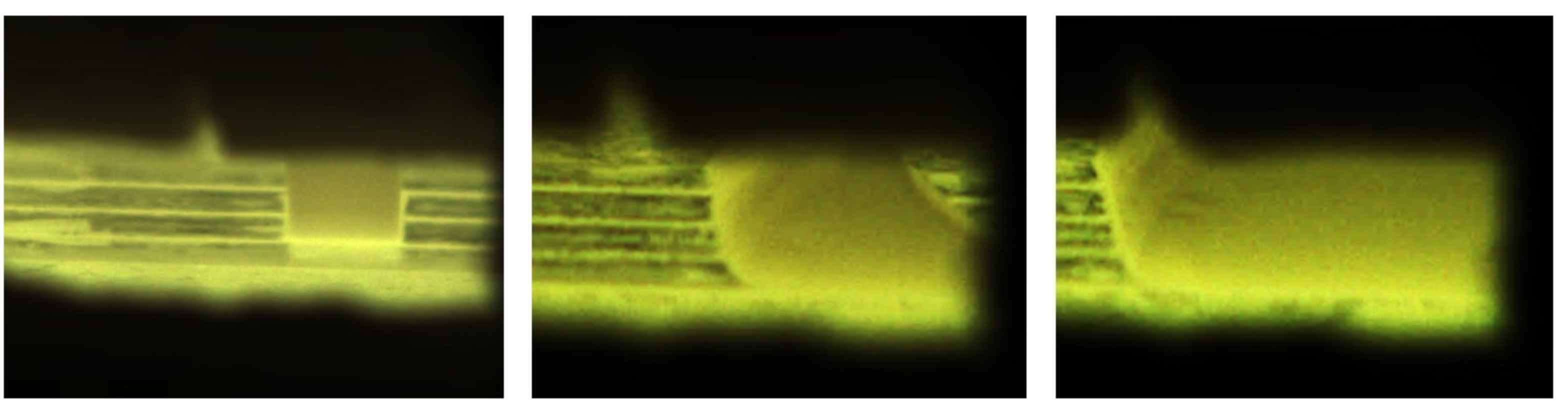

Figure is the process monitoring screen. Case 1. If both of the temperature gradients in the diameter and thickness direction are large, it grows into a thin single crystal only in one to two slits**. Case 2.** Polycrystals occurred with excessively fast growth in one slit, if the temperature gradient in the diameter direction is large but the temperature gradient in the thickness direction is small. **Case 3.** Polycrystals occurred if the temperature gradient in the diameter direction is small but the temperature gradient in the thickness direction is large. **Case 4.** Stable and thick single crystal had grown, when both of the temperature gradients in the diameter and thickness directions are small.

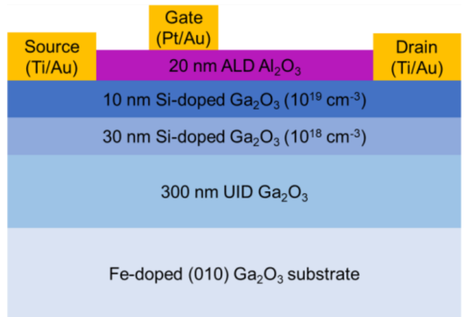

Figure 1. Cross-sectional schematic of the β-Ga_2O_3 MOSFET.

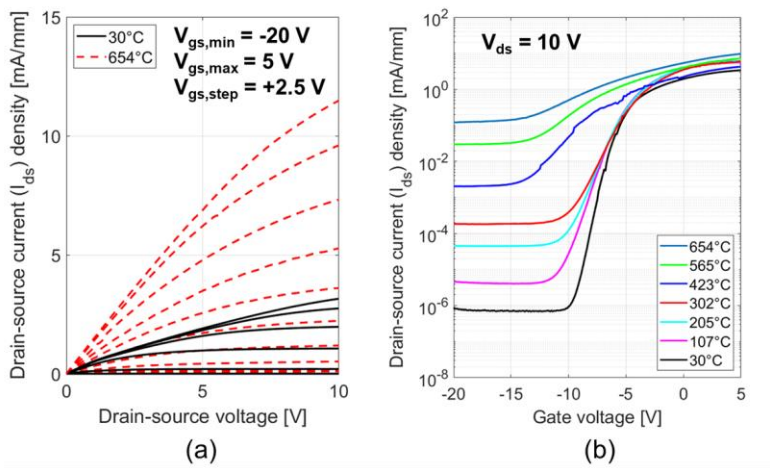

Figure 2. (a) DC output characteristics of a β-Ga_2O_3 MOSFET at 30 °C and 654 °C. (b) DC transfer characteristics of a β-Ga_2O_3 MOSFET from 30 °C to 654 °C.

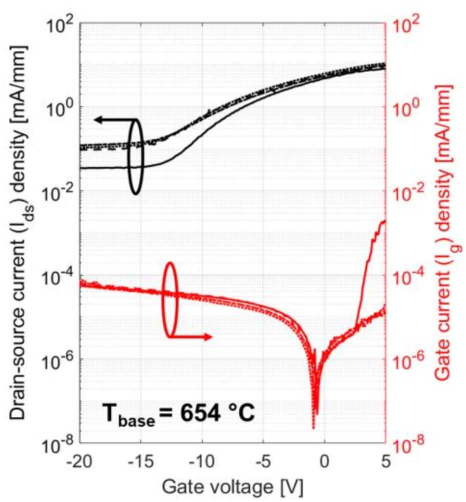

Figure 3. DC transfer characteristics of four different β-Ga_2O_3 MOSFETs operating with a base temperature of 654 °C. The left axis shows the drain-source current density (I_{ds}) and the right axis shows the gate current density (I_g).

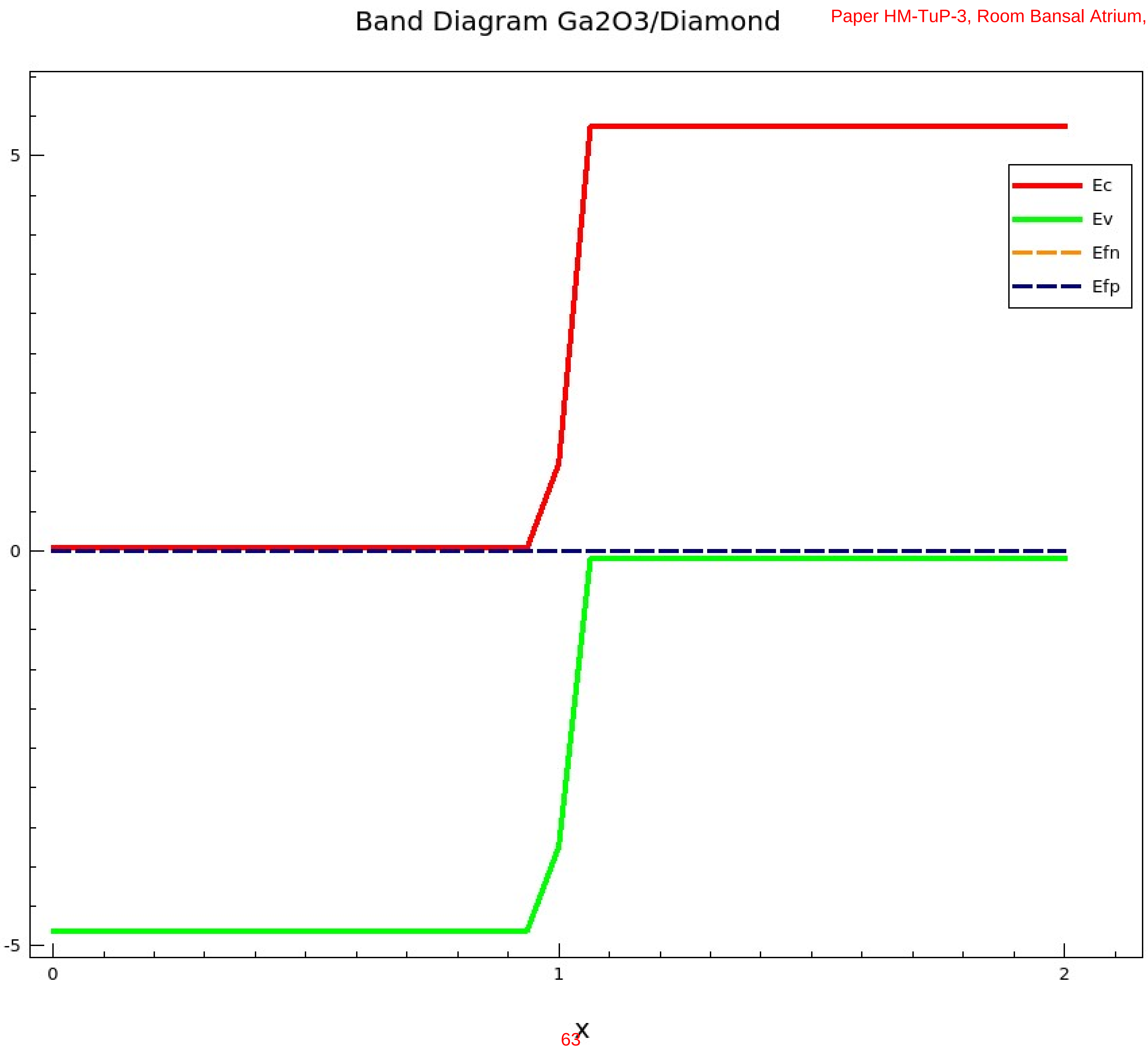
Band Diagram Ga2O3/Diamond
5
0
-5
0
1
2
X
Ec
Ev
Efn
Efp

GOX 2023
6th U.S. Workshop on Gallium Oxide (GOX 2023)
Heterogeneous Material Integration

Mirchandani[1]

[1]*Syrnatec Inc.,95 Pond PL, Middletown, Connecticut 06457-8736, United States*

Table 1 : Radiation Effects between Ga2O3 and Si MOSFETs

Radiation Type	Si MOSFET	Ga_2O_3 MOSFET
Total Ionizing Dose And	Atomic change in lattice: • Carrier concentration altered	Strong bond, reinjection of carriers from Al_2O_3/Al_2N_4 interface • Carrier concentration in 2DEG less affected
Displacement Damage	Metal Oxide layer traps charge: • Threshold voltage changes	Field Effect Transistor: • No oxide layer to trap charge
Single Event Effects	SE Gate Rupture (SEGR) • Catastrophic failure	SE Gate Rupture (SEGR) • No Catastrophic failure observed
	SE Burn Out (SEB) • Catastrophic failure	SE Burn Out (SEB) • Catastrophic failure
Conclusion	Bulkier die to meet tolerance levels	Almost no die change, mainly packaging
	Very susceptible to radiation	Very tolerant to radiation
	High FOM: low performance	Low FOM: good performance

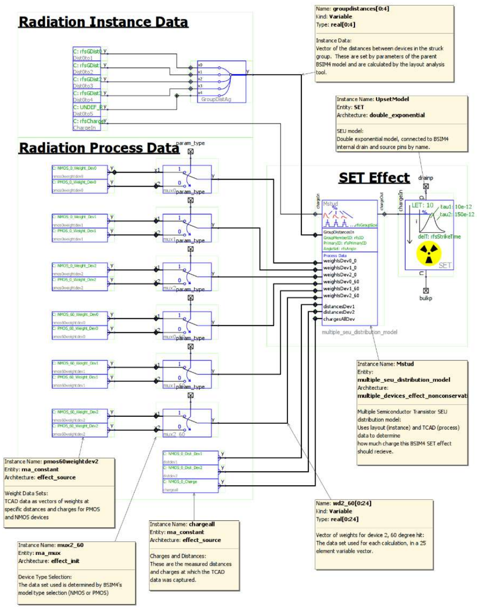

Figure 2: Radiation Modelling

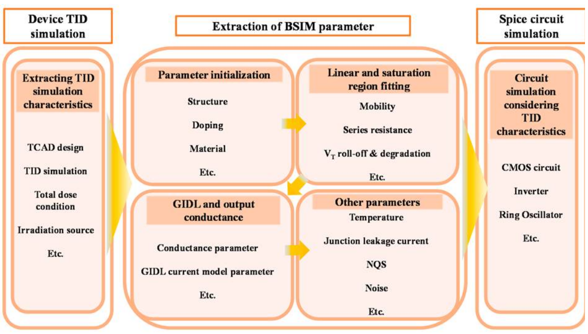

Figure 3: Flow chart of the simulations for TID

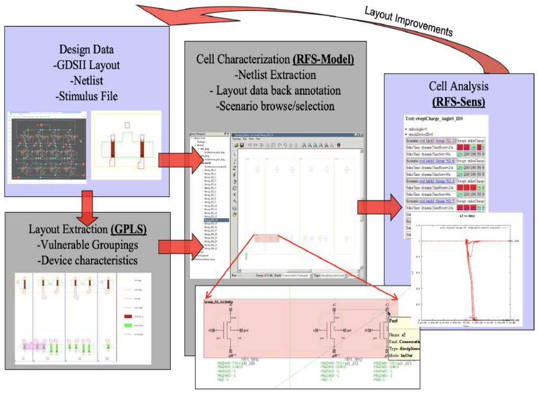

Figure 4: Design Analysis Approach

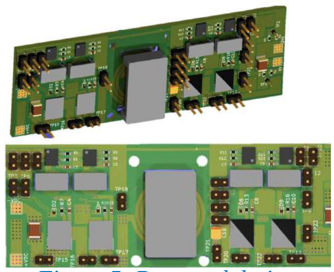

Figure 5: Proposed design

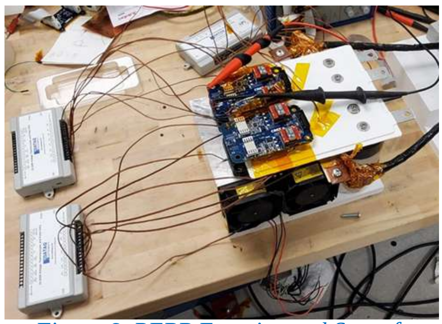

Figure 6: PEBB Experimental Setup for Steady State Thermal Characterization

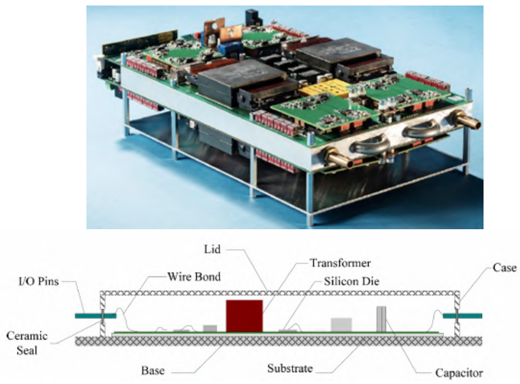

Figure 7: Package for DC-DC converter

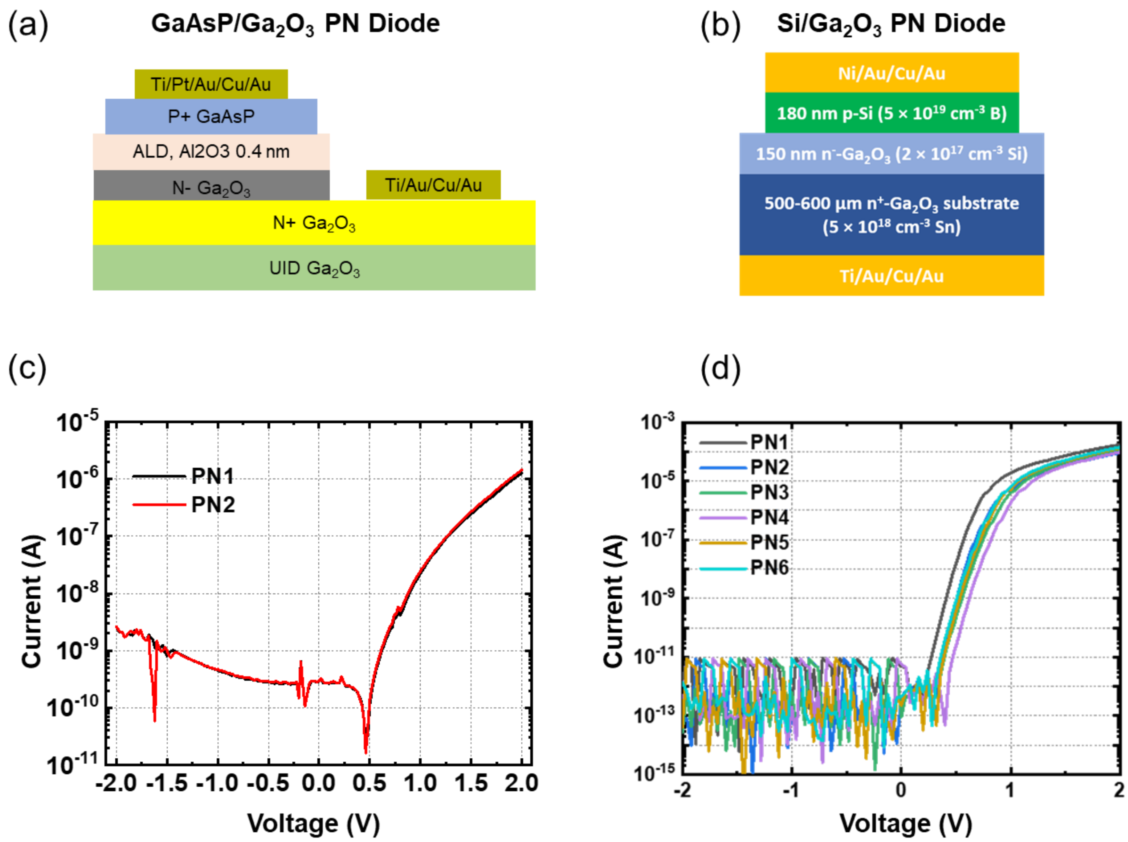

Fig. 1. Device schematics and I-V curves of GaAsP/Ga_2O_3 and Si/Ga_2O_3 PN diodes.

Table 1. Summary of the diode characteristics of GaAsP/Ga_2O_3 and Si/Ga_2O_3 PN diodes.

	GaAsP/Ga_2O_3 PN Diode	Si/Ga_2O_3 PN Diode
On/off Ratio	10^3	10^7
Ideality Factor	1.35	1.13

Performance and traps of Ga_2O_3 Schottky barrier diodes with mesa structure

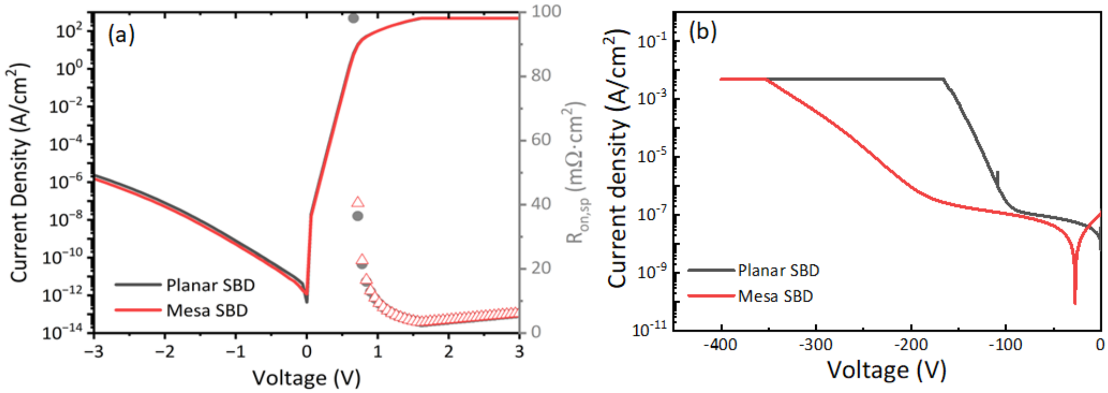

Fig. 1. (a) Current-voltage characteristics of Ga_2O_3 SBD with general and mesa structure. (b) Reverse biased current characteristics of SBDs.

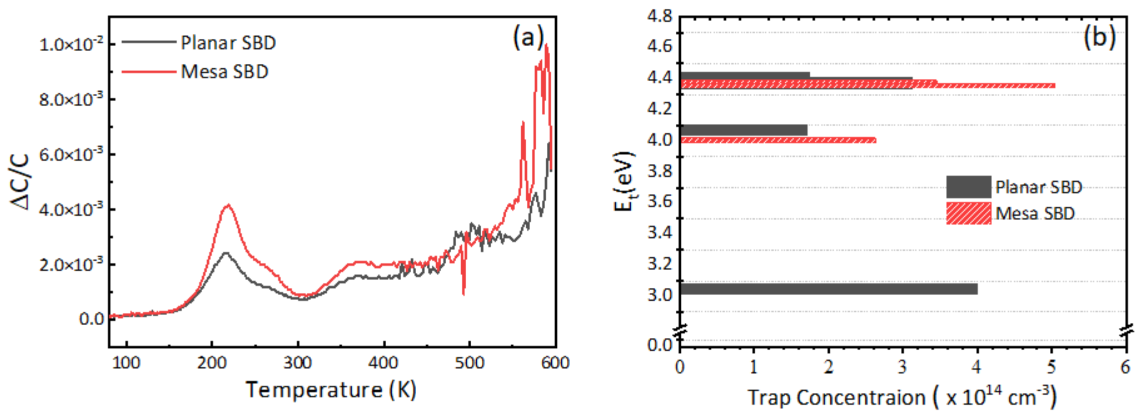

Fig. 2. (a) DLTS spectra of Planar and Mesa SBD. (b) Summary of the trap energy of SBDs from result (a).

References

[1] Tarplee, M. C., Madangarli, V. P., Zhang, Q., & Sudarshan, T. S. (2001). Design rules for field plate edge termination in SiC Schottky diodes. IEEE Transactions on Electron Devices, 48(12), 2659-2664.

[2] Identification and Suppression of Majority Surface States in the Dry-Etched β-Ga2O3. J. Phys. Chem. Lett. 2022, 13, 7094−7099

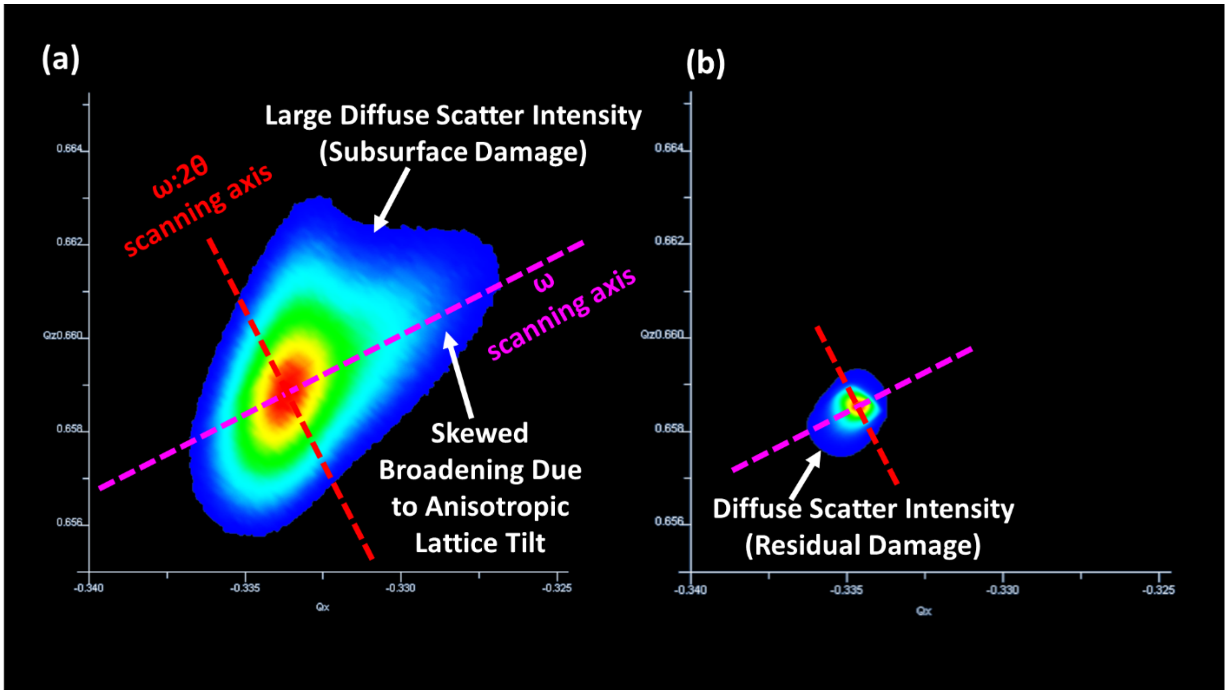

Figure 1. X-ray diffraction reciprocal space maps using the (420) reflection in glancing incidence geometry for the (a) wafer sliced rough substrate and (b) chemical mechanical polished substrate. The ω and ω:2θ scanning axes are marked, which correspond to the directions of peak broadening due to lattice tilt and strain, respectively. The wafer sliced substrate has severe lattice damage, which is predominately lattice tilt in character. The diffuse scatter intensity is also skewed, likely indicative of the anisotropic mechanical response to deformation (damage) in β-Ga_2O_3. After polishing, the diffuse scatter intensity is significantly reduce, which corresponds to removal of subsurface damage.

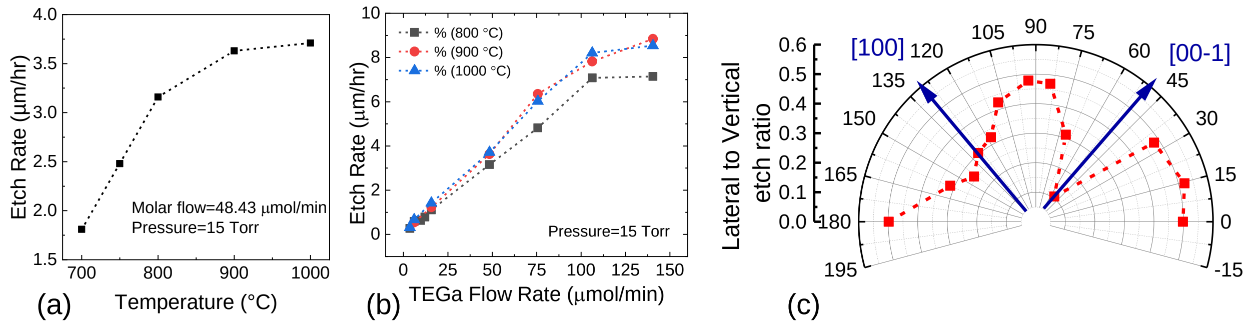

Fig.1 (a) Etch rate as a function of substrate temperature, (b) Etch rate as a function of TEGa flow rate, (c) lateral to vertical etch rate as a function of in-plane orientation.

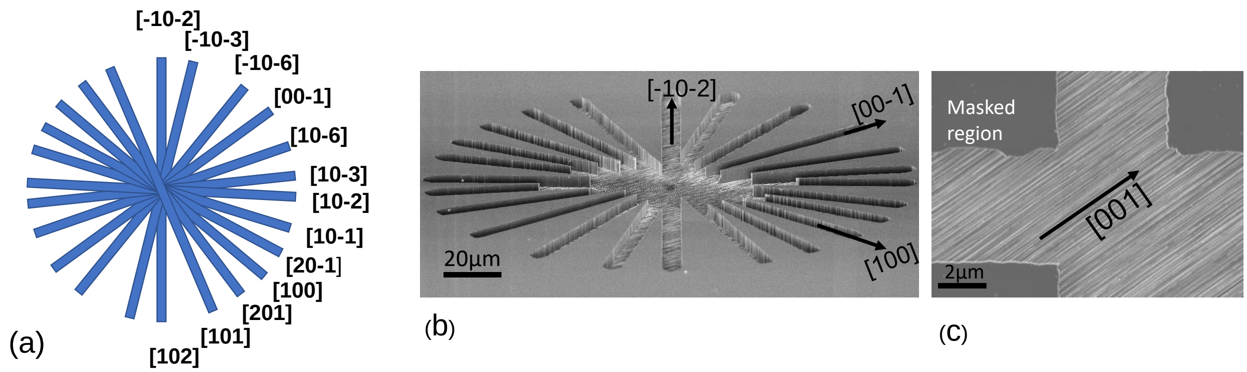

Fig.2 (a) Schematic of the spoke-wheel structure used to study in-plane etch anisotropy. (b) Tilted SEM image of the etched spoke-wheel pattern. (c) SEM image of (010) β-Ga_2O_3 surface after Ga etching.

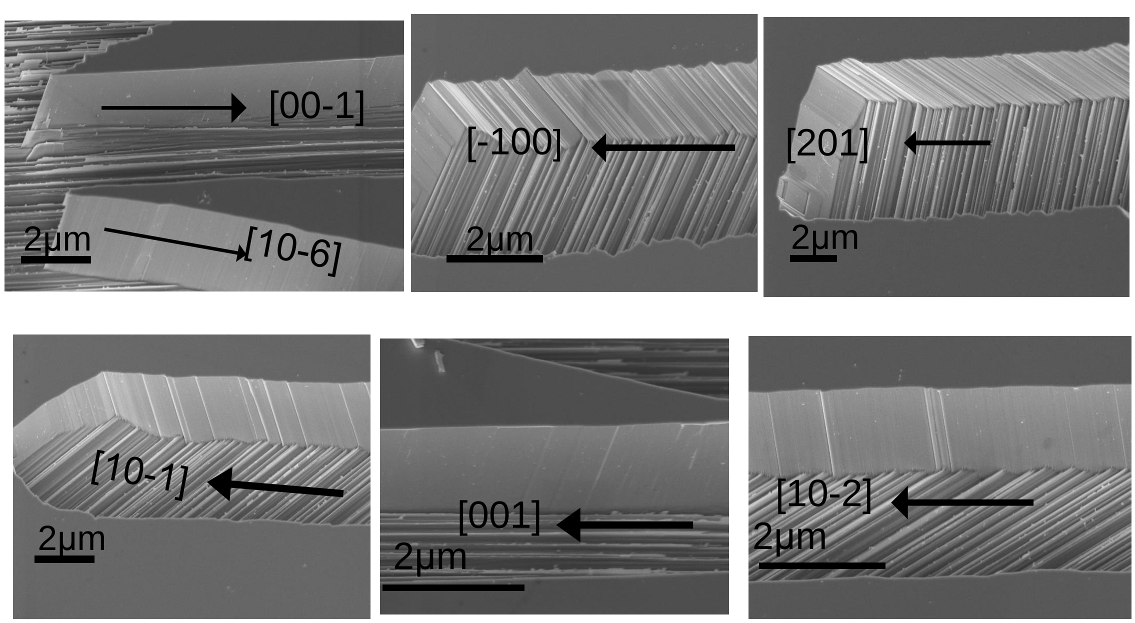

Fig.3 SEM images of various etched sidewall planes formed on the (010) β-Ga_2O_3 sample. The in-plane orientation of the trenches is shown. See Fig.2 (a) and (b) for the schematic of trench orientation.

Supplemental Information:

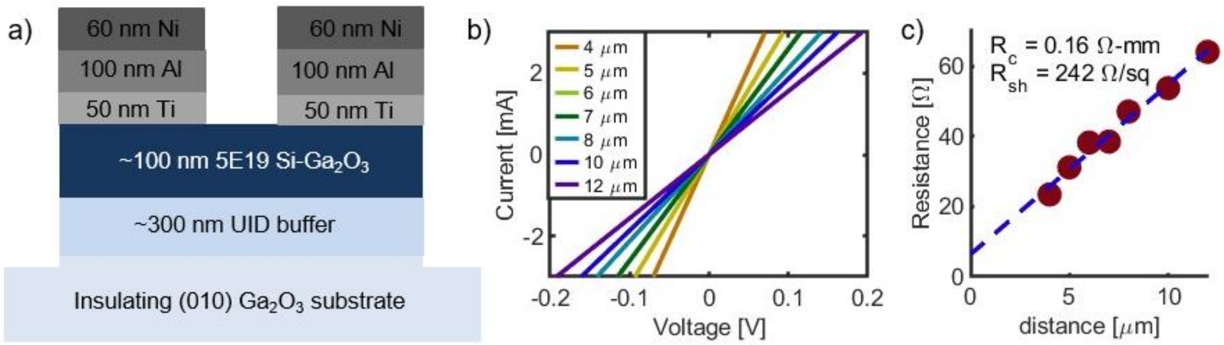

Figure 1: a) Layer structure of the implanted sample. b) IV measurements of alloyed contacts display linear, canonical ohmic behavior. c) TLM extraction of contact resistance gives R_c of 0.16 Ω-mm and sheet resistance of 242 Ω/□.

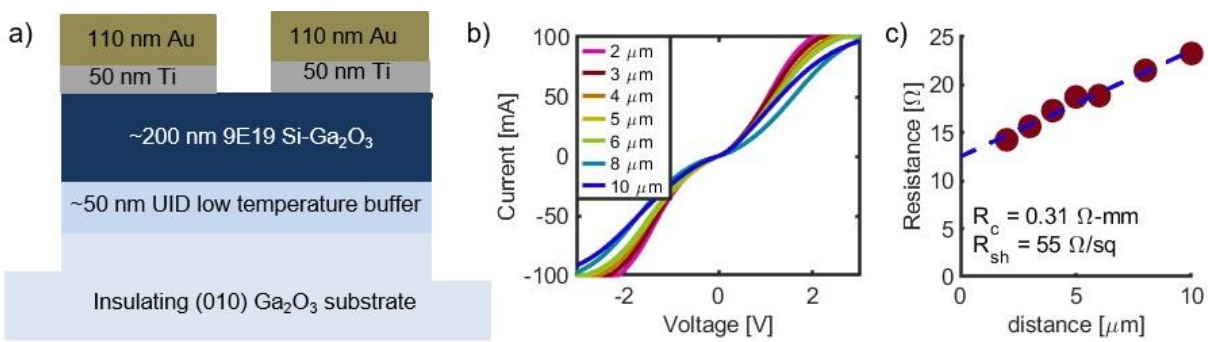

Figure 2: a) Layer structure of non-alloyed contacts to MOCVD grown n+ Ga_2O_3. b) IV measurements display leaky-Schottky behavior. c) TLM extraction of R_c at 50 mA applied current. The extracted R_c is 0.31 Ω-mm, and the R_{sh} is 55 Ω/□.

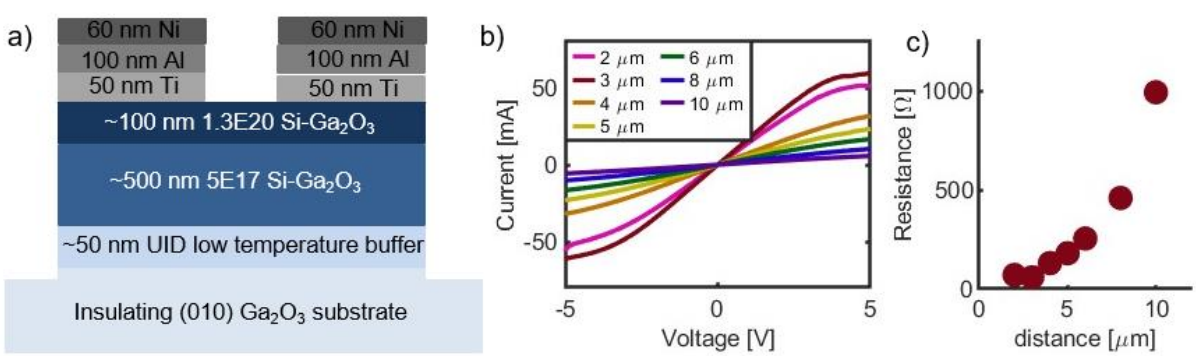

Figure 3: a) Layer structure of alloyed contacts to MOCVD grown n+ on n- Ga_2O_3. b) IV measurements show canonical ohmic behavior with current saturation due to thermal effects and source choke. c) Spatially non-uniform contacts make extraction of R_c by TLM methods impossible.

Acknowledgements: We acknowledge support from the AFOSR Center of Excellence Program FA9550-18-1-0529. This work was performed in part at the Cornell Nanoscale Facility, a NNCI member supported by NSF grant NNCI-2025233.

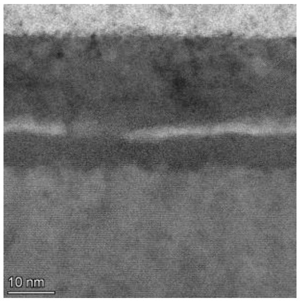

Figure 1: HAADF TEM image showing the ZnO film as-deposited. As will be seen in later slides, the white line shows the intermixing of the ZnO and Ga_2O_3

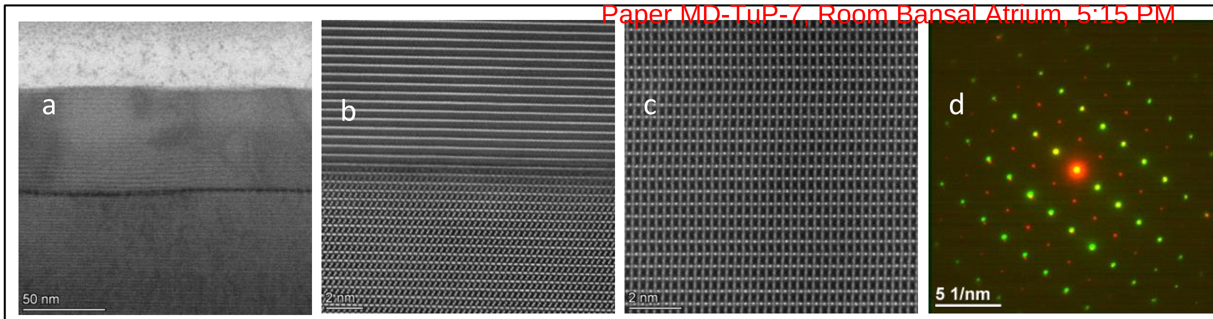

Figure 2: HAADF TEM images of the $ZnGa_2O_4$ film zooming in on the film (a) and interface with the Ga_2O_3 substrate (b) The color-mapped SAED is shown where red is the $ZnGa_2O_4$ film, and green is the Ga_2O_3 substrate. The crystallinity of the film is visible even in the TEM images, and the SAED confirms its semi-concurrent match to the Ga_2O_3 substrate

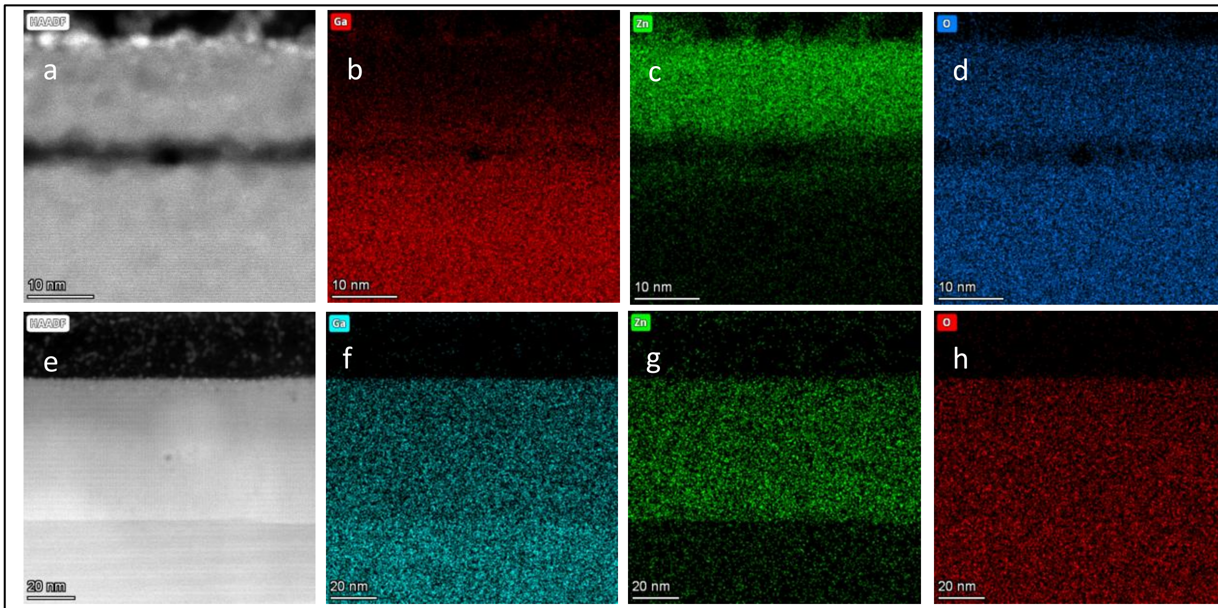

Figure 3: EDS from the TEM scans of the film as-deposited (a-d) and after annealing (e-h) show the intermixing of the ZnO and Ga_2O_3. Even at ALD temperatures, there is some intermixing, and the dark line can be seen as the interface of deposition with some Ga and Zn on either side. After high temperature annealing, the ZnO and Ga_2O_3 have fully mixed to form $ZnGa_2O_3$

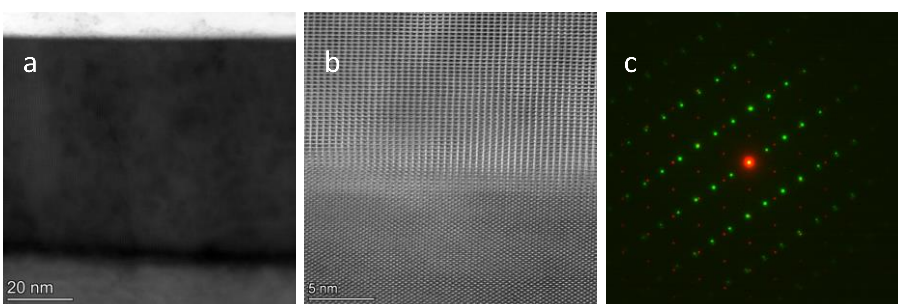

Figure 4: The large area view (BF-S) (a), interface zoom (HAADF) (b), and color-mapped SAED overlay of the $ZnGa_2O_4$ film on a (001) Ga_2O_3 substrate show that this technique works for the (001) orientation

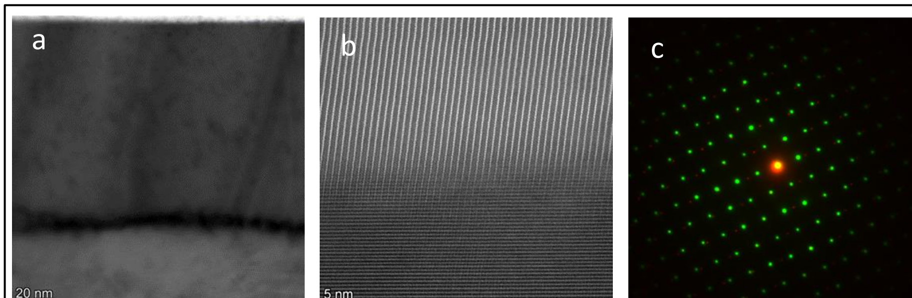

Figure 5: The large area view (BF-S) (a), interface zoom (HAADF) (b), and color-mapped SAED overlay of the $ZnGa_2O_4$ film on a (010) Ga_2O_3 substrate show that this technique works for the (010) orientation

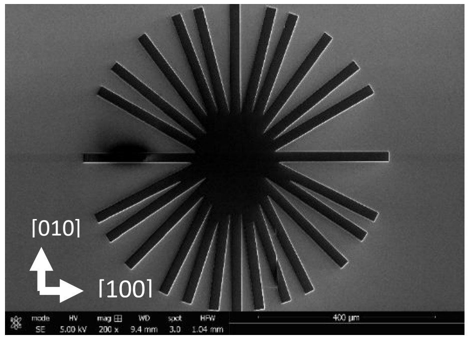

Figure 1. An SEM image of the wagon wheel used in this study following H_3PO_4 etching.

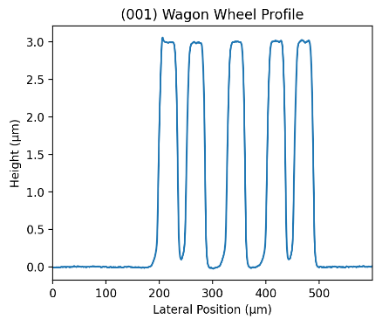

Figure 2. A line profile of the wagon wheel following H_3PO_4 etching.

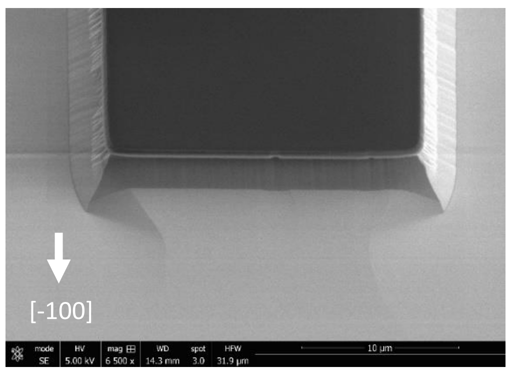

Figure 3. A spoke oriented along the [-100] direction.

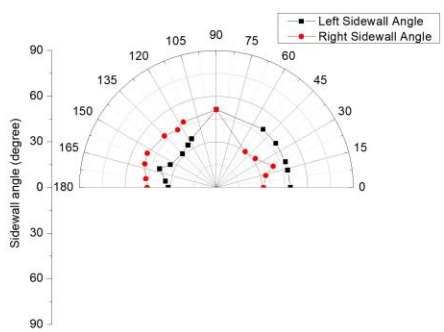

Figure 4. A polar plot showing the sidewall angles for spokes.

Supplementary information: **Electronic band structure and excitons in $LiGaO_2$ and $LiGa_5O_8$**

Niloufar Dadkhah, Klichchupong Dabsamut, and Walter R. L. Lambrecht
Department of Physics Case Western Reserve University, Cleveland OH 44106

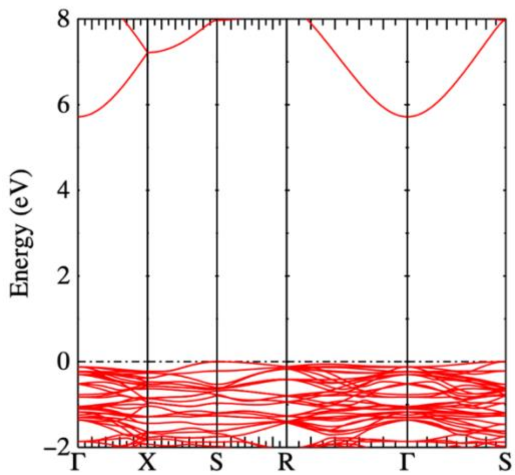

Fig. 1 Band structure of $LiGa_5O_8$ in spinel structure calculated in the QS$GW\Gamma$ method.

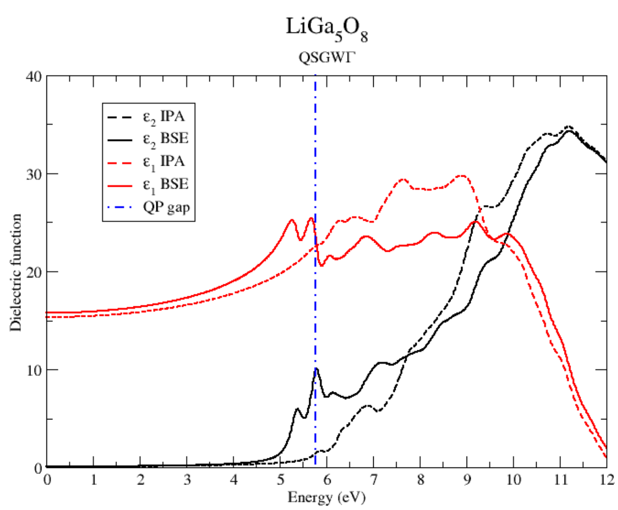

Fig. 2: Real (red) and imaginary (black) part of function of $LiGa_5O_8$, obtained in the Independent Particle Approximation (dashed lines), and the Bethe-Salpeter-Equation approach (solid lines), showing evidence of a strongly bound exciton. The blue dash-dotted line indicates the lowest direct quasiparticle gap.

Two-Dimensional Analytical Modeling of the Surface Potential of a Double-Gate Vertical Fin-Shaped Ga_2O_3 Power Transistor

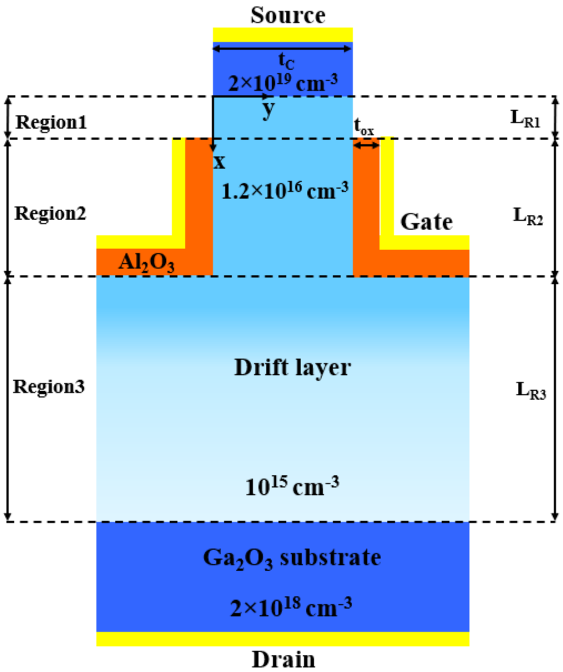

Fig 1: Vertical Ga_2O_3 Device structure used for analytical modeling. The entire unit is divided into three region. The lengths of the depletion region that are created in the source–channel and channel–drain junctions are denoted by L_{R1} and L_{R2}, respectively. The drift layer length is denoted as L_{R3}. The junctions between the source-channel and drain-channel are intended to be abrupt for the sake of simulation.

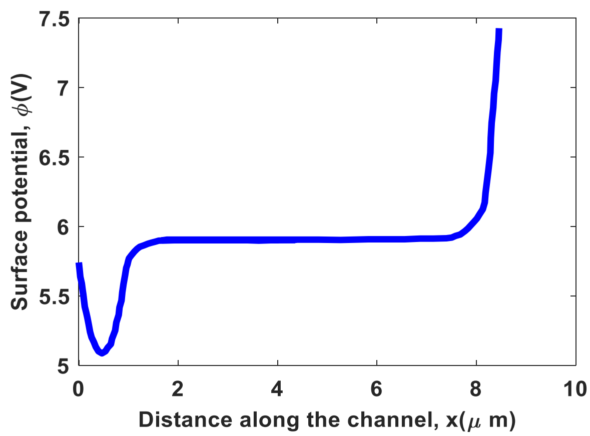

Fig 2: Surface potential of vertical Ga_2O_3 PowerFET. The potential is increased in parabolic manner at the source-channel and channel-drain junction.

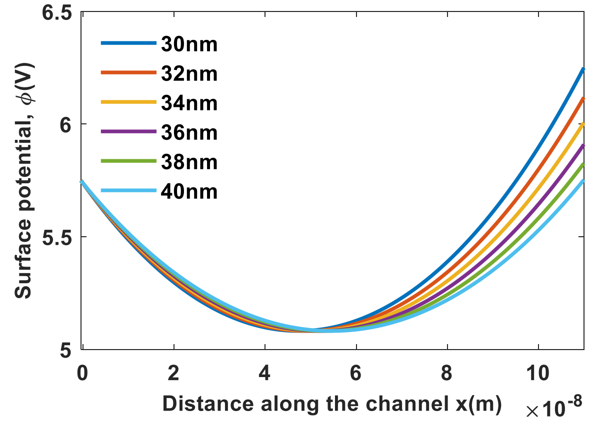

Fig 3: Surface potential profile along the channel with varying oxide thickness. The potential is decreasing as the oxide thickness (t_{ox}) increases, which causes the gate to eventually lose control of the channel.

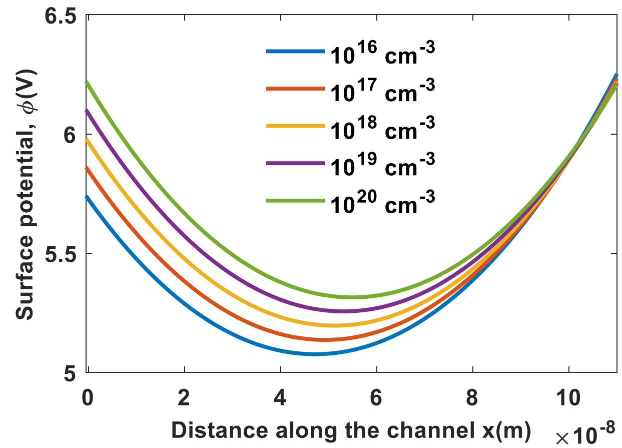

Fig 4. Surface potential profile along the channel for varying doping concentration. The potential on the source-channel junction increases for the same gate-source voltage as the accumulation of charge carrier beneath the channel rises.

Sample	Specific R_C (Ω*cm²)	Mobility (cm²/V·s)	R_{sh} (Ω/sq.)	N_{sh} (cm^{-2})
A (0.3 µm)	1.99×10^{-4}	71	4082	2.15×10^{13}
B (0.5 µm)	1.77×10^{-5}	115	4513	1.20×10^{13}
C (1.0 µm)	2.25×10^{-6}	116	6585	8.12×10^{12}

Table 1. Specific contact resistance from TLM and mobility, sheet resistance, and sheet carrier concentration from room temperature Hall measurements on each MOCVD stack.

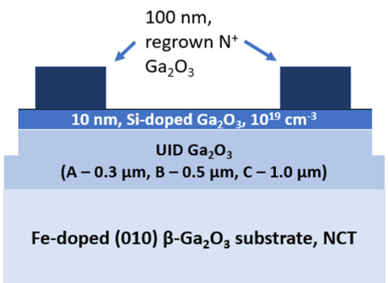

Fig. 1. Cross-section schematic of the MOCVD structures grown on Fe-doped (010) β-Ga_2O_3 substrates from NCT.

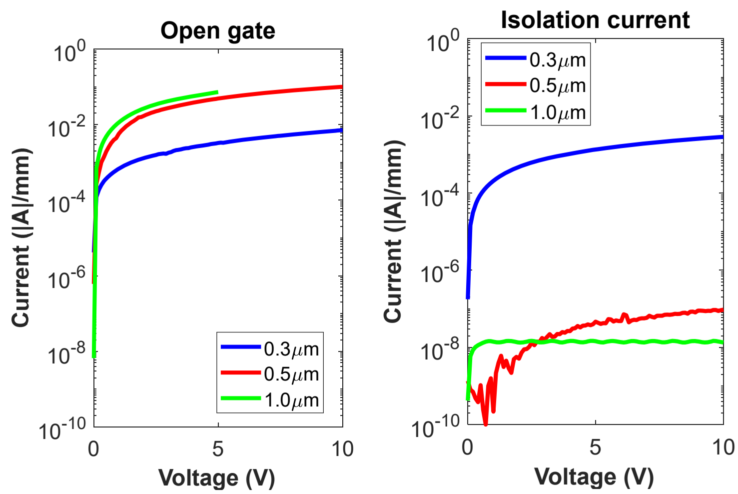

(a) (b)

Fig. 2. (a) Open gate *J-V* characteristics and (b) isolation current of each MOCVD sample (A – blue), (B – red), (C – green).

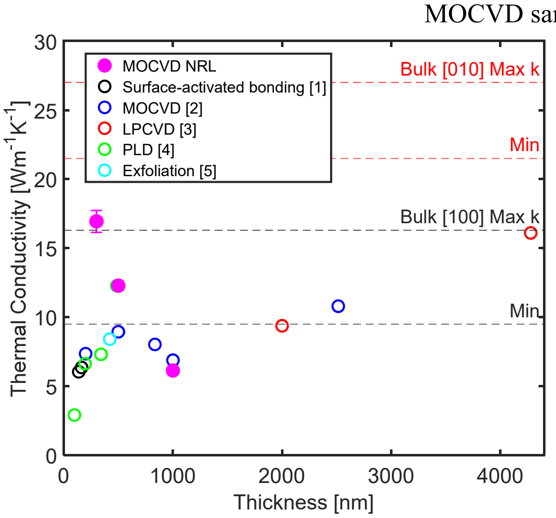

Fig. 2. Thermal Conductivity of this work measured by FDTR compared to literature. References: [1] Z. Cheng et al., ACS Appl Mater Interfaces, vol. 12, no. 40, pp. 44943–44951, Oct. 2020. [2] Y. Song et al., ACS Appl. Mater. Interfaces, vol. 13, p. 38490, 2021. [3] Y. Song et al., ACS Appl. Mater. Interfaces, vol. 13, p. 38490, 2021. [4] N. Blumenschein et al., Oxide-Based Materials and Devices IX (2018). [5] Z. Cheng et al., APL Mater, vol. 7, no. 3, p. 031118, Mar. 2019.

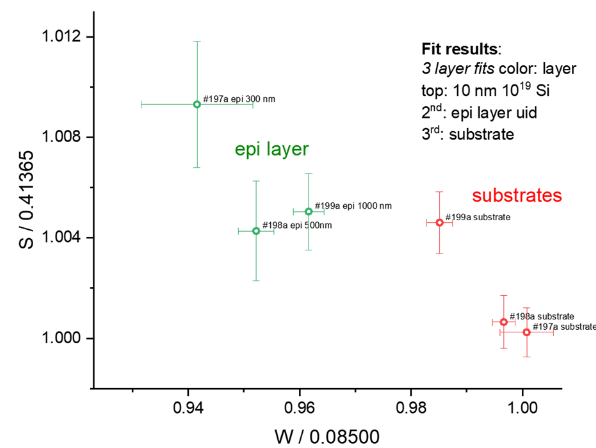

Fig. 3. Normalized S vs. W plot for 3-layer fit of positron annihilation spectra for the three samples.

H.M., M.L. and J.S.L. gratefully acknowledge postdoctoral funding from the National Research Council, Washington DC. Fabrication equipment and support was provided by the NRL Nanoscience Institute and Dr. Brian Downey (NRL). Agnitron β-Ga_2O_3 development work was partially supported

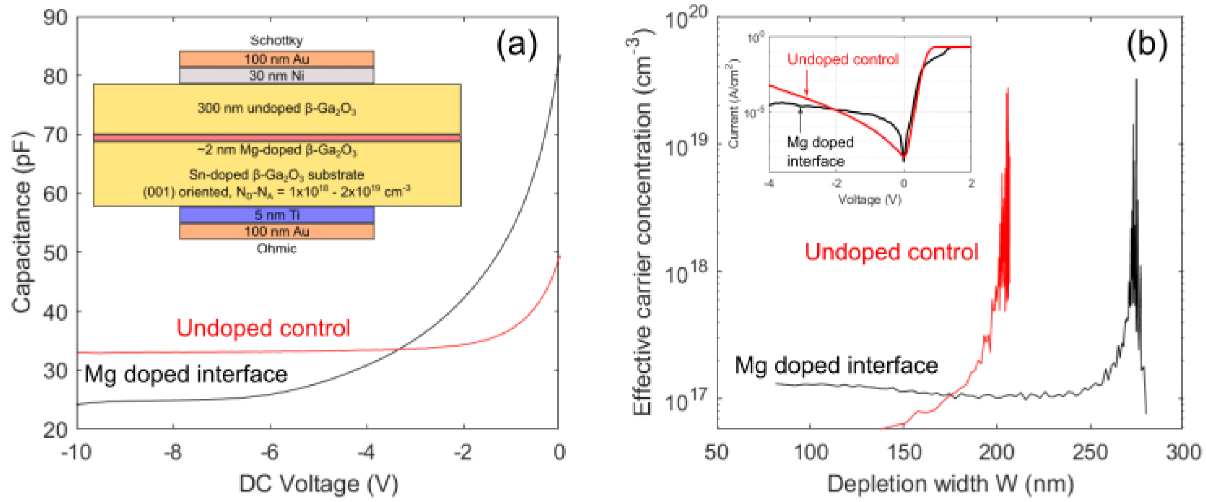

FIG. 1. C-V characteristics of vertical Schottky diodes grown on (001) Sn-doped β-Ga_2O_3 substrates. Schottky contact diameter = 300 µm. (a) Capacitance vs DC voltage for sample counterdoped with 3.8×10^{-9} torr Mg flux (black) and unintentionally doped (UID) control sample (red). Inset: Vertical Schottky diode sample structure. (b) Effective carrier concentration vs depletion width for Mg counterdoped and UID control samples. Inset: Current-voltage curves demonstrating reduced reverse leakage current for Mg counterdoped Schottky diode.

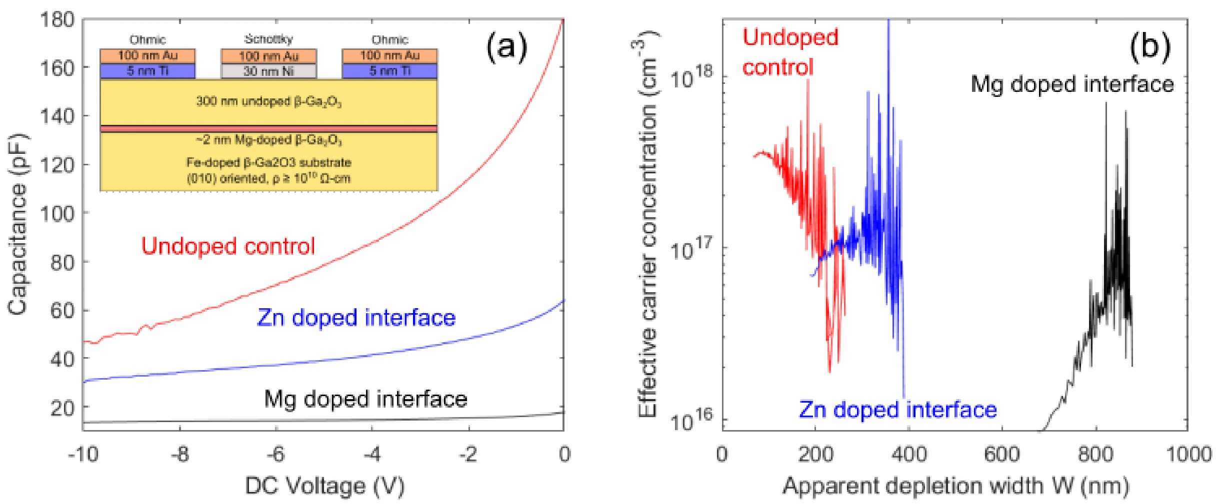

FIG. 2. C-V characteristics of lateral Schottky diodes grown on (010) Fe-doped β-Ga_2O_3 substrates. Schottky contact diameter = 400 µm. (a) Capacitance vs DC voltage for samples counterdoped with 1.0×10^{-8} torr Mg flux (black) and Zn flux (blue) and unintentionally doped (UID) control sample (red). Inset: Lateral Schottky diode sample structure. (b) Effective carrier concentration vs apparent depletion width for Mg and Zn counterdoped and UID control samples. Counterdoping reduces the concentration of uncompensated n-type donors and increases the effective depletion width in lateral β-Ga_2O_3 Schottky devices.

Fig. 1 – Plot of reported mobilities and carrier concentrations for *in-situ* doping methods of β-Ga_2O_3. Results for implant and optimized thermal anneal from this study are shown as blue, red, and yellow dots for MBE β-Ga_2O_3 samples at implant concentrations of 5x10[18], 5x10[19], and 1x10[20] cm[-3], respectively, and green dots for MOCVD β-$(Al_xGa_{1-x})_2O_3$ (x=0.09, 0.1, 0.15). Mobilities and carrier concentrations from Si implant with optimized annealing are highly competitive with *in-situ* doping methods, even for AlGO samples.

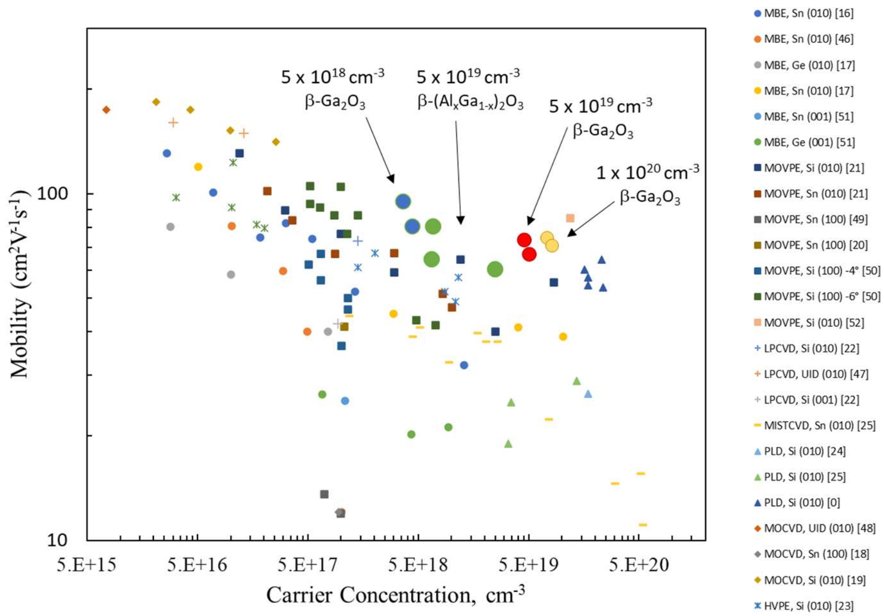

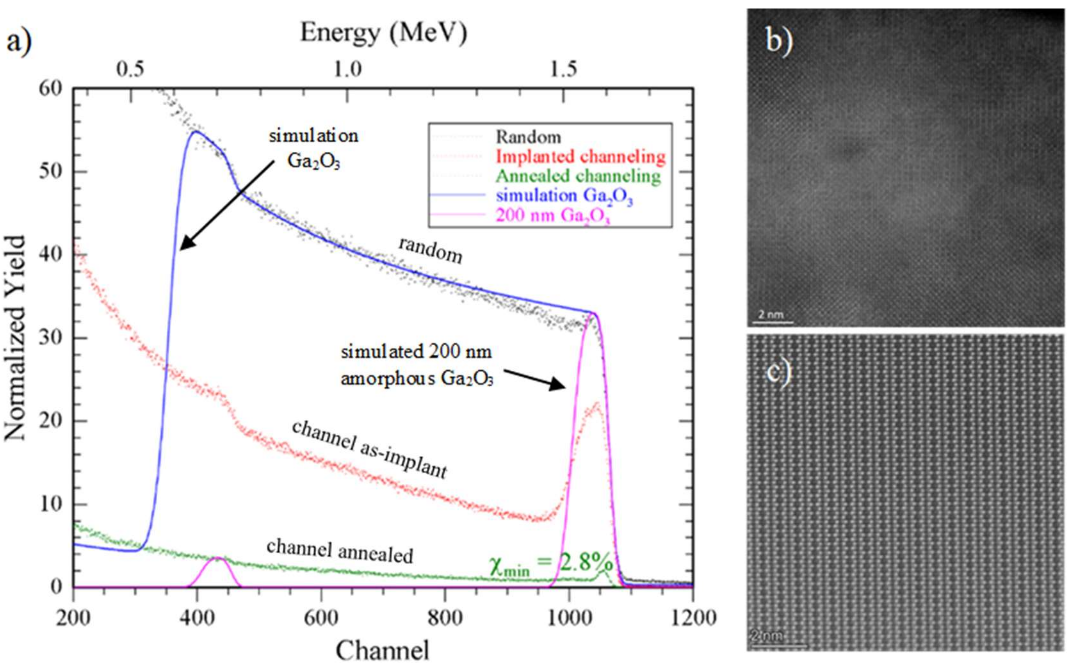

Fig. 2 – (a) RBS/C data showing only partial amorphization of the implant region (red channeling) within the top 200 nm; shown in pink is the expected Ga peak for a fully amorphized 200 nm layer. After annealing, channeling data (green) shows lattice recovery to a near perfect crystal. (b) and (c) show atomic resolution STEM images of the implanted sample showing (b) visible lattice damage and areas of retained crystallinity and (c) fully recovered lattice after annealing at 950 °C for 20 minutes in high purity nitrogen.

Fig. 3 – Plots of (a) sheet resistance, R_s and (b) carrier concentration (cm[-3]), for annealing with controlled amounts (0.25, 2.5, and 25 ppm) of H_2O in otherwise ultra-dry, high purity nitrogen. The increase in R_s is associated primarily with a decrease in carrier concentration (blue points). Subsequent annealing (orange points) in dry N_2 shows partial recovery of carrier density and R_s.

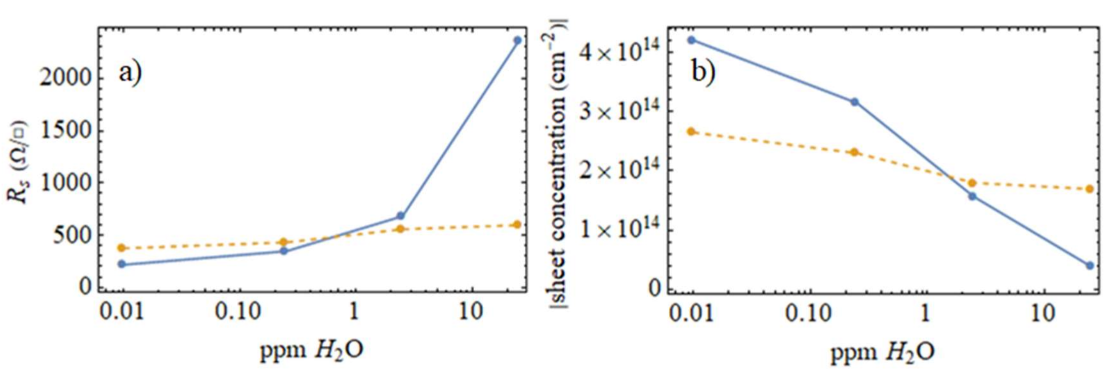

Recent progress of Ga_2O_3 power technology: large-area devices, packaging, and applications

Yuhao Zhang, Virginia Tech, USA   Email: yhzhang@vt.edu

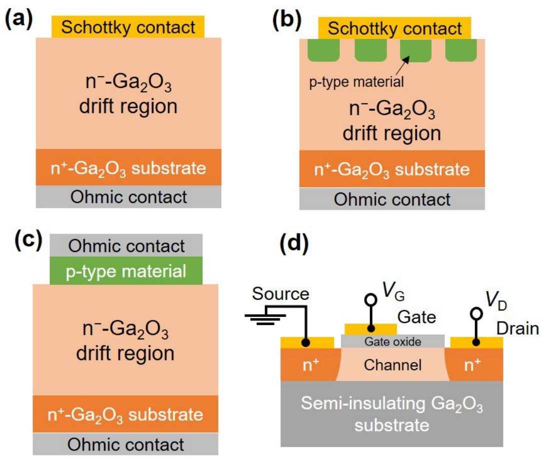

Fig. 1. Schematic of Ga_2O_3 (a) Schottky barrier diodes, (b) junction barrier Schottky diodes, (c) hetero-PN diodes, and (d) MOSFETs that have demonstrated ampere-class performance [1].

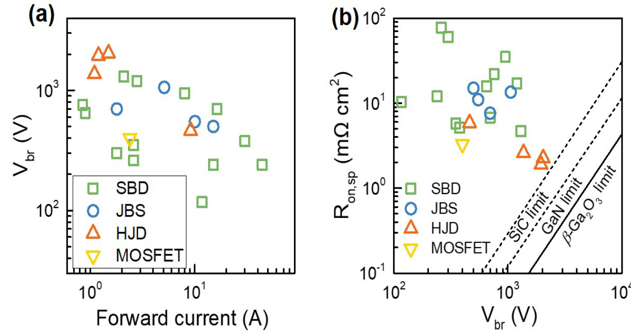

Fig. 2. Summary of (a) breakdown voltage versus forward current trade-off and (b) specific on-resistance versus breakdown voltage trade-off of the reported ampere-class Ga_2O_3 devices [1].

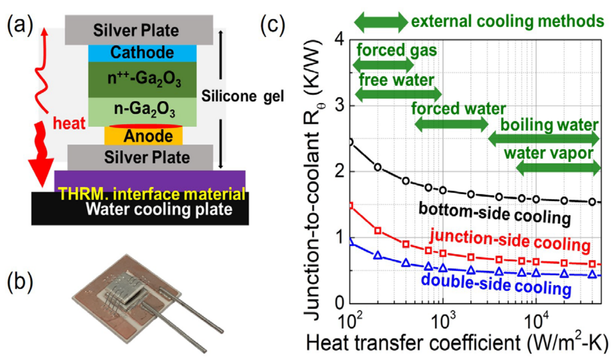

Fig. 3. (a) Schematic of the thermal characterization of a junction-side cooled, packaged Ga_2O_3 Schottky barrier diode on a water-cooling plate [4]. (b) Photo of a fabricated double-side-cooling packaged Ga_2O_3 diode [5]. (c) Junction-to-ambient thermal resistance as a function of heat transfer coefficient (i.e., representative of external cooling method) for bottom-side-cooled, junction-side-cooled, and double-side-cooled Ga_2O_3 devices [5].

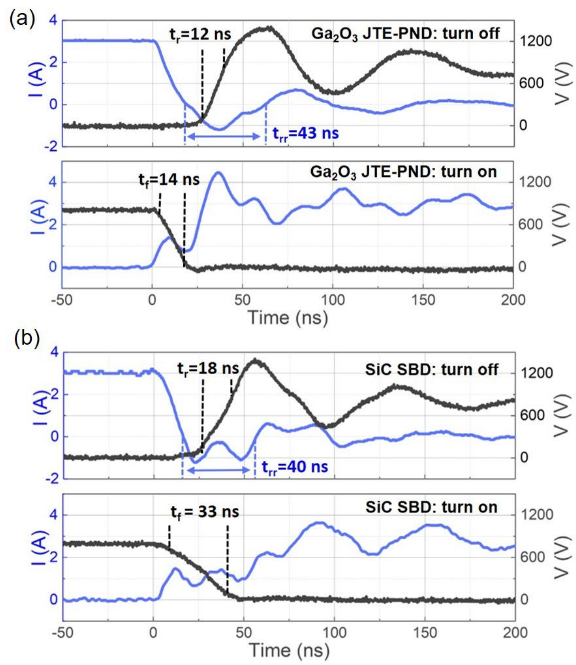

Fig. 4. Turn-ON and turn-OFF waveforms of a (a) Ga_2O_3 diode with NiO junction termination extension [2] and (b) similarly-rated, commercial SiC diode measured using a customized double-pulse test setup for on-wafer device characterizations.

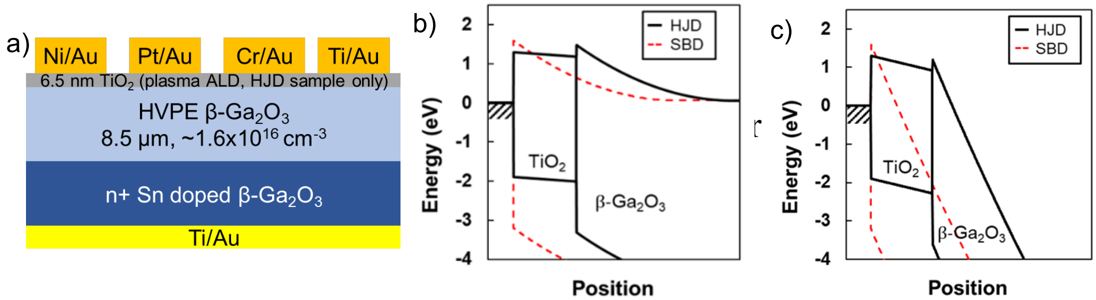

Figure 1: Schematics of a) the fabricated devices and the b) zero bias and c) reverse bias band diagrams of the SBD (red dash) and HJD (black).

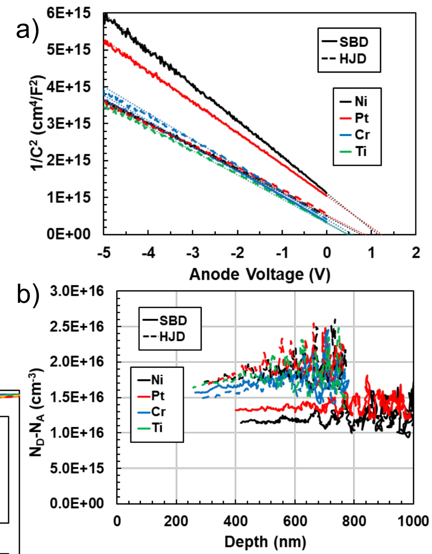

Figure 2: a) $1/C^2$ versus voltage for all devices and b) extracted N_d-N_A versus depth.

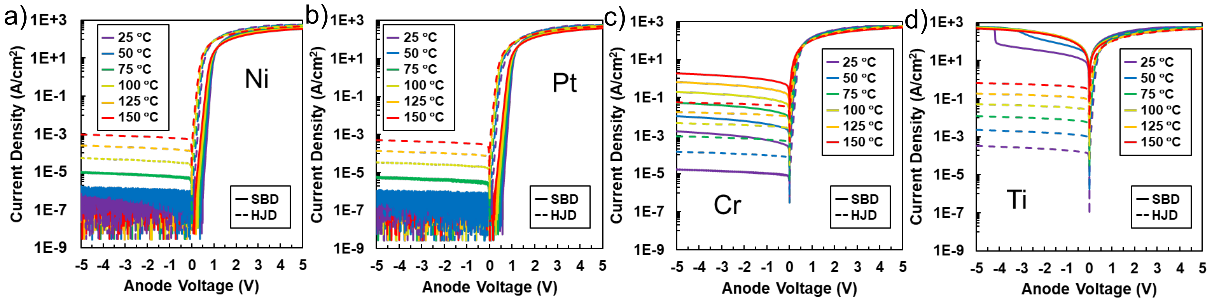

Figure 3: J-V-T data for a) Ni, b) Pt, c) Cr, and d) Ti SBDs (solid) and HJDs (dashed) from -5 to 5 V for 25 °C- 150 °C

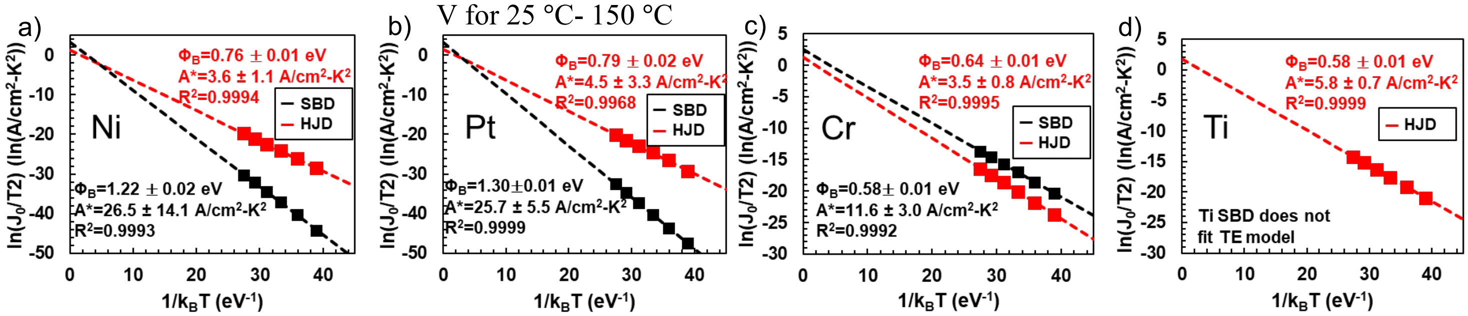

Figure 4: Richardson plots from J-V-T data for a) Ni, b) Pt, c) Cr, and d) Ti SBDs (black) and HJDs (red).

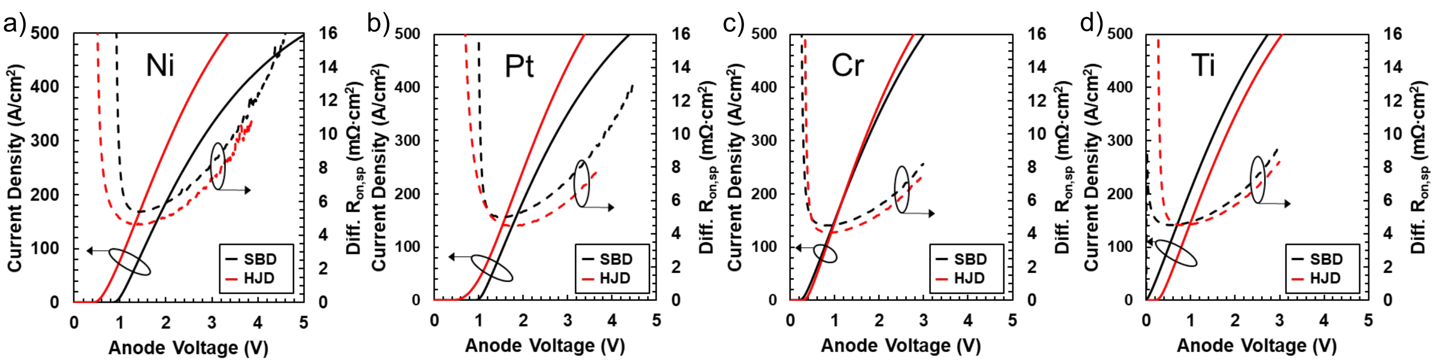

Figure 5: Linear scale forward J-V behavior of a) Ni, b) Pt, c) Cr, and d) Ti SBDs (black) and HJDs (red) with differential $R_{on,sp}$ in dashed lines.

Table 1: Extracted N_D-N_A, Φ_B and A* for all devices.

Device	N_d-N_A x10^{16} cm^{-3}	C-V Φ_B eV	J-V-T Φ_B eV	A* A/cm^2-K^2
Ni SBD	1.17	1.00	1.22	26.5
Pt SBD	1.34	1.23	1.30	25.7
Cr SBD	1.65	0.34	0.54	11.6
Ti SBD	N/A	N/A	N/A	N/A
Ni HJD	1.80	0.64	0.76	3.6
Pt HJD	1.83	0.72	0.79	4.5
Cr HJD	1.58	0.42	0.64	3.5
Ti HJD	1.75	0.34	0.58	5.8

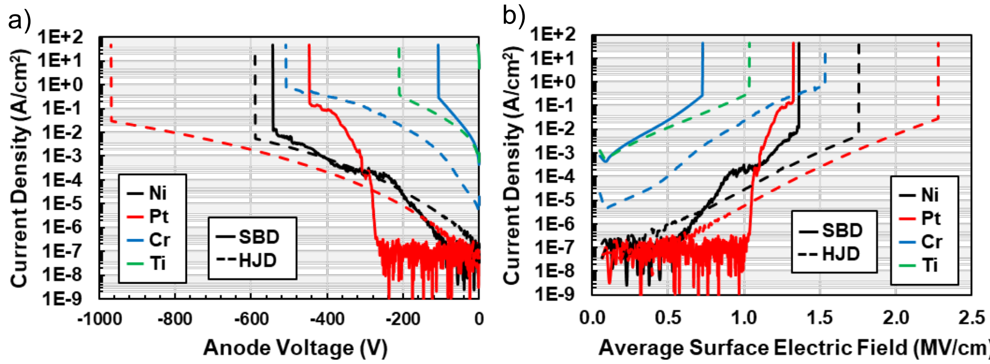

Figure 6: Reverse bias current behavior for all devices tested versus a) reverse voltage and b) average surface electric field (Ti SBD not shown).

[1] Z. Z. Hu et al., IEEE T Electron Dev 67 (12), 5628-5632 (2020)

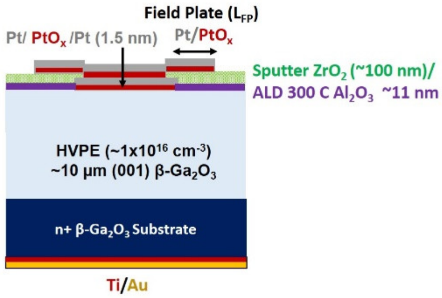

Figure 1: Schematic of the vertical β-Ga_2O_3 SBD of 100 µm diameter fabricated on low-doped 10 µm drift layer HVPE (001) with Pt cap/ PtO_x/Interlayer Pt (1.5 nm) Schottky contacts. The 30 µm field-plate was formed with high permittivity ZrO_2 dielectric with underneath thin Al_2O_3

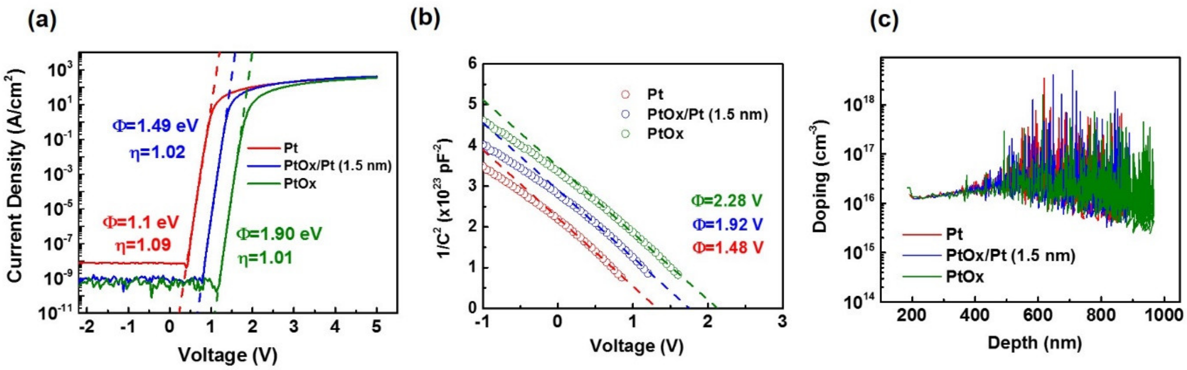

Figure 2: (a) J-V showing lower turn-on voltage and SBH for Pt and PtO_x/Pt(1.5 nm) SBDs than PtO_x (b) C-V extracted SBH showing lower SBH for Pt and PtO_x/Pt(1.5 nm) than PtO_x (c) Similar doping profile observed in all SBDs

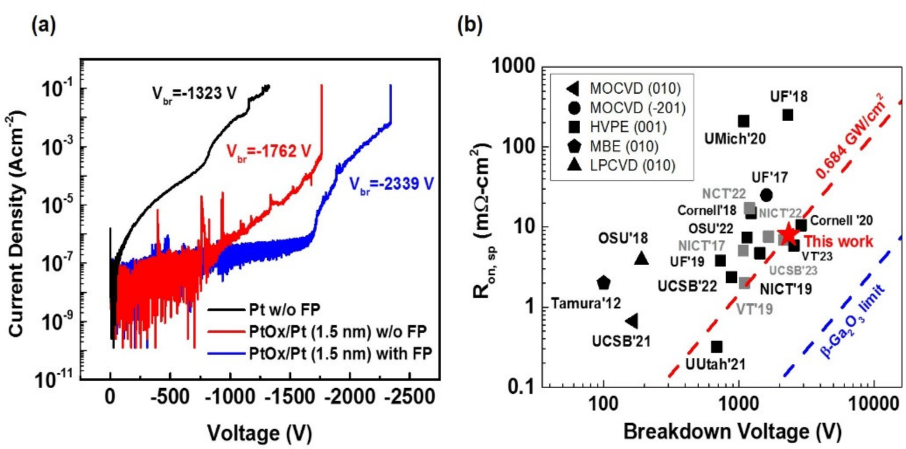

Figure 3: Reverse J-V showing (a) PtO_x/Pt (1.5 nm) provides substantially lower leakage and higher breakdown voltage compared to Pt SBDs. The ZrO_2 field-plate further improves the breakdown voltage to ~2.34 kV (b) Benchmark plot of on-resistance versus breakdown voltage from this work and other reports. A BFOM of 0.684 GW/cm^2 is achieved with the field plate PtO_x/Pt (1.5 nm) diodes.

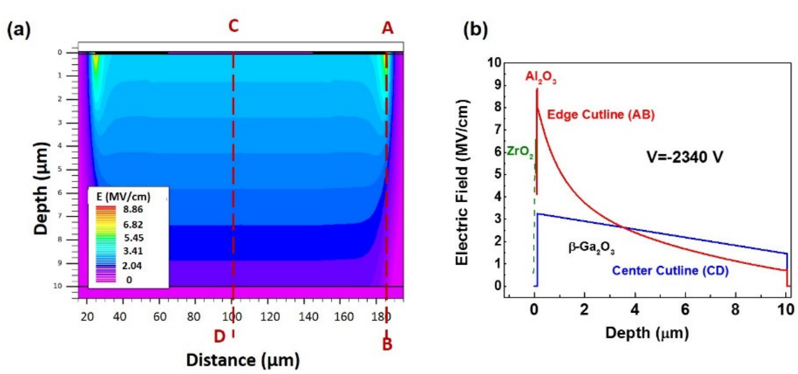

Figure 4: (a) Simulated electric field contour plot of the PtO_x/Pt(1.5 nm) Schottky diode with ZrO_2 dielectric field-plate at voltage V=-2.34 kV. (b) Electric field at the center of the anode through cutline CD shows a punch-through field profile achieved at the breakdown voltage with a maximum value of ~3.25 MV/cm. Electric field at the field-plate edge along cutline AB reveals that a peak field of 8.86 MV/cm and 8 MV/cm appear in Al_2O_3 and β-Ga_2O_3, respectively, indicating either one or both of them can be the critical locations of breakdown.

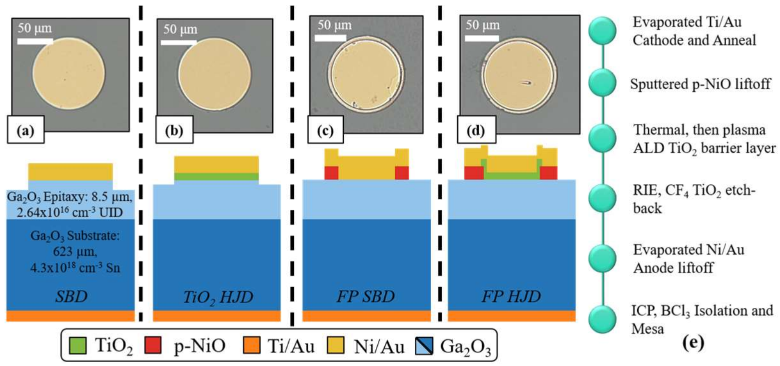

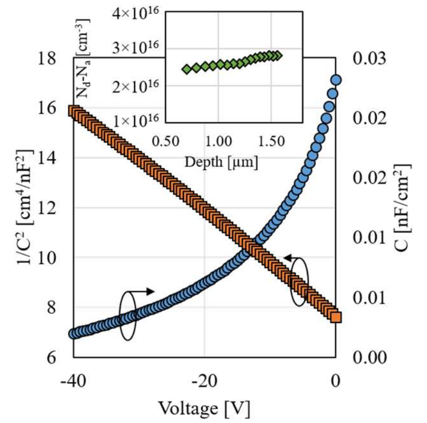

Fig. 1 Optical microscope and cross section graphic depicting each device type: (a) SBD (b) TiO_2 HJD (c) GR SBD (d) GR HJD; and (e) an outline of the fabrication process flow.

Fig. 2 C-V measurements of an SBD device with extracted carrier concentration vs. depth.

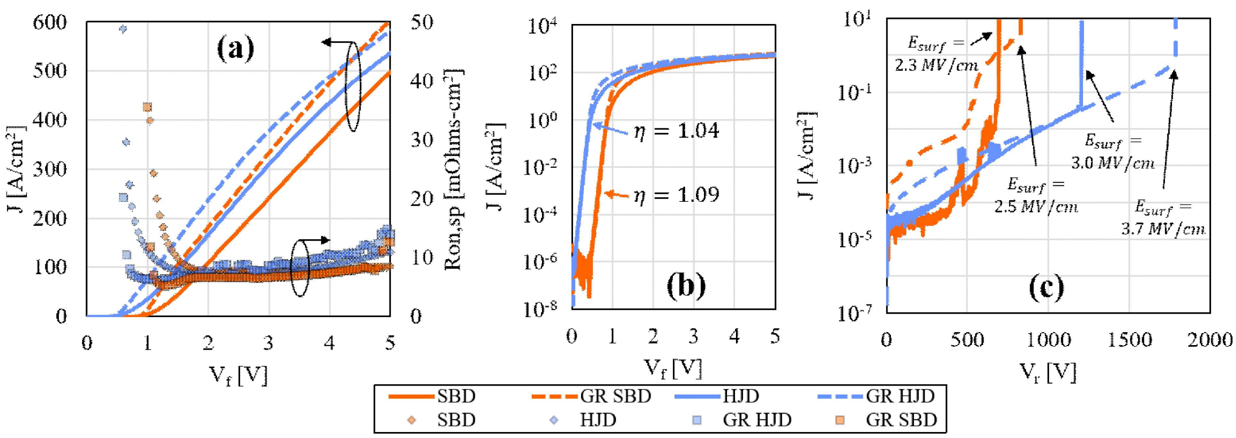

Fig. 3 (a) Forward J-V response of each device on a linear scale with differentially extracted $R_{on,sp}$. (b) Forward J-V response on a logarithmic scale with extracted ideality factors. (c) Reverse bias J-V response and breakdown, with surface electric field at breakdown calculated from C-V derived doping and manufacturer specifications.

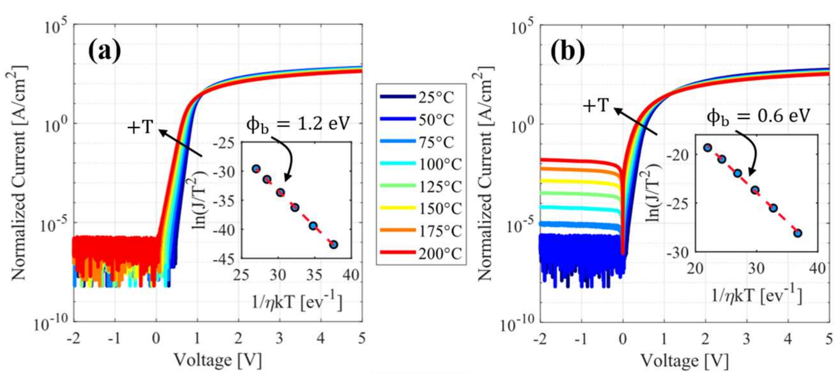

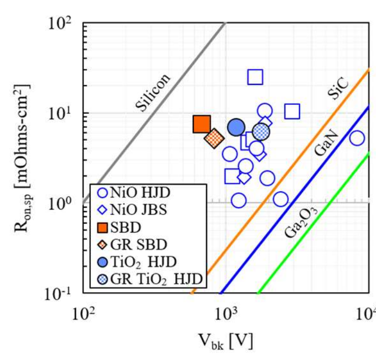

Fig. 4 Temperature dependent J-V response of a representative (a) SBD device and (b) TiO_2 HJD device. The inset shows Richardson plots used for extracting each junction barrier height according to the classical thermionic emission model.

Fig. 5 The devices from this work (filled points) compared with literature (empty points) using BFOM = $V_{bk}^2/R_{on,sp}$.

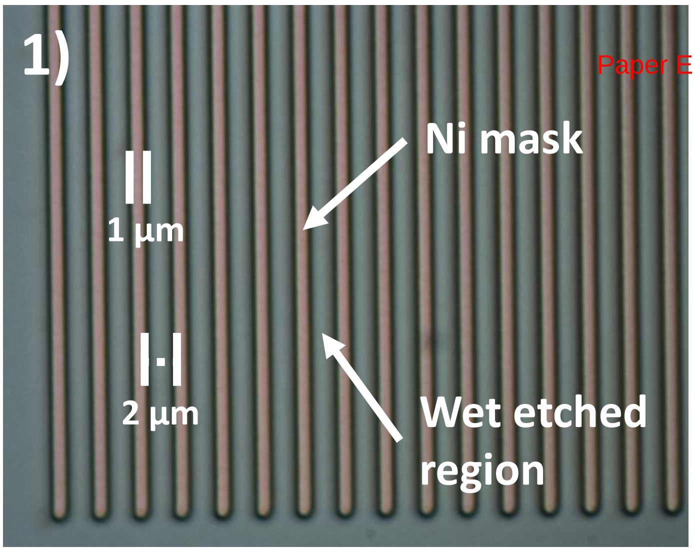

Fig. 1) Demonstration of nickel wet etching down to 1 µm.

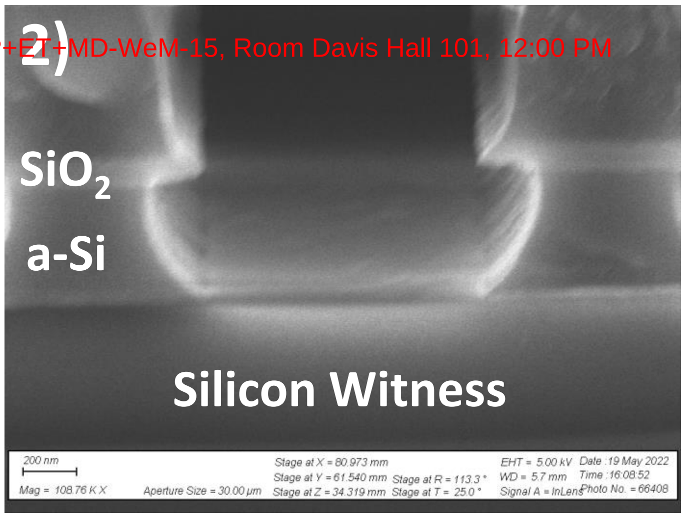

Fig. 2) XeF_2 undercut of the amorphous silicon layer for the lift-off process.

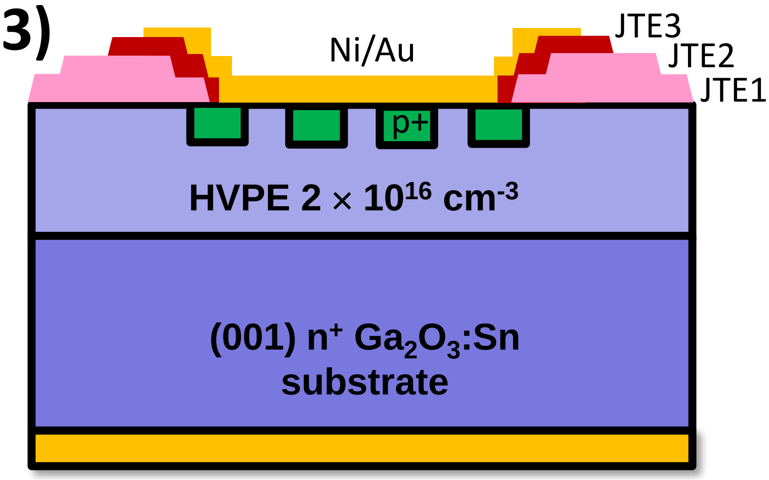

Fig. 3) Schematic of the Ga_2O_3 NiO JBS diode with NiO junction termination extension.

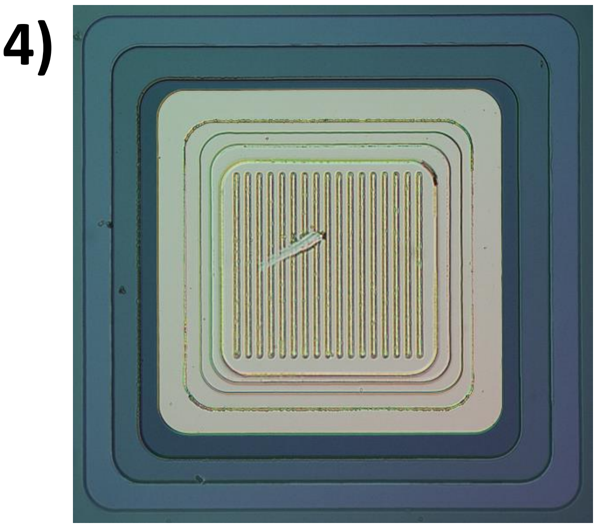

Fig. 4) Fully fabricated Ga_2O_3 NiO.

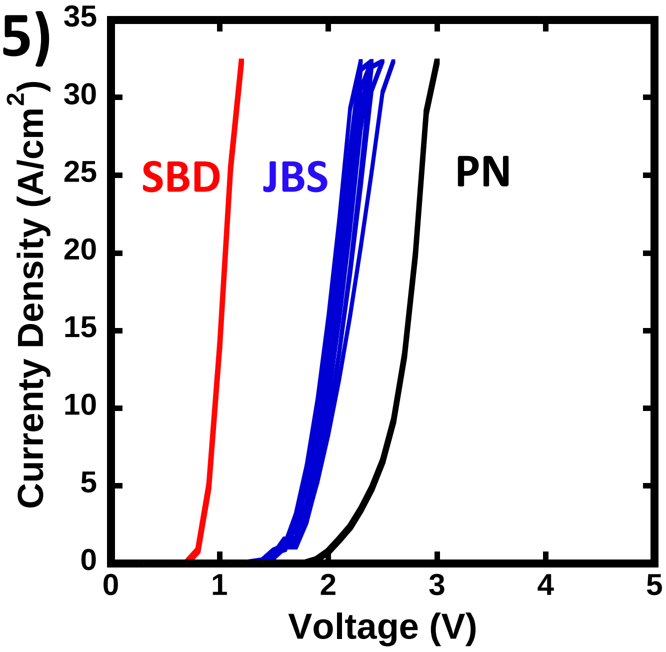

Fig. 5) Forward *J-V* characteristics.

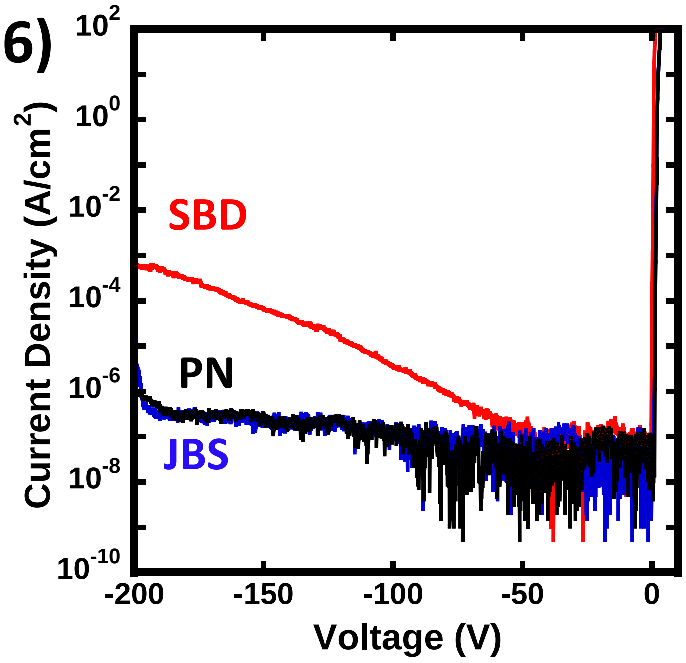

Fig. 6) Reverse *J-V* characteristics.

Abstract References:

[1] Spencer, J.A., et al. *Applied Physics Reviews*, 9.1 (2022): 011315 2022

[2] Lv, Y., et al. *IEEE Transactions on Power Electronics* 36.6 (2020): 6179-6182

[3] Gong, HH., et al. *Applied Physics Letters* 118.20 (2021): 202102

[4] Wang, B., et al. *IEEE Electron Device Letters* (2022).

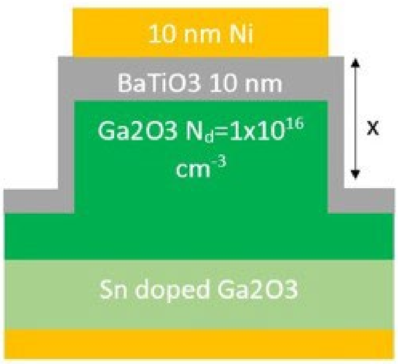

Figure 1: Schematic of the device where X varies between 0, 3, and 6 um.

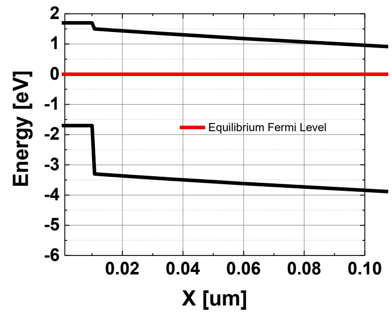

Figure 2: Equilibrium band diagram of BaTiO3- Ga2O3 heterojunction at equilibrium.

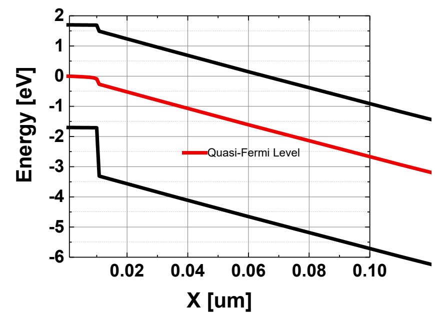

Figure 3: Band diagram of BaTiO3-Ga2O3 heterojunction at -20 V bias.

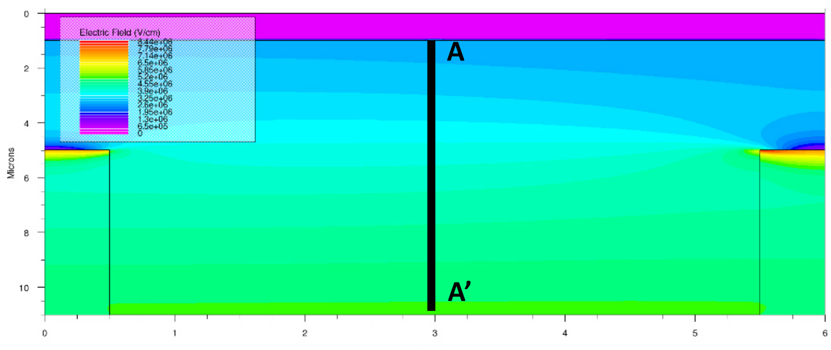

Figure 4: Simulated electric field coutour in 6um-trench device, showing a peak field in the device of 5 MV/cm. A cut-line is defined from A-A'.

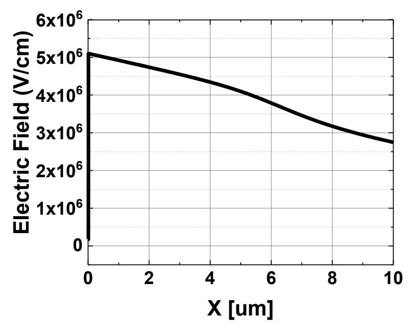

Figure 5: Electric field profile along cutline A-A' from Figure 4. Peak field is at 5 MV/cm.

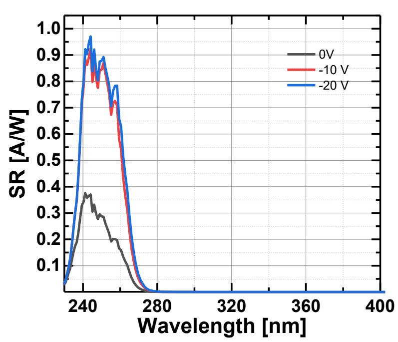

Figure 6: Spectral response of the device at 305K.

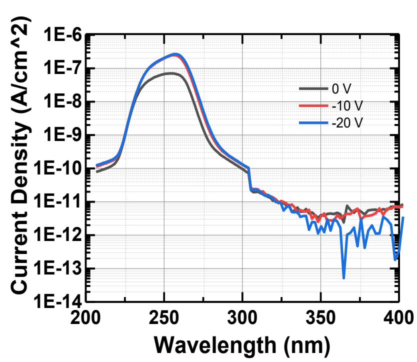

Figure 7: Current vs. wavelength behavior of the device at 305K.

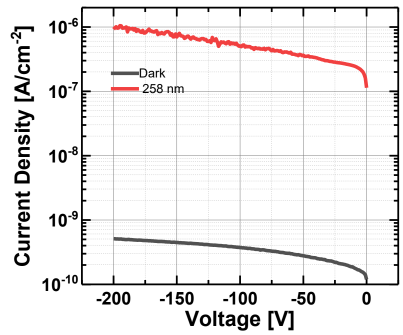

Figure 8: IV curve with and without 258nm illumination.

Supplemental Document Author Index

Bold page numbers indicate presenter